JOURNAL OF QUATERNARY SCIENCE (2022) **37**(2) 142–180 ISSN 0267-8179. DOI: 10.1002/jqs.3354

JQS Journal of Quaternary Science QRA Quaternary Research Association

Neanderthals on the Lower Danube: Middle Palaeolithic evidence in the Danube Gorges of the Balkans

DUŠAN BORIĆ,[1,2]* EMANUELA CRISTIANI,[3] RACHEL HOPKINS,[4] JEAN-LUC SCHWENNINGER,[4] KATARINA GEROMETTA,[5] CHARLY A. I. FRENCH,[6] GIUSEPPINA MUTRI,[7] JELENA ĆALIĆ,[8] VESNA DIMITRIJEVIĆ,[9] ANA B. MARÍN-ARROYO,[6,10] JENNIFER R. JONES,[11] RHIANNON STEVENS,[12] ALANA MASCIANA,[13] KEVIN UNO,[13] KRISTINE KORZOW RICHTER,[14] DRAGANA ANTONOVIĆ,[15] KAROL WEHR,[12] CHRISTINE LANE[16] and DUSTIN WHITE[17]

[1]The Italian Academy for Advanced Studies in America, Columbia University, New York, NY, USA
[2]Department of Environmental Biology, Sapienza University of Rome, Rome, Italy
[3]DANTE - Diet and Ancient Technology Laboratory, Department of Oral and Maxillo-facial Sciences, Sapienza University of Rome, Rome, Italy
[4]Research Laboratory for Archaeology and the History of Art, School of Archaeology, University of Oxford, Oxford, UK
[5]Department of Archaeology, Faculty of Philosophy, Juraj Dobrila University of Pula, Pula, Croatia
[6]Department of Archaeology, University of Cambridge, Cambridge, UK
[7]The Cyprus Institute, Aglantzia, Nicosia, Cyprus
[8]Geographical Institute "Jovan Cvijić", Serbian Academy of Sciences and Arts, Belgrade, Serbia
[9]Department of Archaeology, University of Belgrade, Belgrade, Serbia
[10]EvoAdapta Group, Universidad de Cantabria, Santander, Spain
[11]School of Natural Sciences, University of Central Lancashire, Preston, Lancashire, UK
[12]UCL Institute of Archaeology, London, UK
[13]Lamont-Doherty Earth Observatory of Columbia University, Palisades, NY, USA
[14]Department of Anthropology, University of Harvard, Tozzer Anthropology Building, Cambridge, MA, USA
[15]Institute of Archaeology, Belgrade, Serbia
[16]Department of Geography, University of Cambridge, Cambridge, UK
[17]Department of Chemistry, University of York, York, UK

Received 17 February 2021; Revised 17 June 2021; Accepted 28 June 2021

ABSTRACT: The article presents evidence about the Middle Palaeolithic and Middle to Upper Palaeolithic transition interval in the karst area of the Danube Gorges in the Lower Danube Basin. We review the extant data and present new evidence from two recently investigated sites found on the Serbian side of the Danube River – Tabula Traiana and Dubočka-Kozja caves. The two sites have yielded layers dating to both the Middle and Upper Palaeolithic and have been investigated by the application of modern standards of excavation and recovery along with a suite of state-of-the-art analytical procedures. The presentation focuses on micromorphological analyses of the caves' sediments, characterisation of cryptotephra, a suite of new radiometric dates (accelerator mass spectrometry and optically stimulated luminescence) as well as proteomics (zooarchaeology by mass spectrometry) and stable isotope data in discerning patterns of human occupation of these locales over the long term.

KEYWORDS: cryptotephra; Danube Gorges; OSL dating; Palaeolithic; radiocarbon dating; ZooMS

Introduction

There is a dearth of well-researched and dated Palaeolithic sequences in large parts of the Balkans with uneven quality of the extant data. Our understanding remains coarse-grained even though this region must have represented a key land route along which hominin populations expanded northwards and westwards from Asia Minor at various times during early prehistory. Like other areas of southern Europe, the Balkans and the riparian zone of the Danube catchment (Fig. 1), as an important migration conduit, likely acted as a refugium at different times within the pattern of ebb and flow fluctuations in the occurrence and displacement of different animal, plant and hominin taxa over the long term. Recently, the importance of the Danube River corridor as a route for hominin dispersal and a zone of high resource productivity is emerging through new discoveries and the re-evaluation of previous Palaeolithic finds in the wider catchment of the southern Carpathian Basin in Romania, Bulgaria and Serbia (e.g. Anghelinu *et al.*, 2012; Bălțean, 2011; Chu, 2018; Hauck *et al.*, 2018; Mihailović *et al.*, 2011; Tsanova, 2008).

Over the past decade or so, there has been a growing impetus in various parts of the region to discover and investigate Palaeolithic sites, both in caves and in open-air locations, as well as to acquire high-resolution data with modern standards of data collection, recording and analysis (e.g. Alex *et al.*, 2019; Borić *et al.*, 2012; Boschian *et al.*, 2017; Chu *et al.*, 2014, 2015; Dogandžić *et al.*, 2014; Fewlass *et al.*, 2020; Harvati and Roksandic, 2016; Hublin *et al.*, 2020; Iovita *et al.*, 2014; Karavanić *et al.*, 2008; Mandić and Borić, 2015;

*Correspondence: D Borić, as above.
E-mail: dusan.boric@uniroma1.it, db2128@columbia.edu

Figure 1. Principal sites with Middle and Initial/Early Upper Palaeolithic sequences in south-eastern Europe. Bathymetric contours show the drop of sea levels -110 m; source: the General Bathymetric Chart of the Oceans (GEBCO) https://www.gebco.net/data_and_products/gridded_bathymetry_data/. Base map prepared by Andrea Zupancich. Sites: 1. Asprochaliko; 2. Bacho Kiro; 3. Baranica; 4. Bioče; 5. Coșava I; 6. Crvena Stijena; 7. Crvenka-At; 8. Gajtan; 9. Golema Pešt; 10. Hadži Prodanova; 11. Klissoura; 12. Kozarnika; 13. Krapina; 14. Lakonis; 15. Londža; 16. Mujina; 17. Pešturina; 18. Petrovaradin; 19. Românești-Dumbrăvița; 20. Šalitrena; 21. Samuilitsa II; 22. Smolućka; 23. Temnata; 24. Theopetra; 25. Tinkova; 26. Vindija; 27. Zobište. [Color figure can be viewed at wileyonlinelibrary.com]

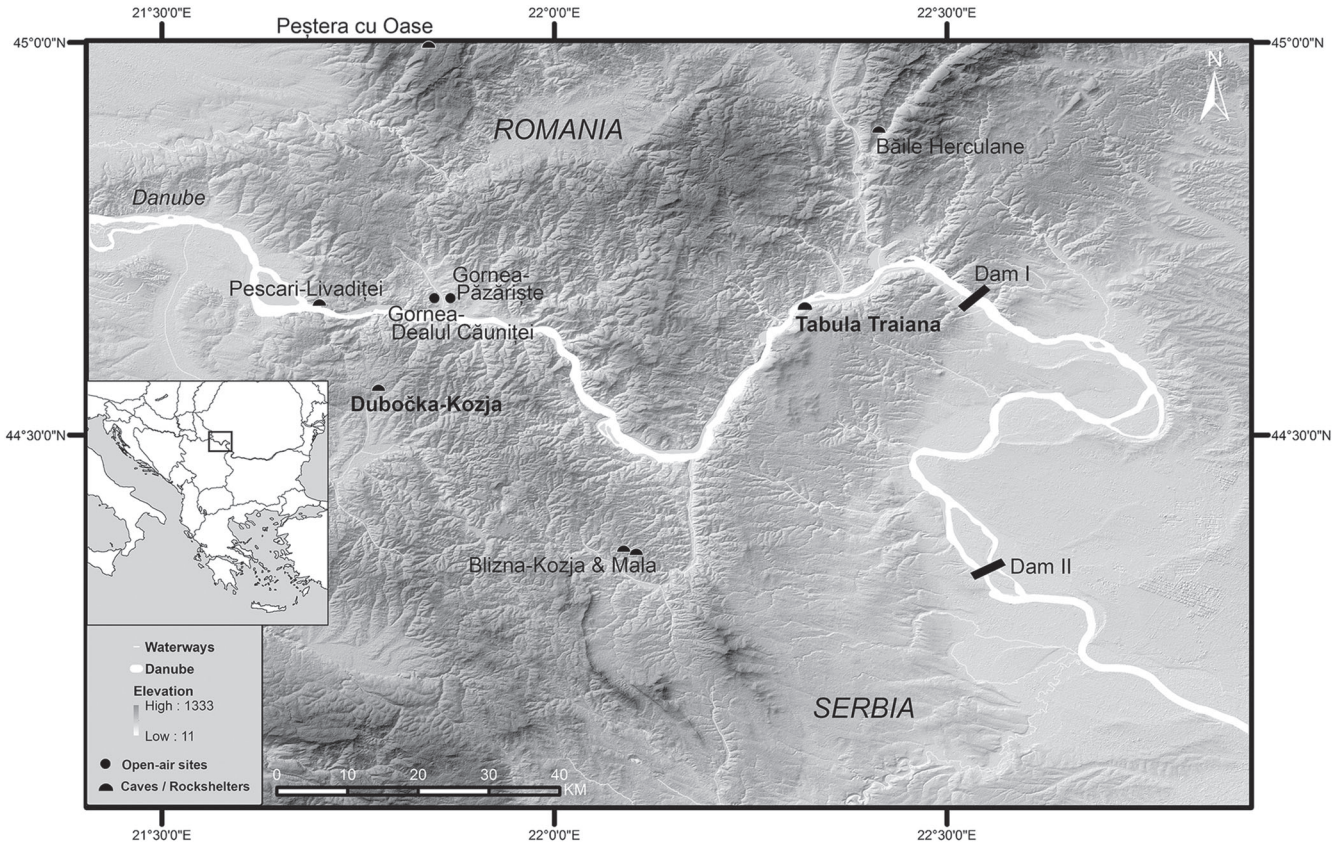

Figure 2. Sites with Middle and Upper Palaeolithic sequences in the Danube Gorges area. Base map elevation data source: ASTER GDEM ('ASTER GDEM is a product of METI and NASA') courtesy NASA/JPL-Caltech. Figure prepared by Karol Wehr and Dušan Borić.

Marín-Arroyo and Mihailović, 2017; Mihailović, 2009, 2020; Sirakov *et al.*, 2010). A part of these efforts by several different research teams is the project, whose first results are presented here, that aims to acquire novel data about the character of the Middle to Upper Palaeolithic transitional interval along the 'Danube corridor' by investigating the karstic region of the Danube Gorges in the north-central Balkans (Fig. 2). The region's importance in later prehistoric periods is already well established by the rich cultural record of terminal Pleistocene–early Holocene Mesolithic forager cultures in the Danube Gorges (Bonsall, 2008; Borić, 2011). Despite years of minimal Palaeolithic research in the Lower Danube Basin, new discoveries are beginning to unlock the potential of this catchment as a hotspot of Palaeolithic archaeology that will shed light on cultural innovation and adaptation during this critical period of human history. We remain interested in better understanding the role of the Lower Danube Basin as a major communication corridor in the transmission of people as well as cognitive, cultural and social novelties in relation to its natural affordances (aspects of terrain, geography and resource bioavailability) throughout the Middle to Upper Palaeolithic in order to define the specific 'pull' factors of this regional context.

In this paper, we present recently collected data from two previously unknown sites found in the area of the Danube Gorges of the wider Lower Danube Basin. Here, the Danube Valley might have acted as an important conduit for the movement of people and animals during different stadial and interstadial conditions. The Danube Gorges are dominated by karstic terrain containing numerous caves and rock shelters (e.g. Constantin *et al.*, 2001). Landscape features such as these commonly preserve both cultural remains, as they have been favoured by hominins seeking shelter for much of the Quaternary, and sediments that can provide important palaeoenvironmental data. Two discussed cave sites – Dubočka-Kozja and Tabula Traiana caves – are characterised by Levallois-based industries along with the likely presence of Early Upper Palaeolithic assemblages at Tabula Traiana Cave (TT). The first site is in the immediate hinterland of the Danube (~10 km) while the second is found directly on the steep banks of the Danube River. In this paper, we summarise the characteristics of knapped stone industries and associated faunal remains from the two sites before presenting new results of accelerator mass spectrometry (AMS) dating of anthropically modified bones and optically stimulated luminescence (OSL) dating of sediments from both sites. Geomorphological observations, micromorphological analyses of sediments, as well as zooarchaeology by mass spectrometry (ZooMS) and stable isotope analyses on faunal remains are further integrated with other available data. Finally, the paper contextualises this new data with other broadly contemporaneous sites in the Balkans and examines to what extent this dataset can fit the refugia model for southern European peninsulas during different phases of the Pleistocene and how these new datasets fit what we currently know about the last Neanderthals and first modern humans in Europe.

Sites' description

Tabula Traiana Cave

Tabula Traiana Cave (N44° 39′ 26.1606″, E22° 18′ 41.1006″, i.e. UTM 7604444 E, 4946683 N) was discovered in the immediate vicinity of the Roman stone inscription *Tabula Traiana*, after which it bears its name, during a survey conducted in the course of the collaborative project 'Prehistory of North-East Serbia' between the Departments of Archaeology of the University of Cambridge and the University of Belgrade in 2004. The cave is situated in the karstic massif of the Miroč mountain, downstream from the Kazan Gorge of the Danube (Fig. 3). The whole stretch of the Golo Brdo karst sloping towards the Danube bears the name *Faca Pešćeri* in the local Vlach dialect and means the 'Face with Caves'. Near TT, several other smaller cave openings, some filled with sediments, have been found. No archaeological material was found on cave floors and no test trenches have been placed in the deposits of these caves, with a detailed test trenching of these prospective sites planned in the near future. The access to TT is difficult, with only a barely visible pathway descending from the present-day arterial road number 25/1 (*Đerdapska magistrala*). TT is found some 22–23 m above the present level of the Danube at an altitude of 90–91 m a.s.l. (Fig. 4).

The cave entrance has a western exposure and is about 4.5 m high and 4 m wide at the base. Its cross section is triangle-shaped, with a clearly visible initial fracture. A small terrace is found in front of TT with a large collapsed block of the cave roof, visible upon excavation, that slid down the sloping side in continuation of the north-western cave wall. TT is developed along a single fracture striking in a west–east direction and was further shaped by water erosion from the hinterland. Today it is out of hydrological function and there are only dripwaters at certain times of the year. Inside, the floor is horizontal for the first 15 m and covered by thick, relatively well-sorted sediments closer to the surface, while very large blocks of collapsed rock and rubble are more prominently found towards the bottom of the stratigraphic sequence (see below for a more detailed description and micromorphological analysis of excavated cave sediments and stratigraphic units). The walls are strongly corroded by long-lasting seepage of mildly acidic karst water. The first part of the cave with a thick layer of sediments ends in a cascade inclined upwards that leads towards the back of the cave, with the back chamber devoid of sediments. There are several chimneys, which end blindly (for more geomorphological details, see Mandić and Borić 2015).

In 2004, a small test pit (Trench 1/2004, 2 × 2 m) was dug at the cave's entrance. Another trench (Trench 1/2005, 4 × 1.5 m) was opened in the central part of the main chamber in 2005. In 2008, a 1 m wide extension was made along the northern profile of Trench 1/2005, while in the same year another trench (2/2008, 1.5 × 3 m) was dug closer to the cave entrance, with its eastern section linked to Trench 1/2004. Consequently, Trench 2/2008 was extended towards the interior of the cave to connect this outer trench with the area excavated inside the cave (Trench 3/2008, 2.5 × 1 m), thus obtaining a continuous longitudinal cross section of the cave's stratigraphic sequence. In 2009, a trench was dug in the back of the main cave chamber in continuation of Trench 1/2005, with a 0.5 m wide baulk separating the two trenches. In 2013, 2017 and 2019, excavations focused on the cave terrace and the zone along the southern cave wall (14 m^2), connecting this outer zone with the cave interior. To date, in total, a horizontal area of 44 m^2 has been investigated in TT, albeit not all parts of the cave have been investigated to the same depth.

The latest occupation (10–30 cm thick) is dated to the Early Iron Age (Basarabi and Kalakača-Gorne style of pottery) (Kapuran *et al.*, 2007). There were also sporadic finds of Late Roman and early Medieval pottery, possibly associated with a pit dug at the entrance of the cave. Only a few pottery fragments can be dated to the Eneolithic period and are stylistically related to the Coțofeni pottery style. A sterile layer separates the late Holocene occupation (SU 200, 201 and 203) from Pleistocene levels (Fig. 5).

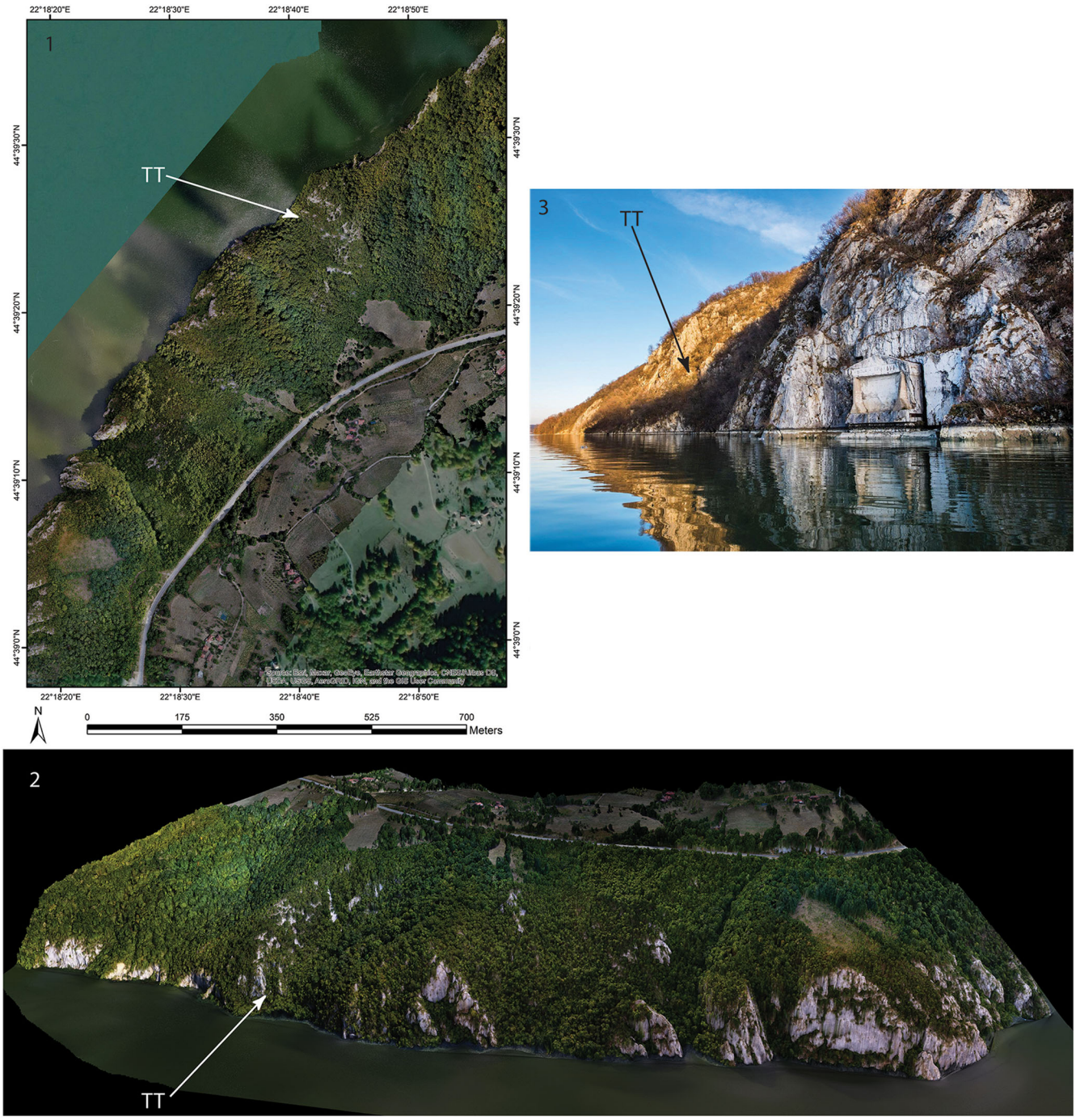

Figure 3. 1: Photogrammetry-derived TT cave area orthomosaic overlain on the World Imagery dataset (Esri – 1 m cell size south-east Europe) demonstrating the improved quality for the investigated area when compared with openly accessible imagery datasets; 2: Snapshot of the TT area 3D model; 3: View of the current location of the Roman plaque *Tabula Traiana* in the vicinity of TT Cave. [Color figure can be viewed at wileyonlinelibrary.com]

During excavations, two major sets of stratigraphic units were clearly distinguished within the Pleistocene deposits, based on the physical properties of sediments. The upper stratigraphic units of Pleistocene age (SU 43, 90, 207, 217) characterised by ashy yellowish brown to greyish brown calcareous silt contained a very low density of knapped flint of largely good knapping quality ($n = 12$) and a large number of animal bones. These upper deposits have a sharp and distinct boundary with lower stratigraphic units characterised by reddish brown silt loam and an abundance of subangular limestone clasts (Fig. 6). In the central part of the interior of the cave, a fireplace was discovered at the bottom of the upper Pleistocene-age chronostratigraphic units (Fig. 5). The lower levels (SU 206, 209, 211, 221, 226) yielded a larger, albeit still a relatively small, assemblage of knapped stone artefacts ($n = 150$) compared with the upper levels. These artefacts were made on a local range of raw materials of poor knapping quality, such as quartzite (*c.* 45%) and quartz (*c.* 45%) (cf. Gurova *et al.*, 2016).

While a more detailed description of the character of the assemblage of knapped stone tools from this site will be provided elsewhere, some of the characteristic pieces from the two major chronostratigraphic horizons are shown in Fig. 7. Although only a very few artefacts were found in the relatively thick deposits of the upper Pleistocene-age horizons, several of these are suggestive of the Early Upper Palaeolithic (EUP) industries, such as Protoaurignacian or Early Aurignacian: a blade with bilateral continuous retouch, a Dufour bladelet, an

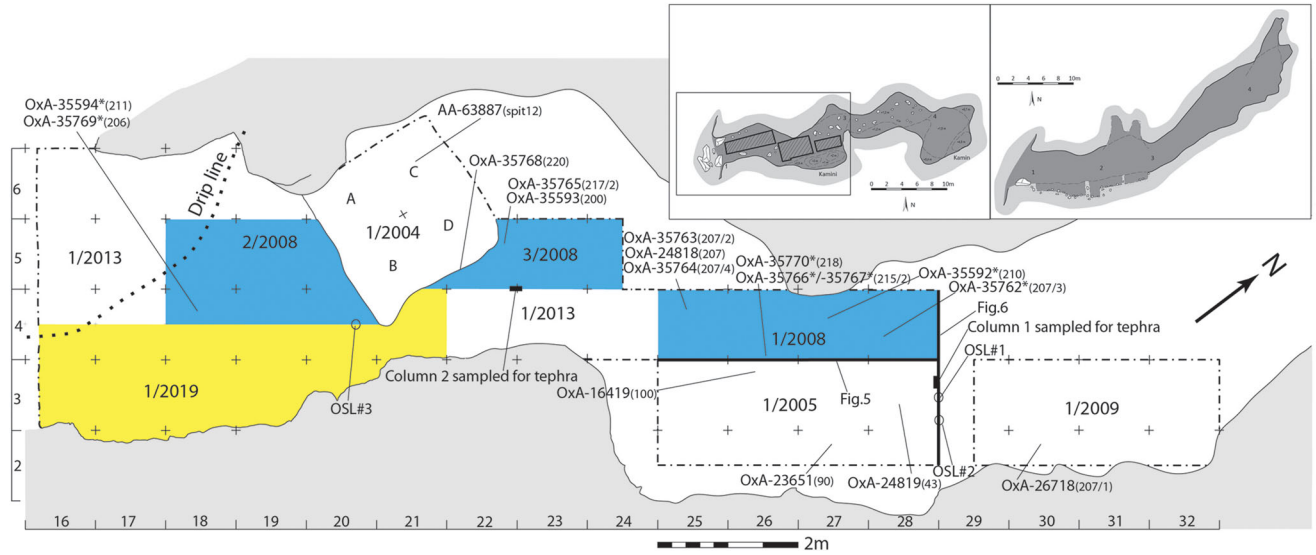

Figure 4. Plan of TT with excavation areas and locations of radiometric and sediment samples. Asterisk marks samples that produced results beyond the limit of radiocarbon dating. [Color figure can be viewed at wileyonlinelibrary.com]

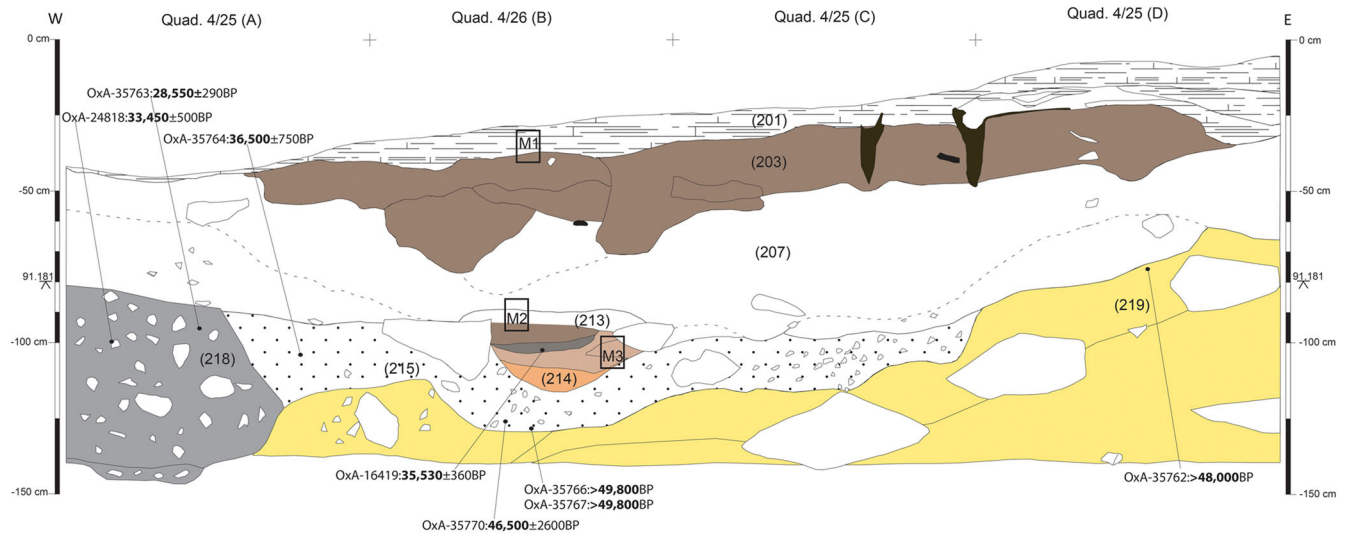

Figure 5. A representative west–east stratigraphic section at TT with the location of micromorphological samples. [Color figure can be viewed at wileyonlinelibrary.com]

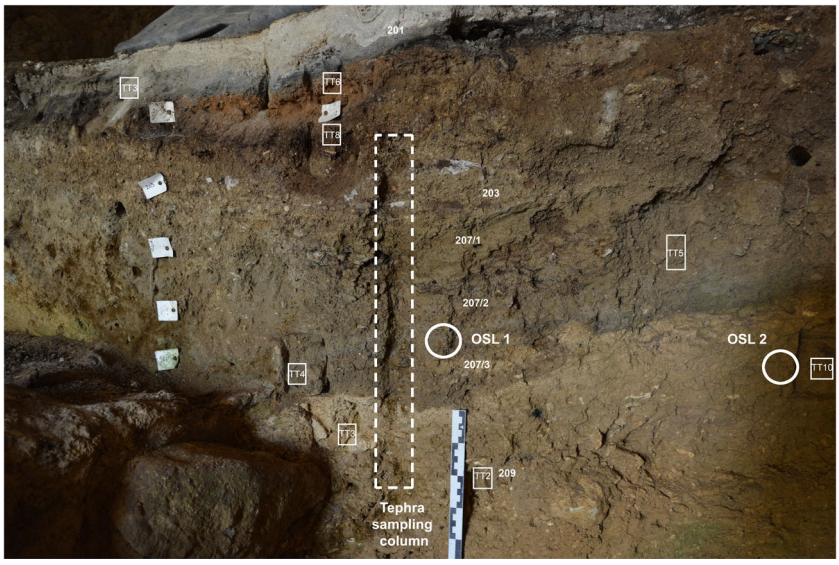

Figure 6. A representative north–south stratigraphic section at TT with the location of micromorphological and OSL samples. [Color figure can be viewed at wileyonlinelibrary.com]

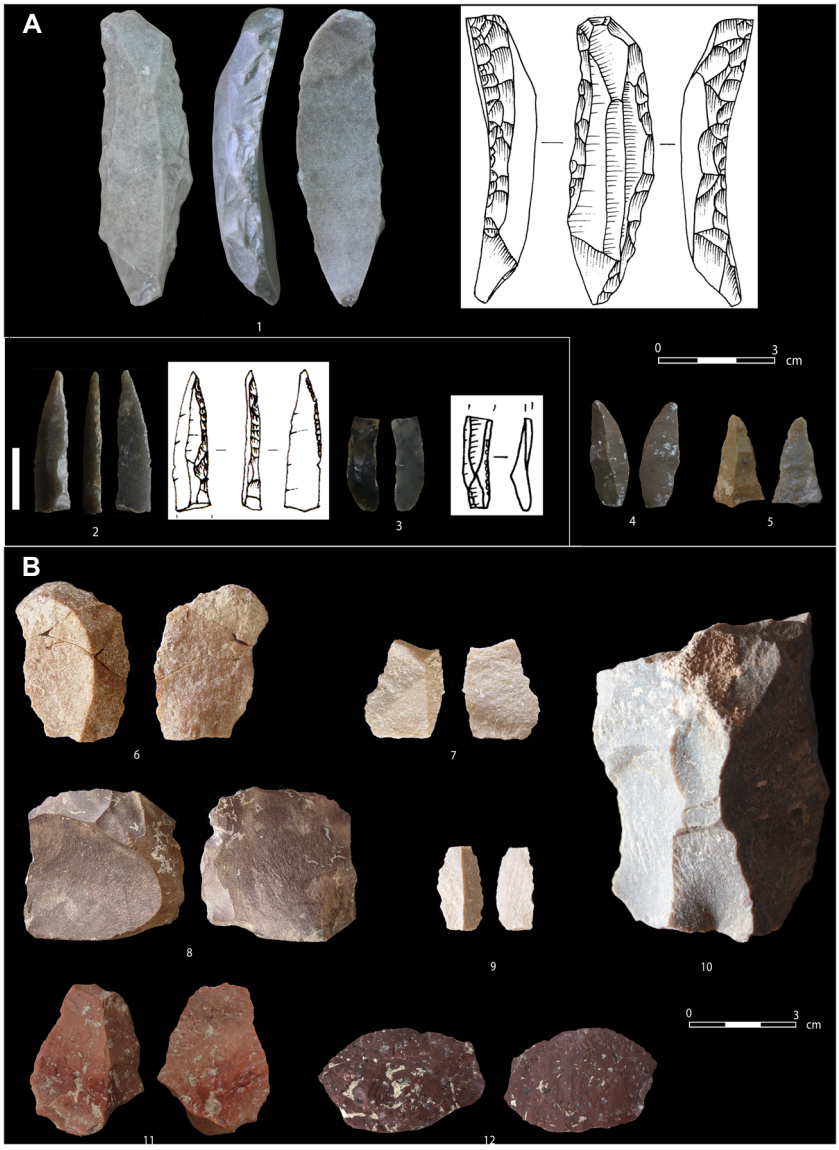

Figure 7. A selection of knapped stone artefacts from (A) Upper Palaeolithic stratigraphic units, and (B) Middle Palaeolithic stratigraphic units at TT; 1: blade with bilateral continuous retouch (SU41, quad. 3/26, depth 91.311 m); 2: Dufour bladelet with abrupt and marginal alternating retouch (SU221, quad. 4.5/16, spit 8); 3: micro-bladelet, bilateral continuous retouch (SU216, quad. 4/25); 4: bladelet blank (SU207); 5: retouched bladelet, distal end (SU207/1, quad. 3/30); 6: rejuvenation flake of the *éclat débordant* type (Tr. 1/2004, quad. A, spit 10); 7: Levallois flake (SU212x.8); 8: rejuvenation flake of the *éclat débordant* type (Tr. 1/2004, quad. C, spit 10); 9: laminar blank (SU212x.4); 10: single-platform core (SU221, quad. 5/18, spit 11); 11: retouched flake (SU226x.89, spit 12); 12: scraper (SU226x.52, spit 11). [Color figure can be viewed at wileyonlinelibrary.com]

unretouched bladelet typical of prismatic-core reduction, and a bladelet with a right and distal direct marginal retouch. In contrast to this small assemblage dominated by curated artefacts indicative of ephemeral visitations of the cave by likely modern humans, the assemblage from the lower chronostratigraphic units is characterised by a low density of tools (only a few scrapers, notches and denticulates) along with the dominance of Levallois flakes, rare laminar blanks and several irregular, single and opposed platform cores ($n = 7$). This latter assemblage could confidently be assigned to Middle Palaeolithic (MP) industries and, by proxy, Neanderthals. Spatially, finds in lower chronostratigraphic units are more abundant in the cave entrance area and on the cave terrace, while few Upper Palaeolithic (UP) tools are found both deeper in the first chamber of the cave and on the terrace.

The detailed results of the complete morphological, taphonomic and spatial analyses of the faunal assemblage from TT is forthcoming, and it suffices to say here that this large assemblage is characterised by the dominance of ibex *Capra ibex* in both the MP and UP levels, while red deer *Cervus elaphus* is also relatively well represented among the herbivorous taxa. Based on the presence in the assemblage of several predatory carnivore species, such as the cave lion *Panthera spelaea*, cave hyena *Crocuta spelaea*, leopard *Panthera pardus*, cave bear *Ursus spelaeus*, brown bear *Ursus arctos*, wolf *Canis lupus*, marten *Martes* sp., lynx *Lynx lynx*, wild cat *Felis silvestris* and fox *Vulpes vulpes*, it is likely that agents of animal bone accumulation were both hominins and carnivores (cf. Milošević 2020). Among small mammals, hare *Lepus europaeus*, beaver *Castor fiber*, Insectivora, Chiroptera, Arvicolidae, and Muridae have also been identified. Fish remains of the genus *Silurus* and family Acipenseridae are also present.

Dubočka-Kozja

The Dubočka cave system was among the first caves in Serbia to be scientifically studied at the end of the 19th century and it contributed to the establishment of karstology in that country. The cave's first mapping and morphological description were made by the celebrated Serbian geographer and geomorphologist Jovan Cvijić (1895a; 1895b), who named it 'Velika Pećina (Big Cave) in the village of Duboka', while subsequently the name Dubočka Cave became the most used. A more recent description and analysis was provided by Branislav Jovanović (1951; see also, more recent findings by Zlokolica-Mandić *et al.*, 2003). The main cave with its large entrance, which is 20 m high and 25 m wide, also has an alternative local name Gaura Mare (meaning Big Cave in the Vlach language). It is situated 2.5 km from the village of Duboka at the end of the Valja Mare Valley in the zone of the isolated fluvio-karst of Dubočka Rudina (with the summit at

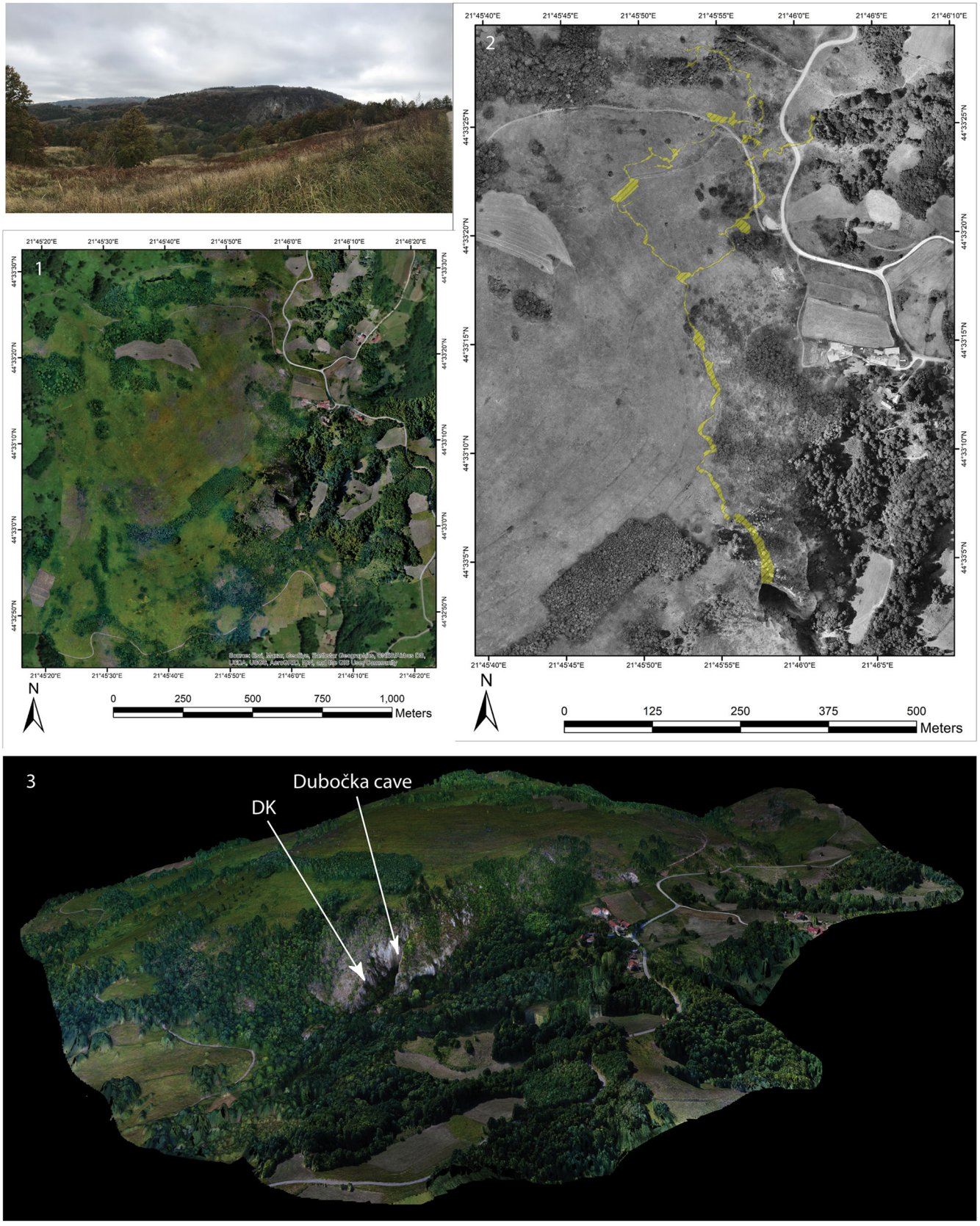

Figure 8. 1: Photogrammetry-derived Dubočka Cave area orthomosaic overlying the World Imagery dataset (Esri composite – 1 m cell size in south-eastern Europe) demonstrating the improved quality for the investigated area when compared with openly accessible imagery datasets; 2: Dubočka area orthomosaic (in greyscale, for contrast) and the outline of the underlying cave systems (after Zlokolica-Mandić *et al.*, 2003: 108); 3: Snapshot of the Dubočka area 3D model. [Color figure can be viewed at wileyonlinelibrary.com]

514 m a.s.l.) known as Veliki Krš (Fig. 8). The cave is formed in Tithonian limestones overlaid by Lower Cretaceous limestones and is situated 11 km from the banks of the Danube as the crow flies. Dubočka Cave is one of the longest caves in Serbia with the total length of 2734 m. It consists of the main channel (1010 m), characterised by an expressive erosional morphology, two longer lateral passages – Rusaljkin or First (472 m) and Glinoviti or Second (590 m) – and several smaller

channels. The cave is characterised by a complex set of secondary morphological characteristics (e.g. chambers, erosional pots, niches, cave karren) and complex processes of clastic and chemical sedimentation. In the Second lateral passage, a 'High passage' was discovered two decades ago above a 7 m high wall. In one of the chambers along this upper level, the remains of several cave bears *Ursus spelaeus*, some still in articulation and covered by a calcium carbonate crust with stalagmites, were discovered, possibly suggesting the existence of a previously passable, but presently closed connection to the modern topographic surface, which is now at *c.* 20 m above this chamber (Dimitrijević *et al.*, 2002). Dubočka Cave is seasonally hydrologically active with the Ponorska River, originating below Kornjecel at 500 m a.s.l., periodically passing through the main channel of the cave during wet seasons, and springing up in front of the cave's entrance, after which it forms a canyon with cascades and a waterfall. The Ponorska River is the right tributary of the Duboka River, which drains into the Pek River.

Approaching the main entrance of Dubočka Cave, on the right side, there is an opening of a small cave known as Ovčja (translated as 'sheep's cave'). On the left side of the entrance, on the steep side of the karst massif located some 30 m directly above the Ponorska River Cave, with a difficult approach and an eastern exposure, there is another relatively large opening (5.6 m wide and 11 m high) known as Kozja (translated as 'goat's cave') (Fig. 9). While Dubočka-Ovčja remains untested, archaeological investigations have so far focused on sediments of Dubočka-Kozja (DK) (N44° 33′ 6.12″, E21° 45′ 59.5″, i.e. UTM 7561314.584 E, 4934278.094 N), where the remains of different prehistoric periods have been documented and reported here for the first time. In 2011, our archaeological team visited DK and noted an illicit digging of a trench along the southern cave wall and possibly also in the small back chamber. Subsequently, a 3.5 × 2 m test trench was excavated in the central part of the cave yielding a relatively thin layer of topmost archaeological strata with ceramic finds dating to later prehistory (Copper and Iron Ages) below which were *c.* 50 cm of cultural strata dating to different phases of the Late Pleistocene based on the characteristics of the discovered lithic industry. Another almost completely filled cave opening (Dubočka 1) is found in the same karstic massif above the Duboka River, some 50 m to the right of the main entrance to Dubočka Cave. A test trench made in this cave has shown a deep stratification of cultural layers and so far, only the layers with the remains of later prehistoric periods have been reached.

Relatively shallow Holocene and Pleistocene palimpsest deposits (~60–80 cm deep) are discovered in DK in the area marked as Trench 1/2013, where excavations have reached the bedrock (Fig. 10). The top levels (SU 1, 2 and 9) of grey colour and ashy consistency are characterised by the presence of organic matter and contained Late Copper Age and Iron Age ceramics and other finds. A large and deep recent robber trench (SU3) significantly damaged Pleistocene sediments beneath. At the interface of Holocene and Pleistocene sediments sits the layer of loose sediment deposits of light colour (SU2, Munsell pale brown 2.5Y 7.3). The main Pleistocene stratigraphic unit (SU4) consists of relatively homogeneous deposits of yellowish brown colour (Munsell 10YR 5/8) with a diffuse boundary between the lower and upper parts of this unit. A couple of other Pleistocene stratigraphic units (5, 10) have also been defined, all containing a fair amount of subangular limestone clasts.

Pleistocene levels at DK have provided a relatively large assemblage of knapped stones from a relatively small excavation area. While a more detailed publication of this assemblage is forthcoming, a summary of the analysis is provided here. The raw material is almost exclusively flint of relatively good knapping quality. Nodules of similar looking flint can be found in the riverbed of the Ponorska River at the entrance to the nearby Dubočka Cave and might have been transported by water from primary deposits. While this would indicate a high availability of good quality materials in the immediate vicinity of DK, there are several artefacts (e.g. Fig. 12:14) that are macroscopically identified as the so-called 'Balkan flint', i.e. yellow white-spotted flint that originates in northern Bulgaria, probably from Upper Cretaceous chalk and chalk-like limestones (Campanian and Maastrichtian age) in the Pleven-Nikopol region (cf. Gurova *et al.*, 2016), more than 150 km from DK. The structure of the assemblage ($n = 1578$) is as follows: debitage at 76.2%, tools at 21.2%, cores at 1.26% and other at 1.4%. The debitage ($n = 1202$) comprises flakes (43.4%), blades (1.4%), bladelets (3.1%), core trimming elements (8.1%), chips (39.7%) and chunks (4.3%). Among tools ($n = 356$, Figs. 11 and 12) retouched flakes dominate (34.1%), followed by denticulates (15.3%), endscrapers (10.8%), notches (7.5%), scrapers (6.6%), retouched blades (4.2%), borers (3.3%), composite tools (3%), points (1.5%), retouched bladelets (1.2%) and retouched core trimming (1.2%), as well as backed bladelets, limaces, backed blades, geometrics (the last four categories all below 1%), and other (9.4%). There are 24 cores, among which are one centripetal core (4.1%) (Fig. 12:22), four Levallois cores (16.2%) (Fig. 12:23–26), irregular multiple platform cores (8.3%), one unpatterned multiple platform core (4.1%), one single platform core (4.1%), core/tools (8.3%) and residual cores (37.5%), all characterised by a very high level of exploitation. Most of the flint assemblage appears homogeneous, and the choice of raw materials is noticeably distinct from flint deposited in the Holocene levels. Artefacts are also found more densely in the lowermost levels of the sequence. While the assemblage does contain some UP tool types (endscrapers, borers, points), the character of the assemblage based on various characteristics (reduction strategies, highly reduced/retouched artefacts, Levallois cores and flakes, domination of retouched flakes with thick profiles, denticulates, faceted and gull-wing/*chapeau de gendarme* platforms) can be defined as MP and, by proxy, Neanderthal.

A relatively small Pleistocene faunal assemblage from DK is highly fragmented and taphonomically altered and the full results of the analysis will be published elsewhere. Among the identifiable remains, the dental remains of cave bear *Ursus spelaeus* dominate, and ibex *Capra ibex*, wolf *Canis lupus*, marmot *Marmota marmota*, and various bird remains are also identified in very small numbers.

Materials and methods

Unmanned aerial vehicle landscape mapping

Drawing on the experiences of other projects utilising cost-effective mapping of the landscape in an archaeological context (Verhoeven, 2009; Comer and Harrower, 2013; Casana *et al.*, 2014; Jorayev *et al.*, 2016; Thomas, 2016, and others), the areas surrounding the excavated caves in the Danube Gorges were recorded using an unmanned aerial vehicle and photogrammetric methods were employed to generate 3D and 2D georeferenced outputs. The team used a DJI Phantom 4 Pro Unmanned Aerial Vehicle with a 20 megapixel CMOS sensor for photography and a handheld GPS unit for ground control points recording. The Dubočka cave area was recorded over four days and the TT cave area over

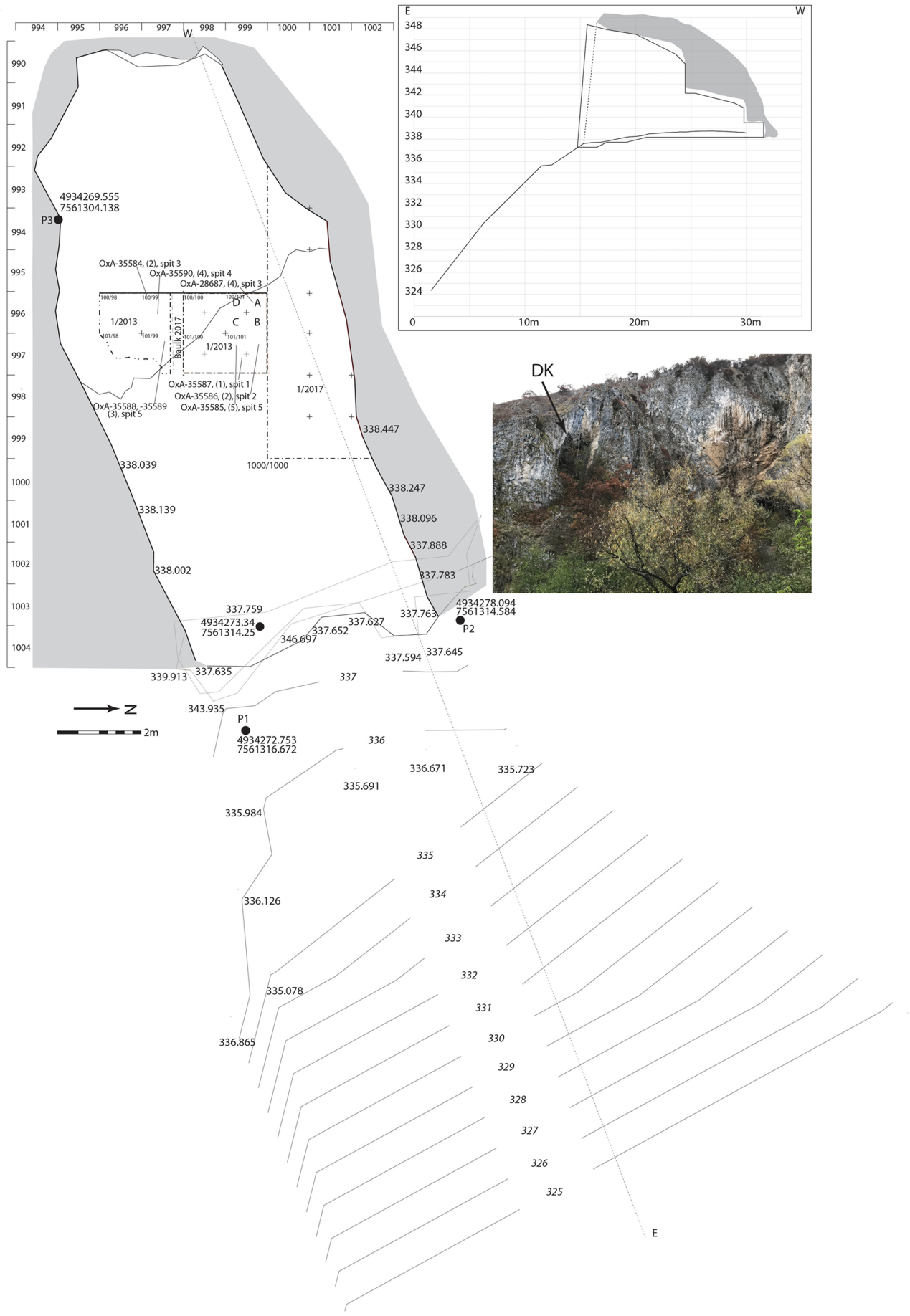

Figure 9. Plan of DK with excavation areas and locations of radiometric samples.

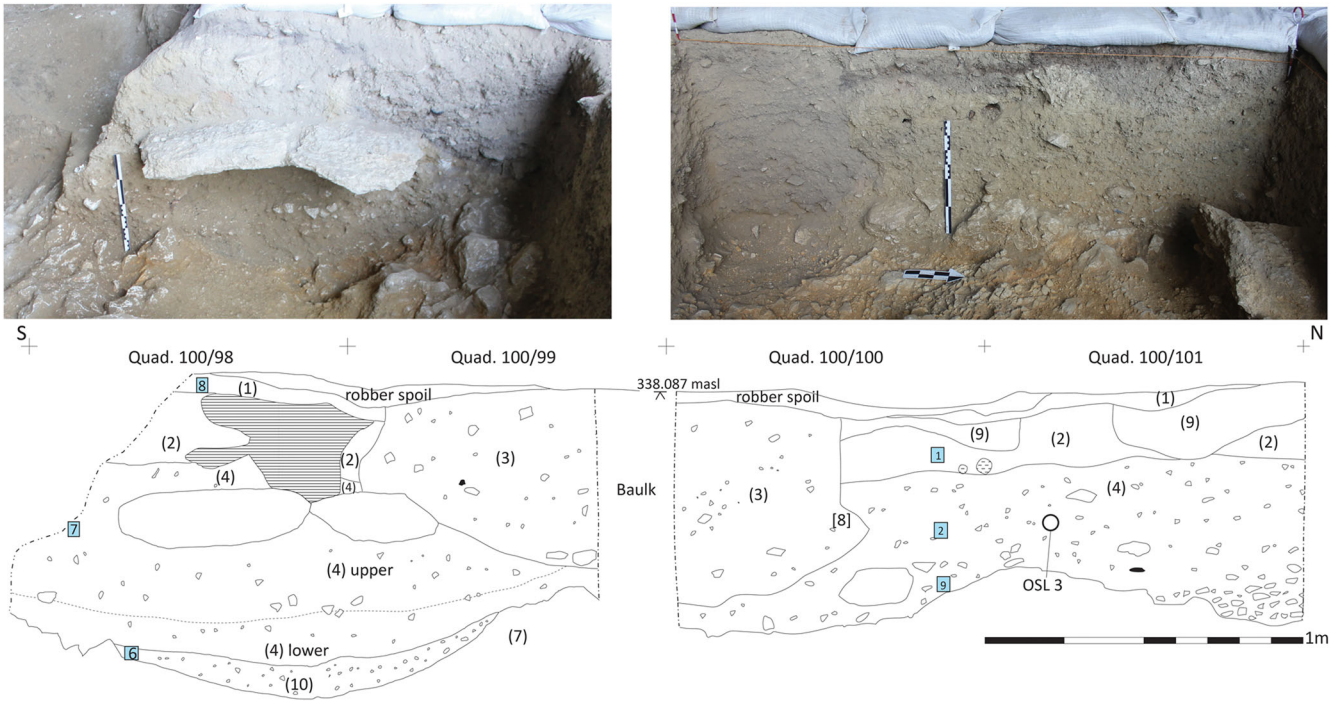

Figure 10. East-facing stratigraphic sections of Trench 1/2013 at DK and locations of micromorphological samples. [Color figure can be viewed at wileyonlinelibrary.com]

two days in late July 2017. Photos were taken at an interval of 3 s at an average altitude of 107 m for the Dubočka cave area, and 115 m for the TT cave area, due to the differences in terrain and vegetation, during manually controlled flights. The datasets were then processed using Agisoft Photoscan (now Agisoft Metashape), Pix4D Mapper and refined using Meshlab (for 3D models) and ArcGIS (for 2D raster datasets) software. The resulting orthomosaics, digital elevation models and 3D models were reconstructed from 2860 images covering an area of 1.9 km^2 and 2442 images covering an area of 0.81 km^2 for DK and TT, respectively. The outputs created were orthomosaics with 2.67 cm and 2.63 cm cell size, digital surface models with 10.7 cm and 6.4 cm cell sizes and 3D models of the areas consisting of 15.6 million faces and 24.9 million faces, respectively.

Sediment micromorphology

In 2008, CAIF took samples from the northern section of Trench 1/2005 (Fig. 5) for micromorphological and associated multi-element and palynological analyses from a Palaeolithic fireplace area and uppermost late prehistoric levels at TT. The soil thin-section samples (Table 1) were prepared using the methodology of Murphy (1986) and described using the accepted terminology of Bullock *et al.* (1985) and Stoops (2003). The geochemical samples were processed using the ICP-AES multi-element analysis process by Als Chemex (www.alschemex.com; 35 element aqua regia ICP-AES, method ICP-41).

In 2017, KG took additional micromorphological samples at TT (Fig. 6) and DK (Fig. 10) on profiles brought into light during previous excavations. This time, 11 undisturbed sediment monoliths for thin-section preparation were collected from TT and eight from DK (Tables 2 and 3). Samples for micromorphological analysis were collected from the profiles, approximately one per unit, or at the boundary between units to observe the boundary morphology. The monoliths were air-dried at 30°C in a ventilated oven until dry. The thin sections were cut by a diamond disc and ground to 30 μm by corundum abrasive powders. The size of all slides is 90 × 55 mm. Thin sections were observed with a standard petrographic microscope at magnifications ranging from 4× to 40× under plane-polarised light (PPL), cross-polarised light (XPL) and oblique-incident light. The descriptions follow the guidelines proposed by Stoops (2003), Bullock *et al.* (1985) and Stoops *et al.* (2010).

Cryptotephra investigations

In June 2010, sediment samples for distal cryptotephra analyses were collected from prepared stratigraphic sections at TT. Sampling involved collection of 20–30 g of *in situ* sediment at 2 cm consecutive and contiguous intervals along continuous vertical profiles. Tephra Column 1 (west-facing section of quadrant 3/28, Trench 1/2005) yielded 30 samples spanning stratigraphic units 201–209 (0.20–0.80 m depth below surface) (Fig. 6). Tephra Column 2 (north-facing section of quadrants 5/22–5/23 boundary, Trench 3/2008) produced 55 samples from units 217–220 (0.10–1.20 m depth below surface). All samples were identified with reference to the site datum and other relevant provenience information.

In the laboratory, cryptotephra searches were carried out in two stages: first at low (6–8 cm) depth resolution, by amalgamation of sub-samples from 3–4 adjacent sediment bags; then where tephra shards were found at this resolution, the individual 2 cm bag samples were processed again to further pinpoint the sediment depth containing the tephra layer. At all stages, samples were processed using the non-destructive density separation method described in Blockley *et al.* (2005). This method concentrates the sediment fraction most likely to contain volcanic glass shards according to grain size and density. The resultant residue was examined under a high-powered polarised microscope and the number of tephra glass shards was counted. Shard counts for the 2 cm depth samples were quantified per gram of dry sediment (s/g).

Individual tephra glass shards were picked out by hand and mounted onto an epoxy resin stub for compositional analysis. Major and minor element oxide concentrations (Table 4) were

FIGURE 11 Continued.

measured on the JEOL JXA8600 electron microscope in the Research Laboratory for Archaeology and the History of Art, University of Oxford (15 kV accelerating voltage, 6 nA beam current, 10 μm defocused beam). Trace element concentrations (Table 5) were measured by laser ablation inductively coupled plasma mass spectroscopy (LA-ICP-MS), using the Agilent 7500 ICP-MS coupled to a 193 nm Resonetics ArF eximer laser ablation system in the Department of Earth Sciences, Royal Holloway University of London (instrumental conditions followed Tomlinson *et al.*, 2010: 5 Hz repetition rate, 40 s sample/gas blank count, 25 μm spot size, NIST 612 calibration standard, ^{29}Si internal standard element). Secondary standard glasses were run alongside all tephra analyses to monitor instrumental precision and accuracy.

Microscopic examination of cutmarks on bones

A select number of bone specimens have undergone a microscopic inspection by means of a Zeiss Axio Zoom stereomicroscope (magnification from 10× and 178×) aimed at recognising anthropic traces related to butchery, namely cutmarks, distinguishing them from non-anthropic modifications (e.g. carnivore and rodent gnaw marks, weathering, root etching and signs of fungal activity), which can mimic human traces on bones (Behrensmeyer, 1978; Shipman, 1981; Fisher, 1995; Lyman, 1994). Archaeological cutmarks were identified through comparison with an experimental reference collection at the DANTE – Diet and Ancient Technology laboratory of Sapienza University of Rome and following criteria widely accepted in literature (Binford, 1981; Blumenschine *et al.*, 1996; Fernández-Jalvo *et al.*, 1999).

AMS dates and stable isotope analyses

AMS dates were processed at the Oxford Radiocarbon Accelerator Unit (ORAU), Oxford University, in 2007 (four measurements from TT), 2013 (one measurement from DK) and 2017 (nine measurements from DK and 11 measurements from TT) (Table 6) using collagen extraction (Law and Hedges 1989), followed by the revised gelatinisation and filtration protocol described by Bronk Ramsey *et al.* (2004a), and dated by AMS as outlined in Bronk Ramsey *et al.* (2004b). One bone sample (AA-63887) was processed in the NSF Arizona AMS facility in 2004.

In total, 14 animal bone specimens from the Middle and Upper Palaeolithic levels of TT were analysed for δ^{13}C and δ^{15}N to provide insights into past environmental conditions and animal habitats at the site (Table 7). Collagen was extracted and analysed at the Dorothy Garrod Laboratory for stable isotope analysis at the University of Cambridge following the procedure outlined in Privat, *et al.* (2002). Samples were analysed using an automated elemental analyser (Costech Analytical, Valencia, CA, USA) coupled in continuous-flow mode to a Thermo Finnigan MAT253 isotope ratio mass spectrometer (Thermo Fisher Scientific, Bremen, Germany) at the Godwin Laboratory, Department of Earth Sciences, University of Cambridge (Cambridge, UK). Carbon and nitrogen results are reported using the delta scale in ‰ relative to internationally accepted standards VPDB and AIR, respectively. Based on replicate analyses of international (IAEA: caffeine and glutamic acid-USGS-40) and in-house laboratory standards (nylon, alanine and bovine liver standards) the precision is better than ±0.2‰ for both δ^{13}C and δ^{15}N values. All but one specimen (TAB12) yielded results within the range of atomic C:N ratios (2.9 to 3.6) that indicate suitably preserved collagen and are thus included in the discussion.

In addition, AMS burn stable isotope values are reported in this paper (Table 6), although these values were not run using a wide range of stable isotope standards and the three-point calibration normally used when specifically measuring C and N isotopes. Instead, only the Oxford lab Alanine stable isotope standard was used (P. Ditchfield, pers. comm). Thus, the AMS burn stable isotope values provide only indicative values and it is problematic to report them alongside the values specifically obtained using the three-point calibration standard (Szpak *et al.*, 2017), even though the differences that the three-point calibration would make would probably be relatively small – perhaps a few tenths of a per mil (P. Ditchfield, pers. comm). In the future, we intend to remeasure all collagen leftovers from AMS-dated specimens specifically for C and N isotopes. For the moment, in the discussion of stable isotope values we briefly discuss AMS burn indicative stable isotope values from TT ($n = 17$) and DK ($n = 4$), which were all made at the ORAU and have ZooMS identifications, in order to understand how comparable these values are with those specifically measured for C and N isotopes. All these values come from directly dated specimens and provide a good chronological control, and they all have acceptable C:N ratios (2.8 to 3.3) (Table 6).

OSL dating

In November 2019, in total, six samples for OSL dating were collected from homogeneous sedimentary units of exposed and freshly cleaned sections of TT (Fig. 6) and DK (Fig. 10) (three from each site) using metal tubes with caps. Additional dosimetry samples of *c.* 30 g were also taken from the sampled units (Table 8). OSL measurements of sand-sized (180–255 μm) quartz mineral grains were extracted from the inner, light-shielded parts of three OSL samples collected at each site. Standard preparation techniques were applied under low intensity light emitting diode (LED) laboratory lighting (peak emission at 594 nm) and included wet sieving, HCl (10%) treatment to remove carbonates, 30% H_2O_2 treatment to remove organic matter and HF (48%) etching to remove the outer (~10 nm) rind of quartz grains affected by alpha irradiation and to dissolve feldspathic minerals. Heavy minerals were removed by density gradient separation using a liquid solution of sodium polytungstate (delta = 2.65 gcm^{-3}) followed by renewed rinsing in HCl (10%) to eliminate potential fluorite contaminants with a final cleaning in demineralised water.

Figure 11. A selection of knapped stone artefacts from Pleistocene stratigraphic units at DK; 1: retouched flake (SU4.x6, quad. 101/100/A, spit 5); 2: scraper (SU4.x1, quad. 101/98, spit 4); 3: retouched blade (SU4, quad. 101/100/D, spit 5); 4: retouched blade (SU2, quad. 100/101/D, spit 3); 5: scraper (SU4.x10, quad. 100/99/B, spit 5); 6: denticulate (SU4.x3, quad. 101/99, spit 4); 7: endscraper (SU4, quad. 100/99, spit 4); 8: retouched flake (SU4, quad. 101/100/D, spit 5); 9: retouched chip (SU4, quad. 101/99/D, spit 5); 10: point (SU4, quad. 100/101/A, spit 3); 11: scraper+truncation (SU4, quad. 100/101/A, spit 5); 12: denticulate (SU2, quad. 100/99, spit 2); 13. denticulate (SU4, quad. 100/101/D, spit 5); 14: point (SU5, quad. 101/101/A, spit 5); 15: truncation (SU4, quad. 101/99/D, spit 5); 16: retouched flake (SU4.x4, quad. 101/100/D, spit 5); 17: convergent scraper (SU4.x28, quad. 100/98/A, spit 6); 18: point (SU4.x15, quad. 100/101/D, spit 6); 19: scraper (SU4, 100/98/A spit 7); 20: denticulate (SU4.x17, quad. 100/98/D, spit 4); 21: sidescraper (SU4.x1, quad. 101/101/A, spit 6); 22: retouched flake (SU10.x2, quad. 100/98/D, spit 8); 23: endscraper (SU4.x18, quad. 101/101/A, spit 6); 24: scraper (SU4, quad. 100/98/B, spit 6); 25: retouched flake (SU4.x39, quad. 101/98/B, spit 7); 26: borer (SU4.x41, quad. 101/98/B, spit 7); 27: scraper (SU4.x35, quad. 100/98/A, spit 7); 28: truncation (SU3, quad. 101/100, spit 2); 29: retouched flake (SU4.x34, quad. 100/98/B, spit 7).

Figure 12. A selection of knapped stone artefacts from Pleistocene stratigraphic units at DK. 1: retouched blade (SU4, quad. 100/98/A, spit 7); 2: retouched blade (SU4.x32, quad. 101/98/B, spit 7); 3: retouched flake (SU4, quad. 100/98/C, spit 7); 4: denticulate (SU4, quad. 100/98/A, spit 7); 5: convergent scraper (SU4.x32, quad. 101/98/B, spit 7); 6: retouched blade (SU4.x25, quad. 101/99/D, spit 6); 7: retouched flake (SU4.x45, quad. 100/98/B, spit 8); 8: retouched blade (SU3, quad. 100/99, spit 3); 9. truncation (SU4.x27, quad. 101/99/D, spit 6); 10: scraper, yellow white-spotted flint (SU4.x43, quad. 101/98/C, spit 7); 11: retouched flake (SU4, quad. 100/98/A, spit 7); 12: retouched flake (SU4.x34, quad. 100/98/B, spit 7); 13: convergent scraper (SU4.x38, quad. 100/98/C, spit 7); 14: retouched flake (SU4.x33, quad. 101/98/B, spit 7); 15: retouched flake (SU4.x5, 100/98/A spit 5); 16: scraper (SU4, quad. 100/98/A, spit 7); 17: endscraper (SU4.x44, quad. 101/98/B, spit 8); 18: retouched flake (SU4, quad. 100/98/C, spit 7); 19: retouched blade (SU4, quad. 101/98/B, spit 5); 20: convergent scraper (SU4, quad. 100/98/A, spit 7); 21: Levallois point (spoil, bag 65); 22: centripetal core (SU4, quad. 100/98/A, spit 7); 23: Levallois core (SU4, quad. 100/98/A, spit 6); 24: Levallois core (SU4.x23, quad. 101/99, spit 6); 25: Levallois core (SU4.x59, quad. 996/997, spit 19); 26: Levallois core (SU4.x22, quad. 101/101/C, spit 6). [Color figure can be viewed at wileyonlinelibrary.com]

Table 1. Selected multi-element analysis results from TT on samples taken from Trench 1/2005.

Sample	Depth from the surface	Al(%)	Ba (ppm)	Ca(%)	Fe(%)	Mg(%)	Mn (ppm)	P(ppm)
1	5–12 cm	0.33	330	20.8	0.33	1.43	1340	>10 000
2	73–85 cm	1.63	100	4.74	1.82	0.34	180	7240
3	84–92 cm	1.91	170	5.84	1.84	0.36	335	>10 000

Dried quartz grains were mounted as multigrain aliquots on aluminium discs with a 2–3 mm spot of silicon oil adhesive (Viscasil 60 000).

OSL measurements were performed in an automated *Lexsyg-Smart* luminescence reader (Richter *et al.*, 2015) manufactured by Freiberg Instruments (Germany) using a single-aliquot regenerative-dose post-IR green OSL measurement protocol (Murray and Wintle, 2000; Banerjee *et al.*, 2001; Wallinga *et al.*, 2002; Wintle and Murray 2006). The instrument was fitted with a ^{90}Sr-^{90}Y ceramic disc β-source providing an activity of ~1.85 GBq and delivering circa 0.11 Gy/s^{-1} to coarse grains (180–255 µm). The source was calibrated against a gamma-irradiated Risø National Laboratory standard (Hansen *et al.*, 2015) from Denmark. For optical excitation, an OSL head unit fitted with 10 green LEDs (emitting at 525 ± 20 nm; max. power 80 mW/cm^2) and 10 infrared LEDs (emitting at 850 ± 20 nm; max. power 300 mW/cm^2) was used. The quartz ultraviolet emission signal at 375 nm was detected using a combination of Hoya U340 and Delta BP 365/50EX optical filters mounted in front of a 25 mm head-on Hamamatsu bi-alkaline cathode photomultiplier tube (model H7360-02; 280–650 nm with peak sensitivity at 420 nm and ~27% quantum efficiency). To detect the presence of potential feldspar contaminants, the 410 nm feldspar emission signal was also detected using a filter combination set comprising a Brightline HC414/46 and a Schott BG 39.

The recorded data was analysed with the Analyst (version 4.57) software developed by Duller (2015) and the weighted mean equivalent dose (De) was calculated using the *Luminescence* package (version 0.9.8) developed by Kreutzer *et al.* (2012) for the statistical programming language *R*. The concentrations of radioactive elements (potassium, rubidium, thorium and uranium) were determined by elemental analysis using ICP-MS/AES and converted to dose rates and luminescence age estimates using the conversion factors of Guérin *et al.* (2011) and the *DRAC* software (v1.02) developed by Durcan *et al.* (2015). The contribution of cosmic radiation to the total dose rate was calculated as a function of latitude, altitude and burial depth, based on data by Prescott and Hutton (1994) and assuming an average overburden density of 1.9 gcm^{-3} and a thickness of 15 ± 5 m for the overlying cave bedrock. In the absence of direct *in situ* gamma-ray spectrometry measurements and in order to achieve the best estimate for the gamma dose rate contribution, layer-to-layer variations in the radioactivity were taken into account by scaling the gamma dose rate as originally proposed by Aitken (1985) and using the *R* function *scale gamma_dose* recently developed by Riedesel *et al.* (2020).

Zooarchaeology by mass spectrometry

Collagen peptide mass fingerprinting analysis, also known as ZooMS (Buckley *et al.*, 2009; Collins *et al.*, 2010), was carried out following the approach published by Buckley *et al.* (2009; see also van der Sluis *et al.*, 2014). In brief, this involved the overnight demineralisation of bone samples in 0.6 M hydrochloric acid, followed by gelatinisation of the acid-insoluble bone residue in 50 mM ammonium bicarbonate at 65°C. The supernatant from this step was digested with sequencing-grade trypsin (Promega, UK) overnight at 37°C, and acidified with 5% trifluoroacetic acid. Then, 0.5 µL of the sample solution was co-crystallised with 0.5 µL of α-cyano-4-hydroxycinnamic acid matrix solution on a Bruker ground steel matrix-assisted laser desorption/ionisation time-of-flight (MALDI TOF) target plate. Samples were analysed using a Bruker UltrafleXtreme mass spectrometer with a frequency-tripled Nd:YAG laser at the Department of Chemistry, Columbia University in the City of New York, USA, with 2000 laser shots acquired over the m/z range 800–3700. Spectra were searched manually for taxonomically informative markers through comparison with the set published by Buckley (2016), Buckley *et al.* (2009, 2017), and Welker *et al.* (2015). All raw spectral file data are available at http://doi.org/10.5281/zenodo.5028649.

Results

TT – stratigraphy and micromorphology

The sampled section on the northern section of Trench 1/2005, beyond the area of roof fall karst boulders in the entranceway (Fig. 4), revealed the following stratigraphic sequence:

	laminated grey/black fine charcoal, ash and dung of late prehistoric periods; spot-sampled for micromorphology
0–10 cm	across this layer boundary;
10–73 cm	fine (<2 cm), sub-rounded to sub-angular karst fragments in a yellowish brown calcitic silt;
73–93 cm	small fireplace feature inset between two large karst blocks infilled with reddish brown calcitic silt and included fine charcoal; two spot samples were taken for micromorphology across the upper and lower boundaries of this feature;
93–118 cm	greyish brown calcareous silt with fine rock fragments (<2 cm);
>118 cm	unexcavated.

The cave sequence suggests that it has received minimal post-depositional disturbance, apart from the solution and deposition of calcium carbonate on the interior cave walls. Three sets of spot samples have been taken for micromorphological and palynological assessment. Only spot sample 1 (TT08/1) from the topmost levels taken to assess pollen preservation produced well-preserved pollen grains, suggesting a broadleaved woodland assemblage with hazel, birch, lime, hop-hornbeam, grass and fern spores, and lots of charcoal. The other two samples were barren. A selection of multi-element results is presented in Table 1. Sample 1 (5–12 cm) exhibits enhanced barium (Ba), manganese (Mn) and phosphorus (P) values. In particular, barium (Ba) may reflect the presence of wood ash (Fleisher and Sulas, 2015; Macphail and Goldberg, 2010; Wattez and Courty, 1987), and the extremely high phosphorus values most probably indicate intensive organic waste accumulation and the possible use of the cave floor by animals (Karkanas and Goldberg, 2010). Similarly, the fireplace deposits also exhibit very high phosphorus values (in samples 2 and 3). The basic

Table 2. Main micromorphological characteristics of the TT sediments. Table abbreviations. Fe – iron; Mn – manganese; AOM: amorphous organic matter. Shape. A: angular; SA: subangular; R: rounded; SR: subrounded. Quantity. Vf: very few; Fw: few; C: common; Fr: frequent; VD: very dominant.

				Coarse material				
Sample	Trench and context	Microstructure	c/f related distribution pattern	Rock fragments	Minerals	Organic and inorganic of biological origin	Micromass	Pedofeatures
TT7	1/2005, 1/2008 201 top	Massive with Fw channels			Fw quartz grains, Vf muskovite flakes	Fr AOM, Fr dark brown tissue, cells and punctuations, VD calcite spherulites, Fw bone fragments, C phytoliths		Fe/Mn nodules
TT6	1/2005, 1/2008 201 bottom	Massive with Fw channels	Open porphyric		C A to SA quartz, C muscovite flakes, C phosphates	C bone fragments, Vf mollusc shells, VD spherulites, C wood ash aggregates	spherulitic ashy	
TT8	1/2005, 1/2008 dark red	Granular and crumb	Single-spaced to open porphyric	C SA limestone frgs,	Fr A quartz, C muscovite flakes, C feldspars, C calcite, Fr R phosphates	Fr AMO and tissue, C sand-sized bone frgs, C wood ash aggregates, Fw ruminant dung frgs		C clay aggregates (pedorelic)
TT5	1/2005, 1/2008 203	Crumb, Fr channels	Single- to double-spaced porphyric	Fw SA limestone frgs	D A to SR quartz, Fr muscovite flakes, Fw biotite, Fw SA feldspars, Vf R glauconite, Fw R phosphates, SA calcite	D phytoliths, Fw bone frgs, Vf charcoal frgs	Calcitic micromass	Fr weekly to strongly impregnated Fe/Mn nodules
TT4	1/2005, 1/2008 207	Crumb	Open porphyric		Fr A to SR quartz, Fw muscovite flakes, Fw biotite, Fw spiritic calcite	VD phytoliths, C bone frgs	Granostriated b-fabric; sometimes opaque	Fw Link cappings, C dusty clay infillings, Fw clay coatings
TT3	1/2005, 1/2008 209	Angular blocky with C channels	Open porphyric		D A to SR quartz, C muscovite flakes, Vf SA feldspars	Vf bone frgs	opaque	C Fe/Mn nodules
TT2	1/2005, 1/2008 219?	Angular blocky	Single-spaced to double porphyric	Fr A to SR limestone frgs	Fr A to SR quartz, C muscovite flakes, C A to SA sparitic calcite, Fw biotite, Fw SA feldspars, Fw phosphates	Fw AMO, Fw bone frgs		C Fe/Mn nodules
TT10/2.1	1/2005, 1/2008 219?	Subangular blocky with Fr channels	Single-spaced to open porphyric		D SA to SR quartz, Fw SA feldspars, Fr muscovite flakes		Clay silt micromass with stipple speckled b-fabric	Fr Fe/Mn nodules, Vf clay papules, Fw calcite infillings
TT1		Subangular blocky and	Single- to double-	Fr A to SA			Calcitic and clay	

(*Continued*)

Table 2. (*Continued*)

Sample	Trench and context	Microstructure	c/f related distribution pattern	Coarse material		Organic and inorganic of biological origin	Micromass	Pedofeatures
				Rock fragments	Minerals			
	1/2005, 1/2008 219?	granular	spaced porphyric	limestone frgs	Fr A to SA sparitic calcite, Fr A to SR quartz, Fw SA feldspars, C muscovite flakes			C Fe/Mn nodules, Fw clay papules
TT11	trench at the entrance of the cave (201)	Crumb	Open porphyric		C SA to SR quartz, C muscovite flakes, C SA to SR calcite	C tissue, Fw bones, C spherulites at the top	Spherulitic at the top, Calcitic at the bottom	
TT12	trench at the entrance of the cave (226)	Granular (pellicular)	Open porphyric	C R to SR limestone frgs	Fr A to SR quarz, C muscovite flakes, C SA ti SR calcite, Fw SA feldspars, C R phospates, Fw biotite	Fw bone frgs	calcitic crystallitic, granostriated b-fabric	cryoturbation-coated grains C Fe/Mn nodules, C calcite hypocoatings

thin-section descriptions are given below, with more detailed descriptions in Appendix 1.

Sample 1 (5–12 cm) was taken through the uppermost late prehistoric fill layer of the cave and exhibits five fabric units. The basal fabric unit 1 (*c.* 12–17 cm) is a finely aggregated, very porous (25%) deposit of micritic and amorphous calcium carbonate with a minor amount of fine sand and pure clay 'staining' the calcium carbonate (Fig. 13a). On its upper surface are three irregular sized and shaped fragments of amorphous sesquioxide (iron oxides and hydroxides) impregnated and replaced organic matter (fabric unit 2; *c.* 12–13 cm). Fabric unit 3 above (*c.* 11–12 cm) is composed of small irregular aggregates of organic matter and plant tissue, all amorphous iron oxide replaced and bioturbated, and micritic calcium carbonate in a 1 cm thick lens. Overlying this is fabric unit 4 (*c.* 9.5–11 cm), which is composed of a dense matrix of amorphous iron oxide replaced organic matter with a horizontal orientation in a 1–1.5 cm thick lens, although it too has been bioturbated (Fig. 13b). In the upper fabric unit 5 (*c.* 5–9.5 cm), there are alternating fine laminae of orangey-brown micrite and amorphous organic matter, and dark brown to black, finely comminuted organic matter and micrite in an excremental matrix (Fig. 13c). This upper unit becomes much disturbed by roots and soil fauna with many large, infilled channels evident.

Overlying weathered karst material derived from the erosion of the cave itself, are a series of superimposed horizons. The first is a discontinuous zone of amorphous sesquioxide replaced organic matter indicative of oxidised and iron replaced organic matter. This appears to be much truncated remnants, possibly a result of water action or human disturbance. Above this is a centimetre-thick zone of plant tissue which is largely replaced by amorphous iron and much bioturbated by the soil fauna. Above this is a second layer of organic matter, very dense, all replaced by amorphous iron oxides and with alternating laminae evident. But what these two organic horizons represent is unclear. It could be byre bedding material, but there is a singular lack of any phosphatic features or phytoliths, which would be expected (Karkanas and Goldberg, 2010: 602), and no micro-artefactual debris typical of people living in the cave is incorporated in this horizon. Perhaps it just represents the storage or accumulation of plant material.

Samples 2 (73–85 cm) and 3 (84–92 cm) were taken through the Late Pleistocene-age fireplace feature. Sample 2 is mainly comprised of calcitic ash and fine bone fragments (Fig. 13d). In addition, at the base of sample 2, there is a fine linear zone of calcitic silt crusts with a fine carbonised dust at a clear planar boundary (Fig. 13e) with the underlying micritic clay or the underlying weathered karst floor of the cave as observed in the base of sample 2 and in sample 3. The calcitic silt crust probably represents a trampled floor containing hearth rake-out material on the weathered natural geology of the cave. Sample 3 exhibited a pellety to aggregated calcitic silt fabric, with abundant phosphatised, very fine sand-size bone fragments and included common very fine charcoal dust and/or plant tissue fragments throughout (Fig. 13f).

The main micromorphological characteristics of the cave sediments examined in 2017 are summarised in Table 2. Field description and micromorphological observations of the most representative west-facing section of Trench 1/2005–1/2008 (Fig. 6) are as follows:

0–10 cm: The surface context 201 (white and grey at the top) is an approximately 10 cm thick layer of ash with lateral variations – it spans from 14 cm in the southern part of the section, and it thins out towards the north to *c.* 2 cm. It varies from laminated ash and burnt organic matter and charcoal (at

Table 3. Main micromorphological characteristics of the DK sediments.Table abbreviations. Fe – iron; Mn – manganese; AOM: amorphous organic matter. Shape. A: angular; SA: subangular; R: rounded; SR: subrounded. Quantity. Vf: very few; Fw: few; C: common; Fr: frequent.

				Coarse material				
Sample	Trench and context	Microstructure	c/f related distribution pattern	Rock fragments	Minerals	Organic and inorganic of biological origin	Micromass	Pedofeatures
DB-K/8/1	1/2013 1	Crumb and granular	Open porphyric	C SA to SR limestone fragments	Fr SA to SR quartz grains, C muscovite flakes, C calcite, Fw SA feldspars, Fw biotite	C AOM Fw bone fragments	greyish brown calcitic crystallithic	Fw silt cappings, Fw carnivore coprolites (possibly hyena), C fresh roots, Fw sheep/goat excrements, Fr moderately impregnated orthic aggregate iron hydroxide nodules
DB-K/7/4	1/2013 4 (upper part)	Angular blocky to vughy	Open porphyric	Fr SA to SR limestone fragments, C quartz aggregates (quartzite)	C quartz grains, Fr SR Feldspars Fr muscovite flakes C Calcite A to SA Vf R glauconite	Fr sand-sized bone fragments C AOM	yellowish brown granostriated	ice lensing (tamo di nisu reworked by soil fauna)
DB-K/6/10	1/2013 10	Pellicular grain and crumb	Single-spaced to open porphyric	Fr SA to SR limestone fragments, Vf A flint fragments	Fr quartz grains, C A to SA calcite, C muskovite flakes, Fw SR feldspars, Vf amphibole	Fr sand-sized bone frgs Vf charcoal frgm	yellowish brown granostriated b-fabric	silt capping phosphates-carnivore coprolite C C Fe nodule
DB-K/5/2	1/2013 2	Crumb	Single- to double-spaced porphyric	Fr SA to SR limestone frgs	C SA to R calcite, C SA to SR quartz grains, C muskovite flakes, Vf SA feldpars, Vf R glauconite, Vf A Pyroxene	C sand-sized bone fragments, Vf shell frgs, Vf AOM, Vf eggshell fragments	greyish brown calcitic crystallithic	Vf carnivore coprolite ice lensing Fw Fe nodules
DB-K/4/4	1/2013 4	Crumb	Single- to double-spaced porphyric	Fr A to SR limestone fragments	FR muscovite flakes, FR SR quartz grains, C SA to SR calicite, Fw A feldspar	FR sand-sized bone fragments	greyish brown calcitic crystallithic	Fr Fe nodules and coatings Vf carnivore coprolites
DB-K/3/ 5-9	1/2013 5-9	Crumb and channel	Double-spaced to open porphyric	FR A to SR limestone fragments	C muskovite flakes, C A to SR quartz grains, C A to SA feldspars, C SA to SR calcite	Fw bone fragments	greyish brown calcitic crystallithic	C R red clay pedorelics (with mostly quartz skeleton) C calcitic hypocoatings
DB-K/2/4	1/2013 4	Crumb	Single-spaced to open porphyric	Fw A flint fragments, Fr limestone fragments	Fr muscovite flakes, Fr SR quartz grains, C SA calcite, FW A feldspars	Fr sand-sized bone fragments	granostriated b-fabric	C carnivore coprolites C silt cappings in lower part of the thin section ice lensing C Fe nodules
DB-K/9/ 4 L (10)	1/2013 10	Pellicular grain and crumb	Single-spaced porphyric	Fr SA to SR limestone fragments	Fr SA to R quartz grains, C SR feldspars, C SA calcite, C muskovite flakes	Fr sand-sized bone fragments	granostriated b-fabric	C carnivore coprolites Fw silty clay coatings

Table 4. Major and minor element oxide wt% compositions of cryptotephra glass shards extracted from Tephra T1 and T2 (Cryptotephra column 1) at TT. Element oxide concentrations are normalised to anhydrous compositions, with original analytical totals shown. *Runfile* links to secondary standard analyses for the two WDS-EPMA sessions used, which are presented in SI Appendix 2.

	SiO_2	TiO_2	Al_2O_3	FeOt	MnO	MgO	CaO	Na_2O	K_2O	P_2O_5	Cl	Total	*runfile*
T1_Col1:207(46–50 cm)													
T1	77.26	0.03	12.68	0.95	0.00	0.01	0.67	2.98	5.29	0.02	0.11	96.73	*b*
T1	77.19	0.02	12.77	0.94	0.09	0.01	0.75	2.79	5.32	0.04	0.09	96.33	*a*
T2_Col1:203/207(30–32 cm)													
T2	61.21	0.41	18.63	2.78	0.22	0.30	1.64	6.81	7.09	0.03	0.88	99.82	*a*
T2	61.63	0.43	18.47	2.65	0.24	0.30	1.66	6.70	7.02	0.03	0.86	99.17	*a*
T2	61.00	0.40	18.44	2.86	0.26	0.30	1.80	6.90	7.07	0.06	0.91	99.06	*a*
T2	61.89	0.42	18.64	2.80	0.16	0.30	1.73	6.19	7.00	0.05	0.82	98.74	*a*
T2	61.05	0.45	18.81	2.81	0.26	0.28	1.73	6.49	7.23	0.03	0.86	98.73	*b*
T2	61.40	0.34	18.69	2.87	0.16	0.34	1.63	6.38	7.19	0.04	0.94	98.45	*a*
T2	61.36	0.41	18.71	2.80	0.24	0.32	1.71	6.45	7.05	0.06	0.91	98.40	*b*
T2	60.22	0.39	18.45	3.86	0.14	0.79	2.88	3.69	8.78	0.16	0.63	98.26	*b*
T2	61.24	0.46	18.80	2.94	0.25	0.30	1.67	6.28	7.18	0.04	0.84	98.23	*b*
T2	60.66	0.34	18.78	3.19	0.16	0.33	1.76	6.51	7.28	0.08	0.90	98.20	*a*
T2	61.40	0.40	18.51	2.96	0.22	0.32	1.66	6.57	6.98	0.08	0.88	98.18	*b*
T2	60.88	0.47	18.74	2.78	0.21	0.29	1.69	6.63	7.42	0.05	0.84	98.14	*a*
T2	61.64	0.37	18.74	3.44	0.10	0.78	2.67	4.45	7.26	0.18	0.37	98.05	*b*
T2	60.96	0.43	18.55	2.89	0.26	0.33	1.73	6.84	7.09	0.05	0.87	97.74	*a*
T2	61.42	0.40	18.66	3.09	0.18	0.32	1.68	6.13	7.27	0.04	0.81	97.53	*a*
T2	61.30	0.43	18.28	3.47	0.08	0.62	2.70	3.56	8.77	0.12	0.66	97.42	*a*
T2	60.95	0.48	18.80	2.85	0.24	0.29	1.68	6.42	7.28	0.07	0.92	97.28	*a*
T2	61.27	0.42	18.71	2.75	0.27	0.33	1.73	6.32	7.26	0.04	0.89	96.74	*a*
T2	61.44	0.46	19.06	2.86	0.28	0.29	1.67	5.91	7.16	0.05	0.82	96.45	*b*
T2	61.10	0.37	18.72	2.87	0.27	0.31	1.68	5.81	7.98	0.04	0.85	96.21	*a*
T2	62.44	0.38	18.26	2.92	0.12	0.46	2.18	3.82	8.65	0.08	0.70	96.20	*b*
T2	61.43	0.42	18.66	2.83	0.19	0.29	1.70	6.36	7.18	0.07	0.86	96.11	*a*
T2	62.69	0.35	18.28	2.75	0.10	0.43	2.08	4.26	8.37	0.06	0.63	95.93	*a*
T2	62.41	0.38	18.23	2.98	0.18	0.43	2.13	4.06	8.39	0.10	0.72	95.70	*b*
T2	61.01	0.47	18.71	2.91	0.12	0.29	1.79	6.61	7.26	0.01	0.83	95.58	*a*
T2	61.84	0.44	18.73	2.95	0.21	0.31	1.66	5.93	6.97	0.04	0.92	95.26	*b*
T2	61.40	0.45	18.73	2.98	0.24	0.27	1.59	6.18	7.16	0.08	0.92	95.05	*b*
T2	78.30	0.12	13.52	1.19	0.05	0.21	1.10	2.20	6.17	0.01	0.07	97.14	*b*
T2	77.47	0.14	13.34	1.09	0.09	0.11	1.09	2.60	6.14	0.03	0.07	97.84	*b*

Table 5. Trace element concentrations (ppm) measured in cryptotephra glass shards from Tephra T2 (Cryptotephra column 1) at TT compared with average values for cryptotephra glass shards from proximal outcrops of the Campanian Ignimbrite (after Lowe *et al.*, 2012). Analyses below limits of detection marked with '–'. For secondary standard analyses see SI Appendix 2.

	Rb	Sr	Y	Zr	Nb	Ba	La	Ce	Pr	Nd	Sm	Eu	Gd	Dy	Er	Yb	Lu	Ta	Pb	Th	U
T2_Col1:203/207(30–32 cm)																					
T2	407	18	52	610	107	13	117	225	24	77	15	–	9	9	5	5	–	5	62	50	17
T2	417	22	54	611	108	16	116	228	23	78	14	–	9	8	5	6	–	5	60	44	15
T2	411	20	49	582	111	17	112	214	22	79	12	–	8	9	5	5	–	5	58	43	15
T2	427	22	53	627	116	16	122	233	24	84	13	–	10	9	5	5	–	5	62	48	16
Campanian Ignimbrite average																					
CI	451	42	52	638	117	24	121	225	23	80	14	1	10	9	5	5	1	5	64	49	17

least three pairs of white and black layers with a thin dark grey layer at the top) to a 10 cm thick more homogeneous layer of ash. Thin layers a few centimetres thick of organic matter/Fe oxides are also visible. At microscopic scale, context 201 (white and grey top) exhibits a spherulitic micromass which is clearly the product of cyclical burning of ruminant (probably sheep and/or goat) dung (Brochier *et al.*, 1992; Boschian and Montagnari-Kokelj, 2000). *In situ* breakage of bones and compaction of the layer are indicators of trampling. Precipitation of secondary iron oxides is also observable. At the bottom (10–16 cm), there is a sandy silt reddish lens in the central part of the profile. It represents a mixture of burnt sediment, herbivore dung and wood ash, with common bone fragments. It has been reworked by earthworms and/or other mesofauna.

16–22 cm: Context 203/dark red is a 10–16 cm thick silt loam filling an erosional feature overlying a thin organic/Fe oxides layer. The microstructure is granular and crumb. At microscopic scale, this context is a reworked mixture of wood ash, amorphous organic matter and tissue, bone fragments, clay aggregates and phosphatic material.

22–43 cm: Context 203: millimetre-thick organic/Fe oxide laminations in a greyish yellow sandy silt which fills up the concave erosional feature. At the bottom of the context (203) there are a few limestone fragments that are a centimetre long, with Fe/Mn coatings. Calcitic micromass with very frequent to dominant phytoliths (Fig. 14:1a) and frequent weakly to strongly impregnated Fe hydroxide nodules.

43–60 cm: Context 207 is a sandy silt ashy layer, yellowish brown at the top, grey in the middle and greyish brown at the

Table 6. Radiocarbon measurements from TT and DK caves with contextual and bone chemistry information, and results of ZooMS identification of the analysed specimens.

Sample ID	Spec. ID	Exc. date	Trench	Quadrant	Context/layer	Depth	Orig-mg	Yield%	OxA-	$F^{14}C$	$F^{14}C \pm$
					TT						
Tab-11	x.11 (y = 22.592; x = 5.199)	14/07/08	3/2008	5/22	217/2	90.233	668.02	2.6	35 765	0.07831	0.00122
	x.98 (y = 30.93; x = 2.845)	2009	1/2009	2/30	207/1	91.975	1330	1.5	26 718		
Tab-14	–	12/07/08	3/2008	5/22	200	–	688.1	2.1	35 593	0.04187	0.00108
Tab-04	x.49 (y = 25.407; x = 4.820)	09/07/08	1/2008	4/25	207/2	91.033	781.16	4.1	35 763	0.0286	0.00104
	TT05/43/1	20/08/05	1/2005	3/28 (D)	43	91.75	500	1.5	24 819		
	–	2004	1/2004	C	spit 12	–			AA-63887		
	TT08/207x.78/2 (y = 25.265; x = 4.516)	11/07/08	1/2008	4/25	207	90.984	630	3	24 818		
Tab-01	x.4 (y = 27.394; x = 4.655)	09/07/08	1/2008	4/27	210	91.096	794.07	6.9	35 592	0.01523	0.00103
	TT05/90/36	2005	1/2005	2.5/27 (F)	90	–	620	4.1	23 651		
Tab-34	–	14/07/08	2/2008	E section T. 1/2004	220	–	839.75	6.2	35 768	0.01404	0.00099
	TT05/100/1	2005	1/2005	3/26 (B)	100	–	1330	1.8	16 419		
Tab-08	x.82 (y = 25.750; x = 4.575)	11/07/08	1/2008	4/25	207/4	90.943	862.96	6.5	35 764	0.01062	0.00099
Tab-39	–	13/07/08	1/2008	4/26	218	–	683.05	4.3	35 770	0.00305	0.00097
Tab-03	x.58 (y = 28.161; x = 4.338)	09/07/08	1/2008	4/28	207/3	91.238	803.36	0.8	35 762	0.00051	0.00102
Tab-17	TT 08/211/2	10/07/08	2/2008	4.5/18	211	–	514.05	1.0	35 594	0	0.00115
Tab-13	x.13 (y = 26.59; 3.989)	13/07/08	1/2008	4/26	215/2	90.721	730.1	1.9	35 766	0	0.00101
Tab-13	x.13 (y = 26.59; 3.989)	13/07/08	1/2008	4/26	215/2	90.721	788.87	1.9	35 767	0	0.001
Tab-38	–	09/07/08	2/2008	0	206	–	699.17	4.6	35 769	0	0.00097
					DK						
DK-01	x.9 (y = 996.639; x = 997.578)	20/07/13	1/2013	100/99	(2), spit 3	387.8	110.45	3.4	35 584	0.57424	0.00208
DK-08	0	17/07/13	1/2013	101/101	(1), spit 1	0	777.84	6.6	35 587	0.50963	0.00196
DK-06	0	18/07/13	1/2013	101/101/A	(2), spit 2	0	768.48	1.7	35 586	0.40263	0.00182
	0	19/07/13	1/2013	100/101/A	(4), spit 3		870.0	5.7	28 687		
DK-17	0	23/07/13	1/2013	101/99	(3), spit 5 (cleaning)	0	799.35	5.6	35 588	0.0136	0.00101
DK-17	0	23/07/13	1/2013	101/99	(3), spit 5 (cleaning)	0	834.35	6.3	35 589	0.01424	0.00102
DK-32	0	22/07/13	1/2013	100/99	(4), spit 4	0	641.07	3.7	35 590	0.0136	0.00104
DK-03	0	22/07/13	1/2013	101/101/D	(5), spit 5	0	926.55	2.4	35 585	0.00157	0.00101
DK-39	0	26/07/13	1/2013	100/93/A	(4), spit 8	0	758.62	3.5	35 591	0	0.00099

Sample ID	^{14}C	$^{14}C \pm$	Cal BP 95% confidence	%C	δ13C	δ15N	C:N	Treat.	ZooMS ID	Taxon	Rationale
						TT					
Tab-11	20 460	120	24 990–24 230	41.5	–19.6	3.7	3.2	AF	PT158	*Bos/Bison* sp.	tentative cutmarks
	24 690	190	29 260–28 550	42.9	–18.7	5.0	3.3			*Capra ibex*, mandible	context
Tab-14	25 490	210	30 100–29 230	40.4	–17.1	12.9	2.9	AF	PT159	Canidae	cutmarks
Tab-04	28 550	290	33 710–31 890	42.1	–19.3	4.6	3.2	AF	PT148	Cervidae	cutmarks
	30 850	390	36 080–34 530	43.3	–18.8	7.8	3.2			*Capra ibex* maxilla	context
	31 200	1200	39 400–33 550		–24.5	8.5	–			*Panthera spelaea*, metapodial	species
	33 450	500	39 570–36 910	43.4	–19.8	6.8	3.1		PT100	*Capra ibex*, metapodial	cutmarks
Tab-01	33 600	550	39 830–36 950	38.9	–20.4	2.6	3.0	AF	PT149	Cervidae	cutmarks
	34 200	550	40 580–37 600	45.3	–19.0	7.9	3.2			*Vulpes vulpes*, femur	cutmarks
Tab-34	34 250	550	40 620–37 630	42.4	–19.3	4.8	3.2	AF	PT163	Cervidae	cutmarks
	35 530	360	41 300–39 890	42.0	–19.4	4.8	3.3			*Capra ibex*, horncore	context

(*Continued*)

Table 6. (*Continued*)

Sample ID	^{14}C	^{14}C ±	Cal BP 95% confidence	%C	δ13C	δ15N	C:N	Treat.	ZooMS ID	Taxon	Rationale
Tab-08	36 500	750	42 350–40 260	42.2	–19.4	5.9	3.2	AF	PT156	*Capra* sp.	cutmarks
Tab-39	46 500	2600	52 350–46 720 (68% confidence)	42.6	–20.0	5.1	3.2	AF	PT165	*Capra* sp.	cutmarks
Tab-03	48 000	0	>48 000	41.0	–20.5	4.0	3.3	AF	PT151	Cervidae	cutmarks
Tab-17	48 800	0	>48 800	41.8	–20.1	5.3	3.2	AG	PT160	*Capra* sp.	cutmarks
Tab-13	49 800	0	>49 800	39.5	–22.0	1.6	3.2	AF	PT157	*Ursus* sp.	cutmarks
Tab-13	49 900	0	>49 900	38.1	–22.0	1.5	3.2	AF	PT157	*Ursus* sp.	cutmarks
Tab-38	50 100	0	>50 100	42.1	–19.4	5.5	3.2	AF	PT164	*Capra* sp.	cutmarks
						DK					
DK-01	4456	29	5290–4960	39.7	–22.2	8.0	3.1	AG		*Sus scrofa*, incisor	pendant
DK-08	5415	31	6300–6120	41.7	–25.4	7.3	3.2	AF	DK 9		cutmarks
DK-06	7308	36	8180–8020	40.2	–21.6	7.6	3.1	AF	DK 8	*Sus* sp.	cutmarks
	25 370	200	30 020–29 200	43.9	–19.1	4.5	3.3				cutmarks
DK-17	34 500	600	41 000–37 860	42,0	–23.1	5.6	3.1	AF	DK 11	*Ursus* sp.	tentative cutmarks
DK-17	34 150	600	40 650–37 470	40.3	–23.1	6.5	3.1	AF	DK 11	*Ursus* sp.	tentative cutmarks
DK-32	34 500	600	41 000–37 860	41.6	–20.9	8.3	3.1	AF	DK17	Cervidae	cutmarks
DK-03	45 200	0	>45 200	39.2	–21.1	9.2	3.2	AF			cutmarks
DK-39	50 000	0	>50 000	39.5	–21.1	9.6	2.8	AF	DK 18	*Ursus* sp.	cutmarks

bottom with a few centimetre long limestone clasts. Wavy boundary. Weakly to moderately separated granular microstructure and granostriated b-fabric. A great amount of phytolith-producing plants are present in this context too (Fig. 14:1b). The phytolith-producing plants in contexts 203 and 207 may indicate bedding or stabling accumulation (Karkanas and Goldberg, 2010: 604).

60–67 cm: Context 209 is from *c.* 30 to a few centimetre-thick silt loam sediment.

67–130 cm: Context 219; common *c.* 20 cm – 1.30 m limestone clasts.

i. Top (sample TT2) – silt loam, mixed with (209), unclear boundary.
ii. Middle (sample TT10/2.1) – silt loam (with more clay than the top) 70–80 cm thick sediment with frequent angular to sub-angular limestone clasts a few millimetres long.
iii. Bottom (sample TT 1) – silt loam with few angular to sub-rounded limestone clasts.

In this group of units at microscopic scale, very scanty traces of human activity are observable with only a very few bone fragments and amorphous organic matter.

Trench 2/2008 at the entrance of the cave, north-facing profile:

i. TT11: Top of thin section (sample collected at the top of the profile) – herbivore dung. Lower part of the thin section – silt loam. Calcitic micromass with common organic matter, fresh roots and bones. Reworked layer.
ii. TT12: Weakly to strongly developed granular microstructure with stress features – granostriated b-fabric indicates cryoturbation due to frequent freeze–thaw cycles (Van Vliet-Lanoë, 2010). Rotation of sediment aggregates and consequent formation of down-turned cappings along the surface are also observed (Fig. 14:2).

TT cryptotephra investigations

The occurrence of tephra in Column 1

Figure 15 shows the Column 1 (Figs. 4, 6) results of tephra glass shard counting within sampled stratigraphy in TT. Tephra was found dispersed in varying concentrations above unit 209 (above 0.56 m depth). When investigated at 2 cm resolution, there appear to be two shard accumulation zones, one of up to 342 s/g, at 0.46–0.50 m depth (T1) and another of up to 214 s/g between 0.30–0.32 m depth (T2). Tephra shards were also present at the depths in between these samples, suggesting that fine particles have been reworked within, or into, the sediment sequence over time. The glass shards in both T1 and T2 show a similar range of morphologies. Both samples contain a high number of clear, cuspate shards, characterised by expanded bubble wall structures, then there are also a number of clear, plate-like shards, with either near-triangular or elongated form. In both samples the glass shards (measurement of longest axis) range up to ~200 μm.

Tephra T1: Table 4 shows the composition of two tephra shards analysed by WDS-EMPA following filtering of the data to those analyses with totals >95 weight percentage (wt%) and that showed no evidence of microlite contamination. The tephra glass shards are rhyolitic (Fig. 15), with normalised major and minor element oxide compositions of 77.2 wt% SiO_2, 12.7 wt% Al_2O_3, 5.3 wt% K_2O, ~2.9 wt% Na_2O, 0.9 wt % FeO and 0.7 wt% CaO. The small plate-like shape of the analysed shards prevented successful analysis by LA-ICP-MS.

Tephra T2: 29 tephra shards were successfully analysed by WDS-EMPA and four of these by LA-ICP-MS (Table 5). All except

Table 7. Stable isotope results and quality indicators for animal bone specimens analysed from Tabula Traiana. *value excluded from interpretation due to unacceptable %C, %N and C:N values.

Chronostratigraphic attribution	Sample code	Bone ID	Species	Element	% Yield	$\delta^{13}C$ ‰	$\delta^{15}N$ ‰	%C	%N	C:N
Middle Palaeolithic	TAB01	PTT 08/211x.10	*Cervus elaphus*	Ulna, carpal	9.9	–19.8	4.8	38.3	13.9	3.2
	TAB02	PTT09/219/1	*Cervus elaphus*	Phalanx II	2.6	–20.5	6.0	22.1	7.7	3.3
	TAB05	PTT11/220/2	*Capra ibex*	Metatarsal	11.3	–19.4	6.0	40.5	14.8	3.2
	TAB06	PTT 08/206x.2	*Capra ibex*	Metatarsal	6.1	–19.8	4.4	30.2	10.8	3.3
	TAB07	PTT08/220/4	*Capra ibex*	Calcaneus	4.4	–20.0	6.6	46.1	16.6	3.2
	TAB08	PTT 08/206/4	*Capra ibex*	Phalanx I	5.8	–20.2	3.6	38.7	13.9	3.3
	TAB09	PTT08/219/1	*Capra ibex*	Phalanx II	11.9	–19.4	4.4	45.9	16.8	3.2
	TAB03	PTT 11/210x.16	*Cervus elaphus*	Phalanx I	4.2	–19.6	6.2	34.3	12.3	3.3
	TAB04	PTT 08/215x.5	large carnivore?	Thoracic vertebra	6.5	–18.0	14.2	40.8	14.9	3.2
Upper Palaeolithic	TAB10	PTT 08/207x.52	*Capra ibex*	Metatarsal	6.7	–19.4	3.4	42.7	15.6	3.2
	TAB11	PTT 08/207/20	*Capra ibex*	Metapodial	4.9	–19.6	5.2	35.8	13.2	3.2
	TAB12*	PTT 08/217/7	*Capra ibex*	Phalanx I	1.9	–21.1	4.6	9.5	3.1	3.6
	TAB13	PTT 08/217/36	*Capra ibex*	Phalanx I	5.6	–19.1	5.3	43.8	16.0	3.2
	TAB14	PTT 08/215/4	*Capra ibex*	Phalanx I	4.0	–18.9	7.4	38.1	13.7	3.

for two of the tephra shards analysed were on curvilinear bubble wall shards and these have phonolite-trachytic compositions, with 60.2–62.7 wt% SiO_2, 18.2–19.0 wt% Al_2O_3, 7.0–8.8 wt% K_2O, 3.6–6.9 wt% Na_2O, 2.7–3.9 wt% FeO, and 1.6–2.9 wt% CaO. The two outlying shards both have plate-like morphologies and have rhyolitic compositions, which plot close to those of shards in T1 (Fig. 16).

Figure 16 compares selected major and minor element concentrations in T1 and T2 cryptotephra glass shards to published glass shard data from widespread tephra layers generated by central to eastern Mediterranean volcanic eruptions dated to between 50 and 29 ka BP. The composition of the two glass shards from T1 plot close to the compositions of tephra derived from the ~50–30 ka Epoch 5 eruptive activity of Ciomadul Volcano, which lies ~320 km to the north-east of TT in the Carpathian Mountains, Romania (Harangi *et al.*, 2015; Karátson *et al.*, 2016; Molnár *et al.*, 2019). Published sources disagree on the possibility of distinguishing between the eruption products of the Ciomadul Epoch 5 activity (Harangi *et al.*, 2020; Karátson *et al.*, 2016). The compositional subdivision shown in Fig. 16 reflects the identification of deposits by Karátson *et al.* (2016) and using these data would suggest that T1 belongs to the most evolved late or early Ciomadul Epoch 5 eruption products. However, with only two successful glass shard analyses from TT, we do not attempt to make a secure correlation to a specific dated eruption event. The composition of the Nisyros Upper Pumice, dated to ~47 ka BP and from the Greek Island of Nisyros ~1000 km to the south-southeast of TT, also plots close to the T1 glass shard compositions (Fig. 16). Not only have no deposits from Nisyros Island been found as far from source as this in the past, but a Nisyros source can be discounted for T1 based on glass shard TiO_2 compositions (not shown).

As observed by Lowe *et al.* (2012), the main population of glass shards from T2 correlates to the Campanian Ignimbrite (CI), which was a major caldera-forming eruption of the Campi Flegrei Volcanic Zone in southern Italy, ~39 ka BP (Giaccio *et al.*, 2017). The two outlying shards from T2 that plot close to the Ciomadul rhyolites could represent reworking of older material from within the cave system, or primary ashfall from a contemporary eruption (Harangi *et al.*, 2020).

The occurrence of tephra in Column 2

Figure 15 shows the Column 2 (Fig. 4) results of tephra glass shard counting within sampled stratigraphy. Tephra was found dispersed in very low concentrations (<11 shards per sample) throughout the sequence (0.10–1.20 m depth). When investigated at 2 cm resolution between 0.10–0.18 m depth, few shards were found, and this horizon was not followed up any further. The observed tephra shards are plate-like, with maximum longest axis lengths <150 μm.

DK micromorphology

The main micromorphological characteristics of the cave sediments are summarised in Table 3. In the field, the sediments are almost homogeneous, with some differences between contexts regarding minor colour variations and degree of cementation. The frequency of subangular to subrounded limestone clasts varies from common (contexts 2, 4) to very frequent (context 10).

In thin section, the sediments are also quite homogeneous, but some more differences could be observed. Microstructure is always crumb or granular, sometimes with coated grains in context 10 (Fig. 17:1), weakly to well developed, and more or less disturbed by channels and chambers with the exception of context 4 which is angular blocky to vughy. The granular microstructure is often referred to as a cold-climate feature (Van Vliet-Lanoë, 2010). The occurrence of silt cappings on skeleton grains (Fig. 17:2) also indicates seasonal frost action on sediments (Van Vliet-Lanoë, 2010), i.e. freezing and thawing cycles in contexts 1, 4 and 10.

The related distribution pattern is always porphyric, single-spaced to open. The b-fabric is calcitic crystallitic (contexts 1, 2, 4, 5–9) or granostriated (4, 10). Granostriated b-fabric may indicate wetting and drying of the sediment (Lindbo *et al.*, 2010).

Bone is the most frequent organic component of the sediments; very few are burnt. In contexts 2, 4 and 10, these bone fragments are very frequently sand-sized (Fig. 17:3). Sand-size bone fragments were observed at several Middle and Upper Palaeolithic sites, such as Riparo del Poggio (Boscato *et al.*, 2009), Riparo Mochi (Douka *et al.*, 2012) in Italy, or Mujina pećina in Croatia (Boschian *et al.*, 2017). In some contexts (especially in contexts 4 and 10) very frequent small bone fragments could indicate the characteristics of the diet. A possible explanation for bone splinters is that they were deliberately smashed and kneaded to extract the bone marrow and grease, activities that were performed *in situ* (Rabinovich and Hovers, 2004). However, given that phosphates, which can be identified as carnivore coprolites (Kolska Horwitz and

Table 8. Summary of luminescence dating results.

Sample field code	Laboratory code	Water content[a](%)	Betadose rate[b] (Gy/ka)	Gamma dose rate[c](Gy/ka)	Cosmicdose rate[d] (Gy/ka)	Totaldose rate[e](Gy/ka)	De[f](Gy)	OSL age[g](ka)
TT Cave OSL 1 [context 207]	X7525	27 ± 5	1.39 ± 0.08	0.70 ± 0.07	0.04 ± 0.01	2.13 ± 0.11	50.36 ± 3.32	23.60 ± 1.98
TT Cave OSL 2 [context 209]	X7526	22 ± 5	1.18 ± 0.07	0.68 ± 0.09	0.04 ± 0.01	1.90 ± 0.11	34.08 ± 7.62	17.93 ± 4.15
TT Cave OSL 3 [context 226]	X7527	11 ± 3	0.75 ± 0.04	0.51 ± 0.02	0.04 ± 0.01	1.30 ± 0.04	70.27 ± 4.27	53.90 ± 3.76
Dubočka OSL 1 [context 4a]	X7528	2 ± 2	1.12 ± 0.05	0.72 ± 0.37	0.04 ± 0.01	1.89 ± 0.38	18.36 ± 0.99	9.73 ± 2.01
Dubočka OSL 2 [context 4b]	X7529	3 ± 2	0.99 ± 0.05	0.68 ± 0.18	0.04 ± 0.01	1.71 ± 0.19	29.65 ± 2.41	17.34 ± 2.39
Dubočka OSL 3 [context 4]	X7530	5 ± 2	1.22 ± 0.05	0.82 ± 0.03	0.04 ± 0.01	2.08 ± 0.06	57.88 ± 2.77	27.76 ± 1.57

[a]The recorded water content expressed as a percentage of the dry mass of the sample mineral fraction.

[b]Dose rates were calculated using the dose rate and age calculator *DRAC v.1.2* developed by Durcan *et al.* (2015) and are based on elemental concentrations of radioisotopes derived from powdered sediment samples (~8 g) analysed by fusion ICP-MS/AES at a specialist accredited laboratory (Actlabs in Canada). Specific activities and radionuclide concentrations were converted to dose rates using the updated conversion factors proposed by Guérin *et al.* (2011), making allowance for beta-dose attenuation due to grain size effects and HF etching (Brennan, 2003).

[c]In the absence of *in situ* gamma-ray spectrometry measurements, layer-to-layer variations in radioactivity for samples X7525, X7526, X7528 and X7529 were taken into account by scaling the gamma dose rate using the R function *scale gamma_dose* developed by Riedesel *et al.* (2020) and based on the approach and data outlined in Aitken (1985).

[d]The contribution of cosmic radiation to the total dose rate was calculated as a function of latitude, altitude, burial depth and an average overburden density of 1.9 gcm^{-3} based on the data reported by Prescott and Hutton (1994). For both sets of samples, the thickness of the cave roof was assumed to be circa 15 m and this value was added to the burial depth recorded for each sample. A large error of ±5 m was attributed to the overburden height in order to account for the uncertainty in accurately estimating the cosmic ray contribution.

[e]The total dose rate includes a small internal dose rate of 0.03 ± 0.02 Gy/ka, based on intrinsic trace amounts of ^{238}U and ^{232}Th found in etched quartz (Mejdahl 1987; Grün and Fenton, 1990; De Corte *et al.*, 2006; Vandenberghe *et al.*, 2008). An alpha efficiency factor of 0.04 ± 0.01 (Rees-Jones, 1995; Rees-Jones and Tite, 1997) was also included in the dose rate calculations.

[f]The equivalent dose (De) is expressed as a weighted mean with a standard error calculated from repeat measurements ($n = 14–35$) made on small-sized (3 mm) multi-grain quartz aliquots. OSL measurements were analysed using the Analyst (ver.4.57) software developed by Duller (2015). The De calculations were made using the *Luminescence* package (version 0.9.) developed by Kreutzer *et al.* (2012) for the statistical programming language *R* and the reported error includes a systematic component of ±4% to account for uncertainty related to the calibration of the laboratory beta source.

[g]The date is reported in 10^3 years (ka) before 2019 and the uncertainty is the quadratic sum of the random and systematic uncertainties expressed within one sigma (68% confidence interval).

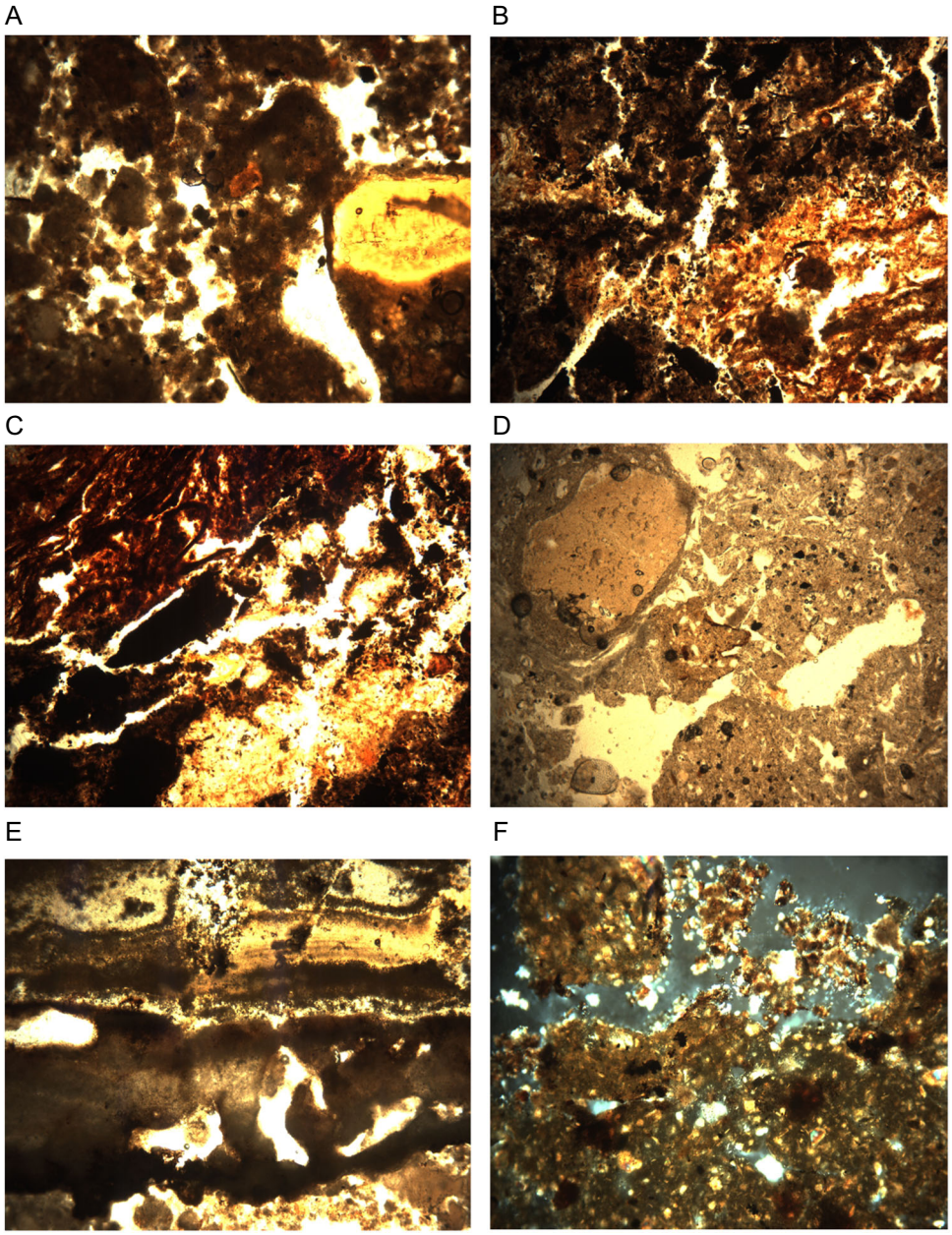

Figure 13. Tabula Traiana Cave; a. Photomicrograph of the bioturbated calcitic fabric with a few bone fragments, basal fabric unit 1, sample 1 (plane-polarised light; frame width = 4.5 mm); b. Photomicrograph of the bioturbated, heterogeneous mixture of calcitic silt, comminuted very fine charred and plant material and amorphous sesquioxide-replaced plant tissues, fabric unit 4, sample 1 (plane-polarised light; frame width = 4.5 mm); c. Photomicrograph of the phosphatised micritc silt with common amorphous sesquioxide-replaced plant tissue matter and included very fine to fine charcoal, upper fabric unit 5 sample 1 (plane-polarised light; frame width = 4.5 mm); d. Photomicrograph of the calcitic ash fabric and a weathered bone fragment (upper left), sample 2 (plane-polarised light; frame width = 4.5 mm); e. Photomicrograph of the thin linear zone of calcareous silt and fine charcoal dust crusts at a clear planar boundary on the underlying weathered karst floor of the cave, sample 2 (plane-polarised light; frame width = 4.5 mm); f. Photomicrograph of the bioturbated calcitic silty clay with abundant included fine sand-size phosphatised bone fragments, sample 3 (cross-polarised light; frame width = 4.5 mm). [Color figure can be viewed at wileyonlinelibrary.com]

Goldberg, 1989; Goldberg, 1980) are common in the same contexts, gnawing and digestion of the bones by carnivores cannot be ruled out.

At the microscopic scale, sand- and silt-sized amorphous organic matter aggregates (Fig. 17:4), which are common in contexts 1 and 4 and occur occasionally in context 2, are the main evidence of human activity at the site; charcoal fragments are also present but very scanty (context 10).

Radiometric chronology of TT

Eighteen AMS measurements on 17 bone fragments are available from TT (Table 6). The rationale in sample selection was primarily the presence of cutmarks as evidence of anthropically modified specimens (Figs. 18 and 19), and hence human activity in cave deposits. However, four dated specimens did not bear any trace of anthropic modifications as the choice of their selection was related to other criteria: interest in knowing the age of the dated species in the case of AA-63887, which dates a cave lion metapodial, and in providing the age of certain contexts lacking anthropically modified bones in the case of OxA-16419 (fireplace), -24819 and -26718. All dates provided late Pleistocene ages, out of which five measurements produced infinite ages beyond temporal limits of radiocarbon dating.

A borderline case is OxA-35770 that at 95% confidence provides an infinite date but produces the range of 52 350–46 720 at 68% confidence and would thus represent the earliest

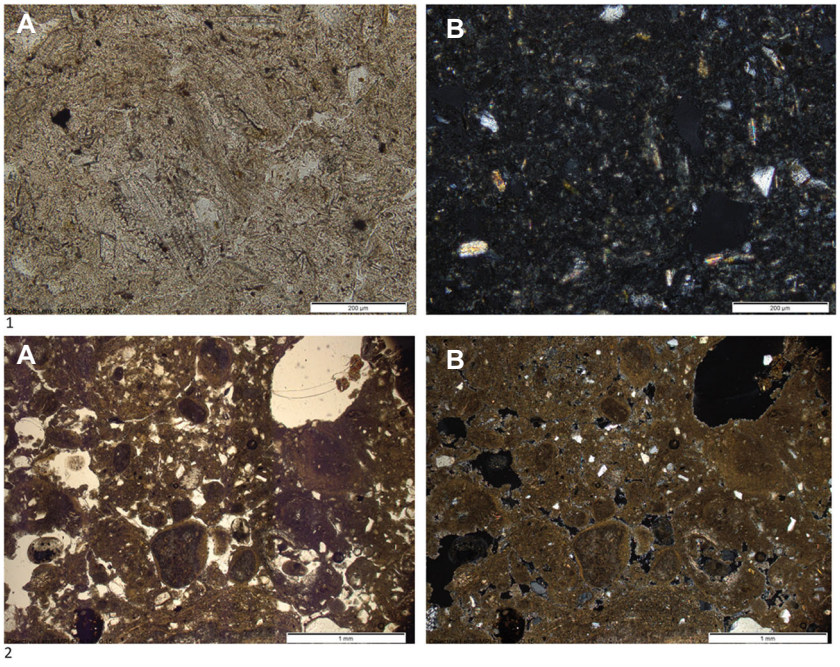

Figure 14. Photomicrographs of sediment thin sections from Tabula Traiana. 1. a: phytoliths in context 207, PPL. b: same as a, XPL; 2. a: granostriated b-fabric; silt capping coating skeleton grains, PPL. b: same as a, XPL. [Color figure can be viewed at wileyonlinelibrary.com]

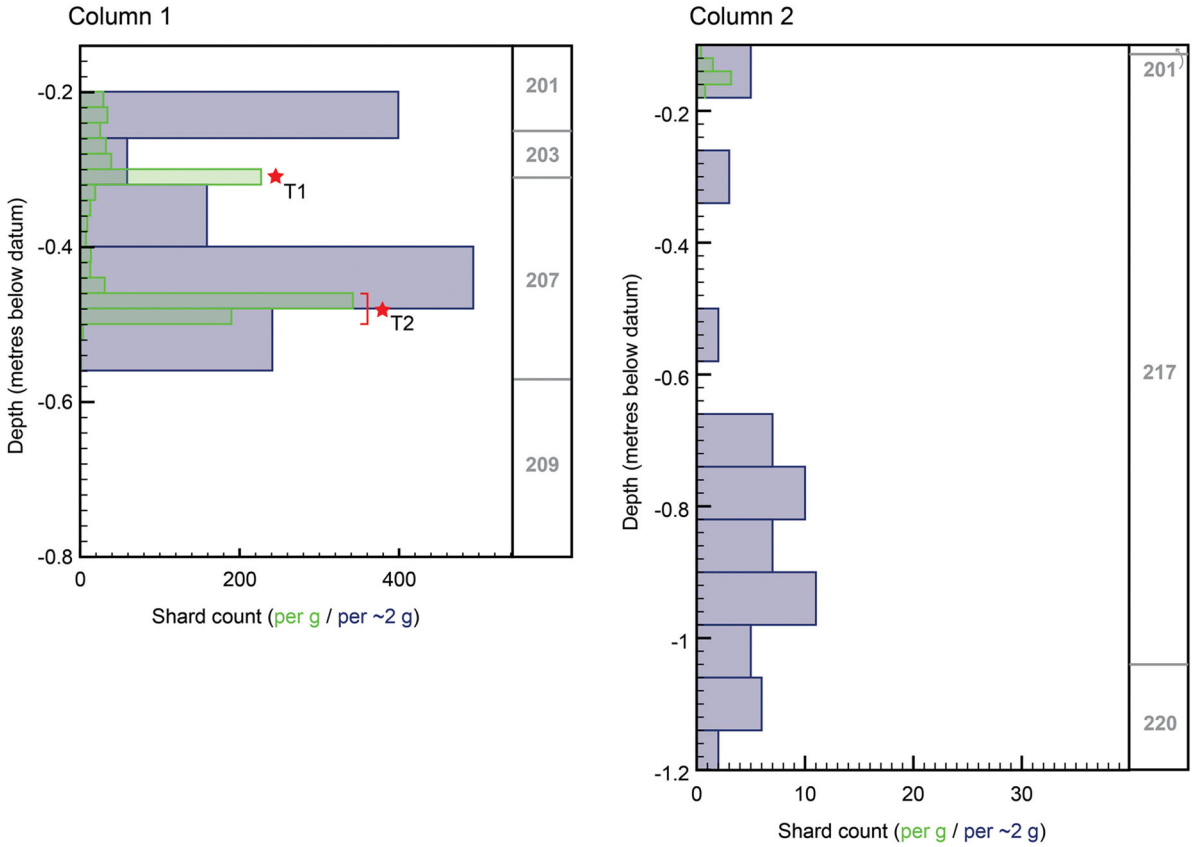

Figure 15. The column 1 and 2 results of tephra glass shard counting within sampled stratigraphy in TT. Distribution of tephra glass shards by depth within cryptotephra column 1 and column 2. Right-hand columns indicate archaeological units and boundaries. Wide blue bars show indicator shard counts from initial low-resolution samples (aggregated from multiple bag samples), estimated as shards per ~2 g dry sediment weight. Green bars show high-resolution (2 cm depth intervals) samples spanning intervals where tephra glass shards had been found in above-background concentrations and are quantified as shards per 1 g dry sediment. Red stars pinpoint tephra layers T1 and T2 for which samples were re-extracted and run for geochemical analyses. [Color figure can be viewed at wileyonlinelibrary.com]

AMS-dated specimen from this site. The stratigraphic position of this cutmarked specimen in the lower stratigraphic units would correspond with the obtained age. The estimated age of OxA-35770 broadly fits the OSL-3 measurement from TT (Table 7), which gave the date of 53.90 ± 3.76 BP. This OSL sample comes from the lowest reached levels of stratigraphic unit (226) at the cave entrance (Fig. 4) and, based on its stratigraphic position, this date would represent a *terminus post quem* for the MP occupation horizon with the Levallois-based technology described earlier. On the face of this evidence, we may tentatively suggest that the MP occupation of TT took place sometime between *c.* 52.3 and 46.7 kya cal

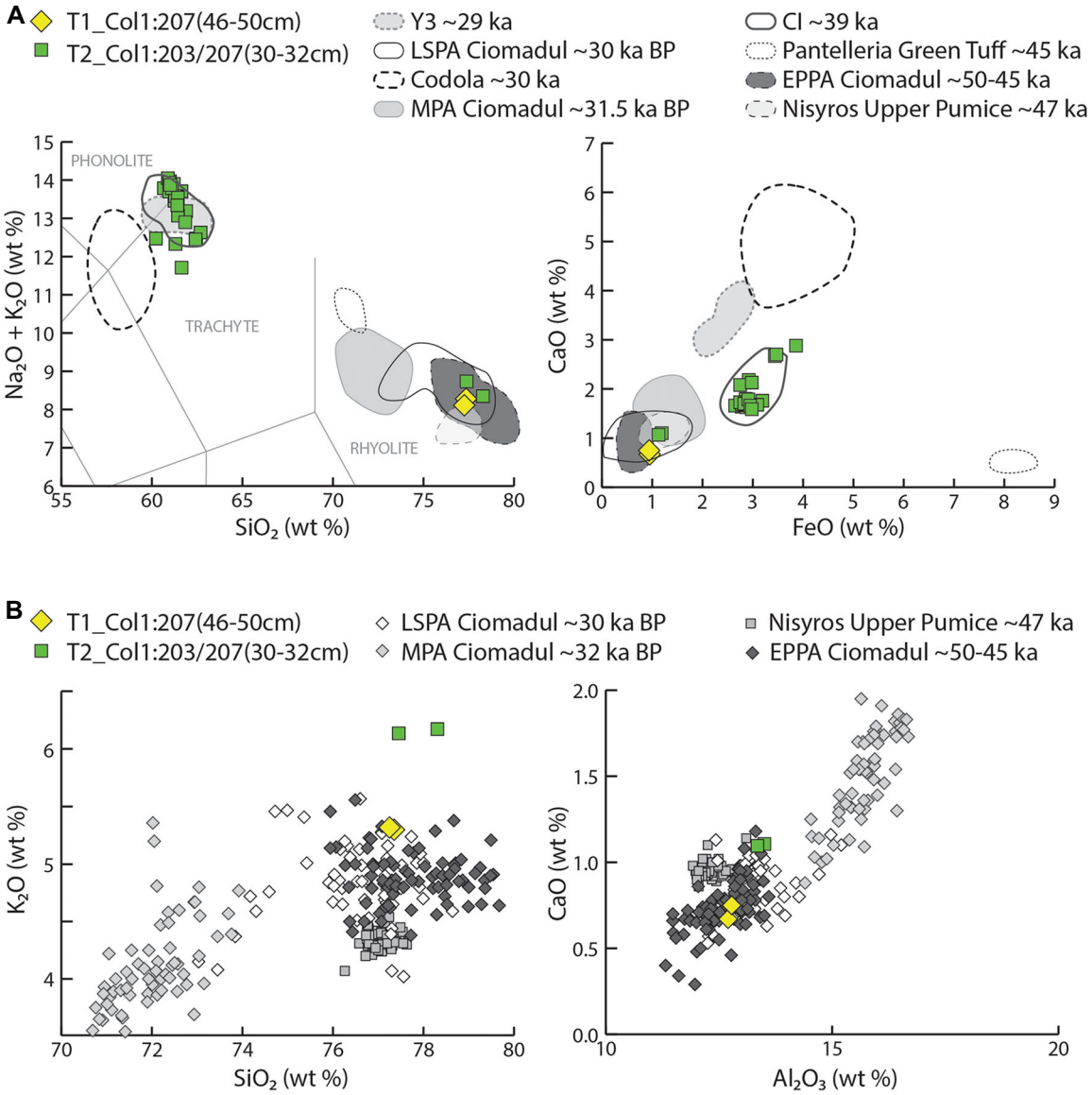

Figure 16. Selected major and minor element concentrations in T1 and T2 cryptotephra glass shards compared with published glass shard data from widespread tephra layers generated by central to eastern Mediterranean volcanic eruptions dated to between 50 and 29 ka BP. [Color figure can be viewed at wileyonlinelibrary.com]

BP. Five infinite dates obtained on four cutmarked bones all consistently come from lower stratigraphic units and thus confirm the MP age of these deposits around or earlier than 50 kya. While lower chronostratigraphic units at TT probably document a MIS3 Neanderthal occupation of the cave, this late MP presence at TT may still have ceased several thousand years before the earliest appearance of modern humans in the Balkans by *c.* 45 kya cal BP (cf. Hublin *et al.*, 2020). The ZooMS identifications of some of the dated fragments (Table 7, Fig. 20) reveal that cutmarks were left on the remains of bovids (*Capra* sp., likely ibex), cervids and bears (likely cave bear), suggesting the subsistence role of these taxa during the MP occupation.

The EUP date ranges obtained for TT fall between *c.* 42.3 and 36.9 kya cal BP (Fig. 19). These dates document rather ephemeral and transitory (based on small artefact densities) UP and, by proxy, modern human presence in the cave, possibly already before but also after the CI eruption (see above). OxA-35764 with the range of 42 350–40 260 cal BP (95% probability), which dates a cutmarked bone fragment (Fig. 18e), is the earliest anthropically modified specimen attributed to UP levels at TT, and its range overlaps with that of OxA-16419 made on an anthropically non-modified ibex horncorn fragment from the context of the fireplace at the bottom of the UP sequence (Fig. 5). Human presence at TT is also now unambiguously confirmed during the early phases of the Gravettian, between *c.* 33 to 29 kya cal BP, based on the obtained dates on two cutmarked specimens (Fig. 18c,f). One of these specimens, dated by OxA-35593 is identified as Canidae based on ZooMS analysis and shows particularly elevated isotope values (Table 6), which could be indicative of high freshwater protein consumption, presumably from fish, seen in dog specimens from this region during the Mesolithic (Borić 2011; Borić *et al.*, 2004).

Finally, the results of OSL dating of samples 1 (23.60 ± 1.98 kya cal BP) and 2 (17.93 ± 4.15 kya cal BP) (Table 7), supposed to date two stratigraphically superimposed units (Fig. 6), seem to underestimate the known age of these deposits based on other proxies. OSL-2 seems particularly problematic as it has large error terms, and its age is inverted to OSL-1 from what is expected stratigraphically. Measurements on additional samples including more advanced single grain analyses will be required in forthcoming studies in order to help explain the apparent age underestimation observed for these samples. Meanwhile, both OSL dates should be interpreted with caution.

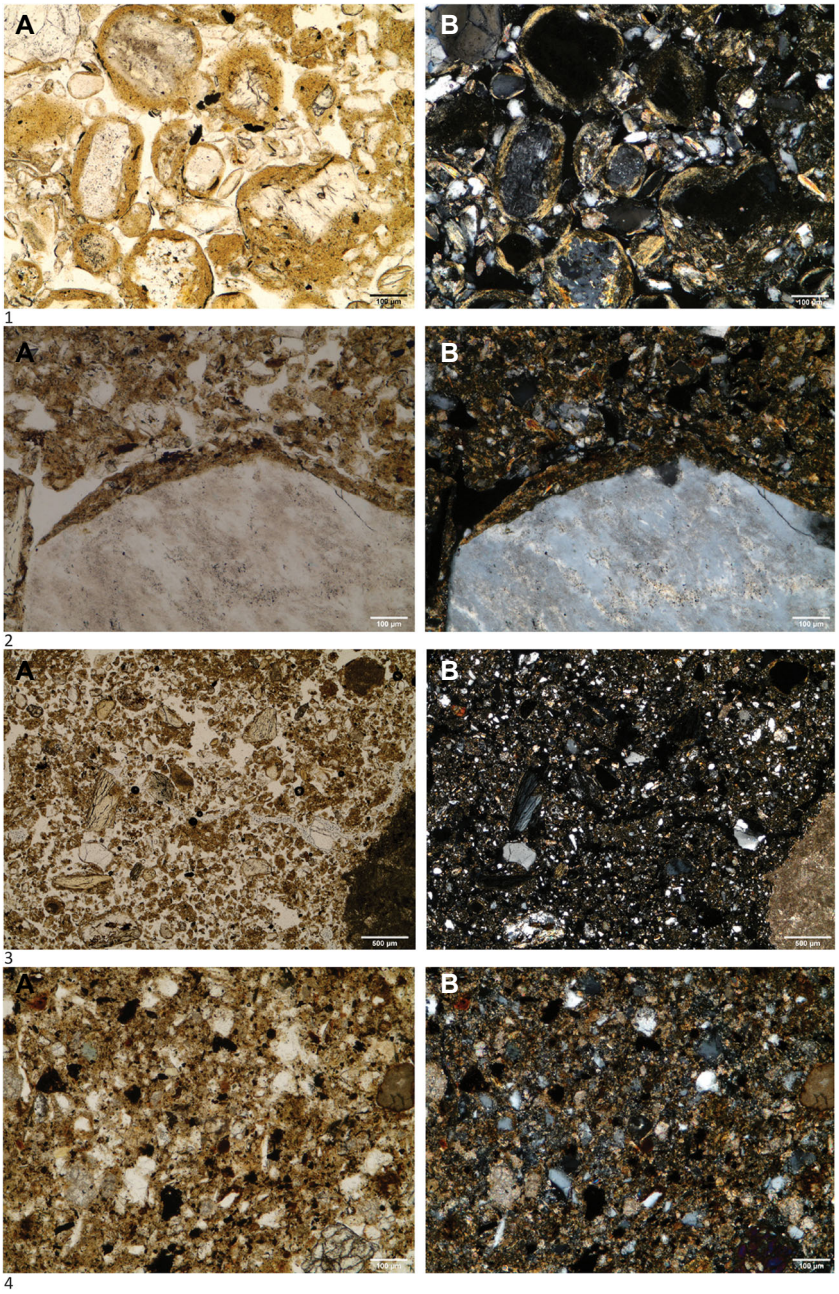

Figure 17. Photomicrographs of sediment thin sections from DK. 1a: cryogenic loose granular microstructure with granostriated b-fabric; silt cappings completely coating skeleton grains, PPL, context 10. 1b: as in a, XPL; 2a: silt capping on metamorphic quartz, PPL, context 10; 2b: as in a, XPL; 3a: bone-dominated sediment, PPL, context 10. 3b: as in a, XPL; 4a: amorphous organic matter, PPL, context 1; 4b: as in a, XPL. [Color figure can be viewed at wileyonlinelibrary.com]

Radiometric chronology of DK

Nine AMS measurements on eight bone fragments are available from DK (Table 6). As with the dating of TT, the rationale in sample selection was the presence of cutmarks or other modifications on bones as evidence of anthropically modified specimens (Fig. 21). Apart from some minor inversion in the topmost, Holocene levels, the dates consistently show increasing age with depth. Three dates from the topmost levels provide Holocene dates on cutmarked or modified specimens dating human presence in the cave to the Late and Early Copper Age and the Final Mesolithic/Early Neolithic. It seems that the latter trace of visitation of the cave comes from people who did not leave traces of material culture indicative of this period.

Two dates from the bottommost Pleistocene-age levels provide infinite dates beyond temporal limits of radiocarbon dating. Three other dates on two cutmarked specimens provide overlapping ranges between 41 and 37.5 kya cal BP, and one date from the topmost Pleistocene levels provides an early Gravettian date between 30 and 29.2 kya cal BP (Fig. 22). In the absence of more diagnostic UP material culture in the excavated area of the cave, for the moment, it must remain an open question whether the two obtained dates around 40 kya cal BP should be associated with the confirmed modern human presence in this region at this time, not leaving much material culture trace in the cave sediments apart from cutmarked bones, or with surviving Neanderthal groups inhabiting this area from before the temporal reach of radiocarbon dating up to the transitional period, during which they might have been contemporaneous with modern humans. The overall homogeneity of the abundant knapped stone assemblage from DK with MP characteristics may perhaps tip the weight of the argument in the direction of the latter scenario, but this suggestion must remain a mere speculation at present. As we currently pursue further AMS dating of the anthropically modified specimens and other contextual analyses on the material from DK, this picture may become clearer soon.

Proteomic/ZooMS analyses on two AMS-dated specimens with cutmarks identified the remains of *Ursus* sp. (Fig. 23). This may tentatively suggest that morphologically

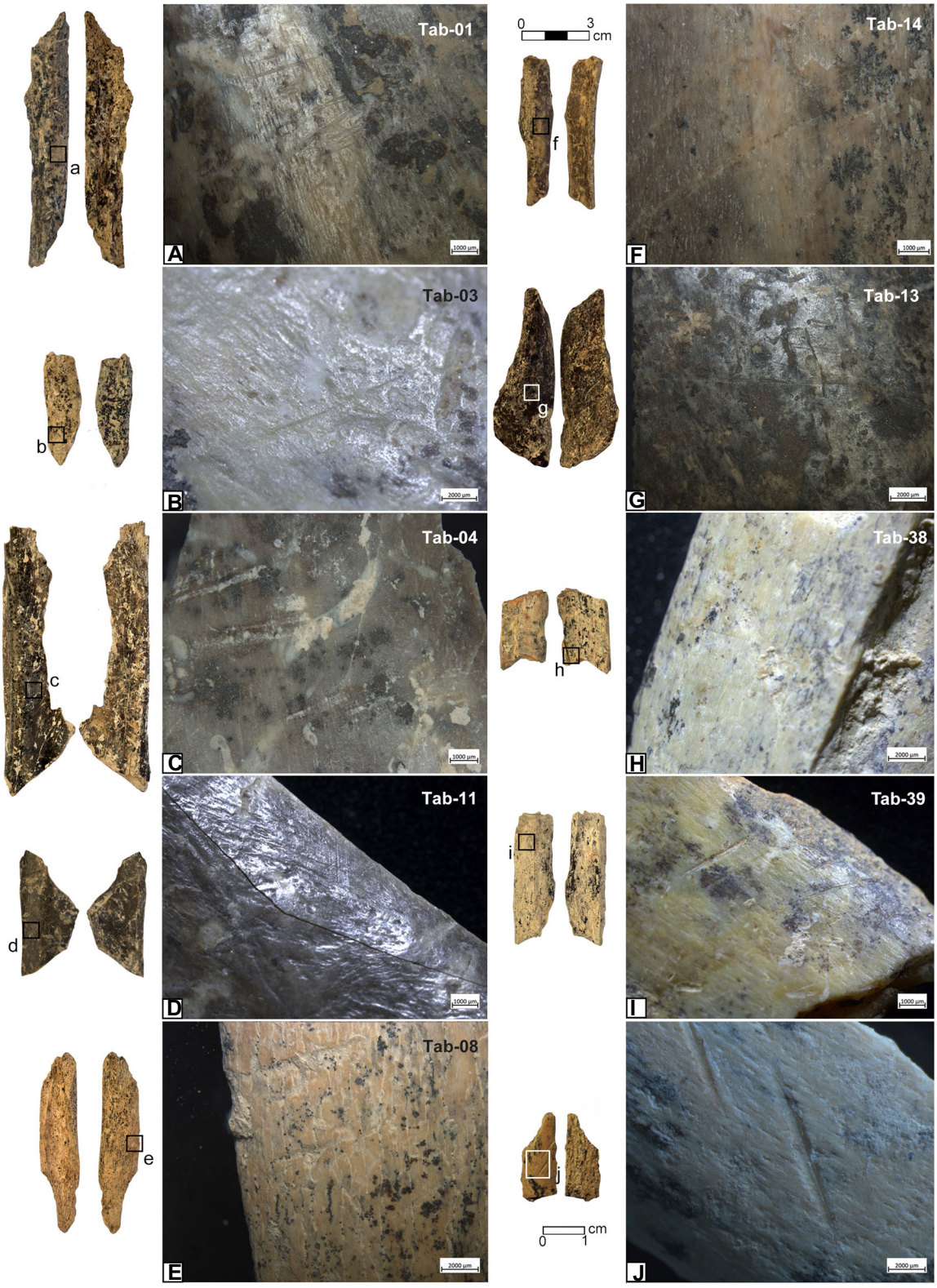

Figure 18. Cutmarked bone specimens from TT selected for AMS dating. [Color figure can be viewed at wileyonlinelibrary.com]

identifiable cave bear specimens found in Pleistocene-age sediments at DK should be linked to the manipulation of cave bear by hominins both in earlier and later phases of the MP occupation of the cave.

The attempt to provide more chronological clarity for DK sediments by means of OSL dating did not result in the expected outcome. The obtained dates from two superimposed samples, OSL-1 (9.73 ± 2.01 BP) and OSL-2 (17.34 ± 2.39 BP), taken from the west-facing section of Trench 1/2013, while internally consistent regarding their stratigraphic position, seem to underestimate the assumed age of these sediments. A similar case is with the date on OSL-3 (27.76 ± 1.57 BP) from the east-facing section of the same trench, supposed to date context 4 (Fig. 10), containing the MP industry described above. OSL redating of these sediments may provide some more clarity in the future.

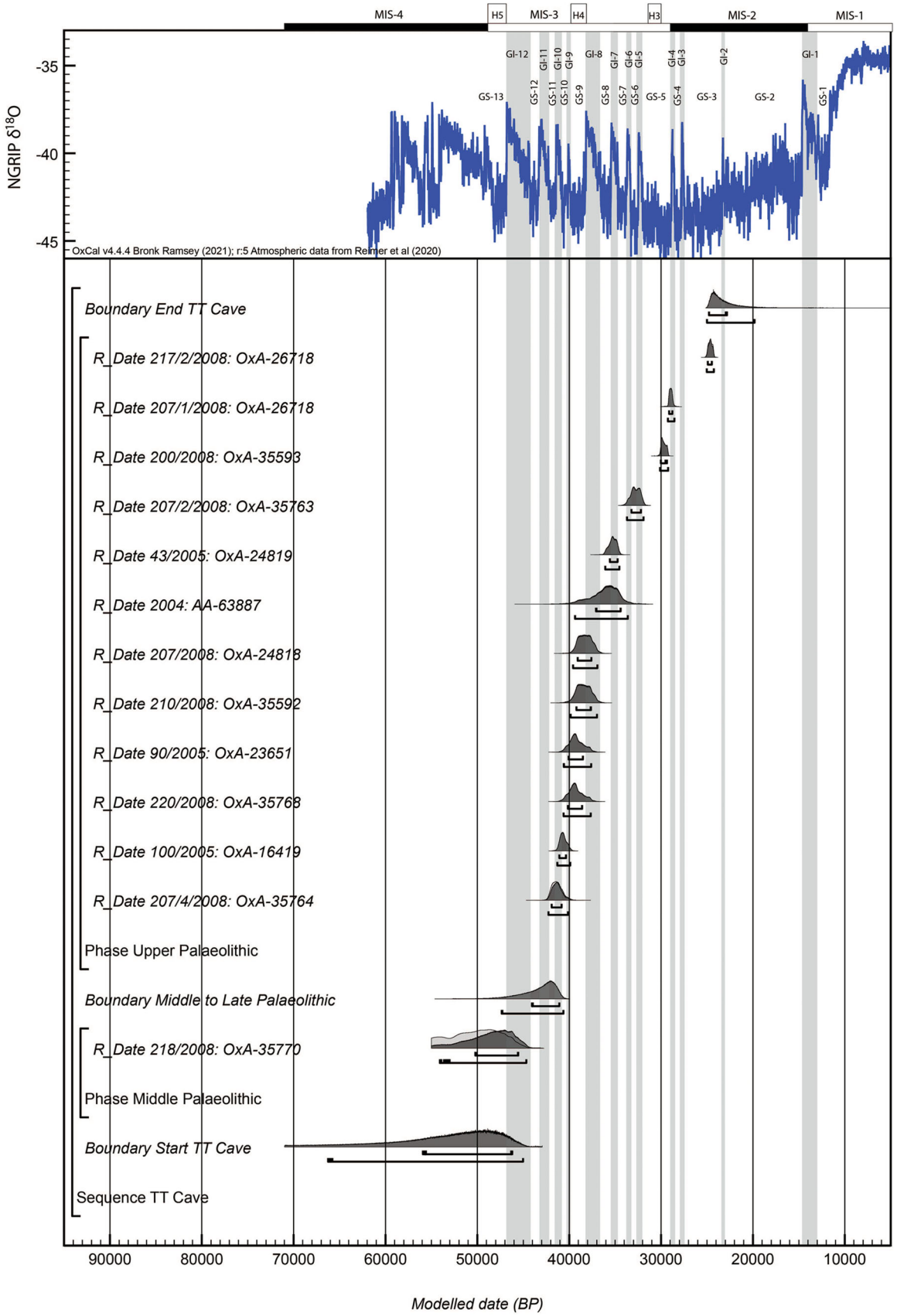

Figure 19. Bayesian modelling of all available dates from TT plotted against the North Greenland (NGRIP) $\delta^{18}O_{ice}$ record and event stratigraphy; Greenland Stadial/Interstadial (GS/GI) cycles for the last 48 kyr BP (before 2000 AD). For the radiocarbon measurements, distributions in outline are the results of simple radiocarbon calibrations and solid distributions are the output from the chronological model. The large square brackets and OxCal v. 4.4 CQL2 keywords define the overall model exactly. [Color figure can be viewed at wileyonlinelibrary.com]

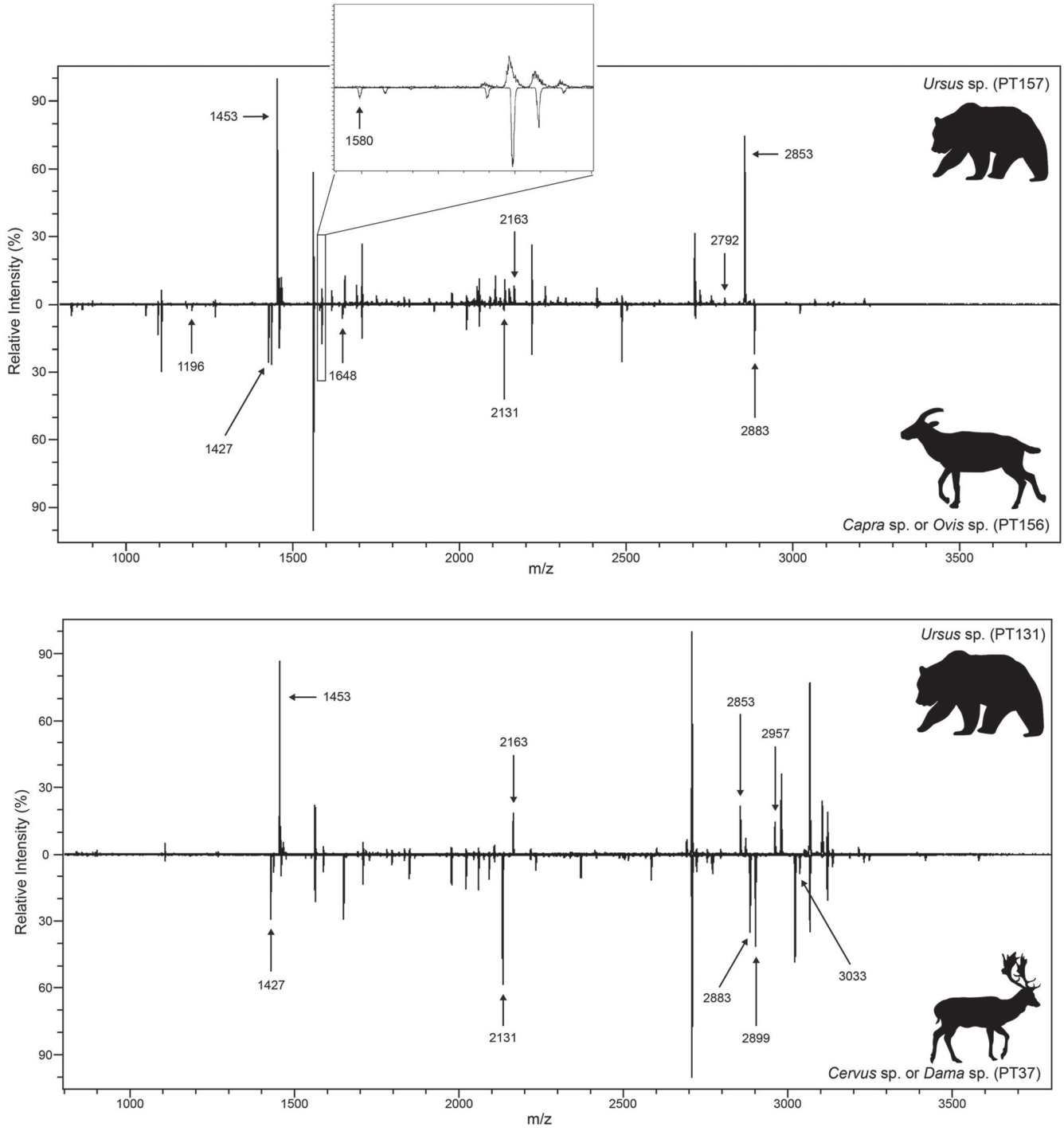

Figure 20. MALDI spectra identifications of fragmented bone specimens from TT. Masses of the key markers used for taxonomic identification are indicated with arrows. The inset highlights that even markers with relatively low intensity values which are not visible in the full spectrum can be used for identification.

Stable isotope analysis on the macromammals from TT

All herbivorous taxa analysed had a diet typical of the consumption of C3 vegetation, in an open landscape, with no evidence of the canopy effect, which can produce lower $\delta^{13}C$ values (van der Merwe and Medina, 1989, 1991) (Table 8, Fig. 24). This may in part be related to the species sampled. Ibex, the most commonly sampled species, typically inhabit rocky, craggy locations, whereas red deer are more flexible in their habitats, and can inhabit woodland and reflect the canopy effect (Drucker *et al.*, 2008, 2011). We could infer that at least some of the deer at the site were predominantly living in open environments. Further analysis of a greater number of red deer specimens, alongside palynological analysis would help to explore vegetation cover in the vicinity of the site further. One AMS-dated specimen of Bos/Bison clusters together with other herbivorous taxa and it seems that overall there is a good correspondence among the specimens belonging to the same species when we compared specifically obtained stable isotope values reported in Table 8 and indicative stable isotope values from AMS burns (Table 6, Fig. 24).

The UP ibex specimens have slightly elevated $\delta^{13}C$ values in relation to the MP samples. This could indicate that there may have been a shift in environmental conditions between these two periods. Modern ibex preferentially inhabit higher altitude, rocky environments (Grignolio *et al.*, 2004; Parrini

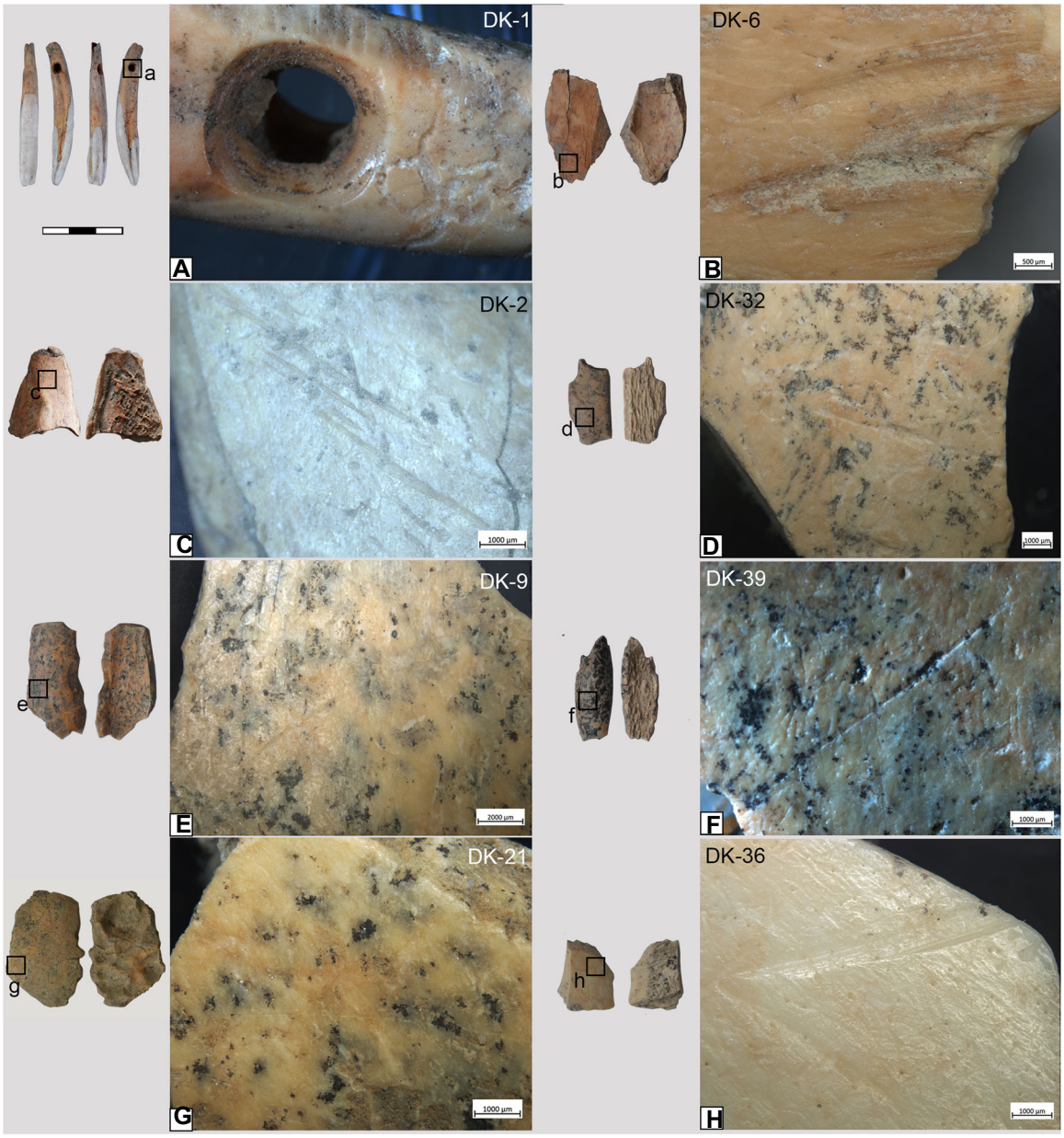

Figure 21. Cutmarked bone specimens from Dubočka-Kozja selected for AMS dating. [Color figure can be viewed at wileyonlinelibrary.com]

et al., 2009). A possible explanation for the slightly higher $\delta^{13}C$ values in the UP may be due to conditions changing slightly between the two periods. Elevated $\delta^{13}C$ values in plants and their consumers can be produced by a multitude of environmental factors, including moisture availability and rainfall (Farquhar, *et al.*, 1982; Stewart *et al.*, 1995; Gröcke, *et al.*, 1997; Diefendorf *et al.*, 2010; Kohn, 2010), and changes in temperature have also been seen to impact on $\delta^{13}C$ values (Heaton, 1999). Additionally, increased $\delta^{13}C$ values are also associated with higher altitude locations (Farquhar *et al.*, 1989; Körner, *et al.*, 1991; Hultine and Marshall, 2000), and could suggest that ibex were perhaps living further up mountain slopes during the UP, possibly due to improved conditions at higher altitudes as well as increased vegetation availability at these higher elevations. Alternatively, a change in the type (DeNiro and Epstein, 1978; Bocherens and Drucker, 2003) or parts of plants (Ehleringer, *et al.*, 1987) being consumed can affect $\delta^{13}C$ values, and it might have caused the UP ibex to have slightly elevated $\delta^{13}C$ values relative to the MP individuals. If so, this could suggest a type of vegetation available in the habitats of the ibex. There might have been a change in environmental conditions between the two chrono-cultural periods, although larger sample sizes, in combination with wider environmental indicators would help to explore this further.

Specimen TAB04 was originally identified as red deer *Cervus elaphus* but has a $\delta^{15}N$ value of 14.2‰ and a $\delta^{13}C$ value of −18.0‰ (Fig. 24, Table 7). These isotopic values are way outside of the $\delta^{15}N$ ranges for European deer in Palaeolithic Europe (Drucker *et al.*, 2003; Stevens *et al.*, 2014; Jones *et al.*, 2018, 2019), suggesting that the specimen might have been misidentified and that it probably comes from a large carnivore. The sample was taken from a fragment of thoracic vertebra, which are notoriously challenging to identify to species using traditional zooarchaeological methods. The size and the upper part of the spine is fused, suggesting that this individual is at least two years of age. This vertebra has a rounded spinal process, which is typical in carnivores and bears, and is consistent with being the size of a medium–large mammal. Carnivore gnawing was noted on both the transverse and spinal processes, suggesting that the bone may not necessarily be linked to the periods of human activity at the site. The high $\delta^{15}N$ value would be highly unusual for a cave bear (*Ursus spelaeus*), when compared with studies of other late Pleistocene individuals.

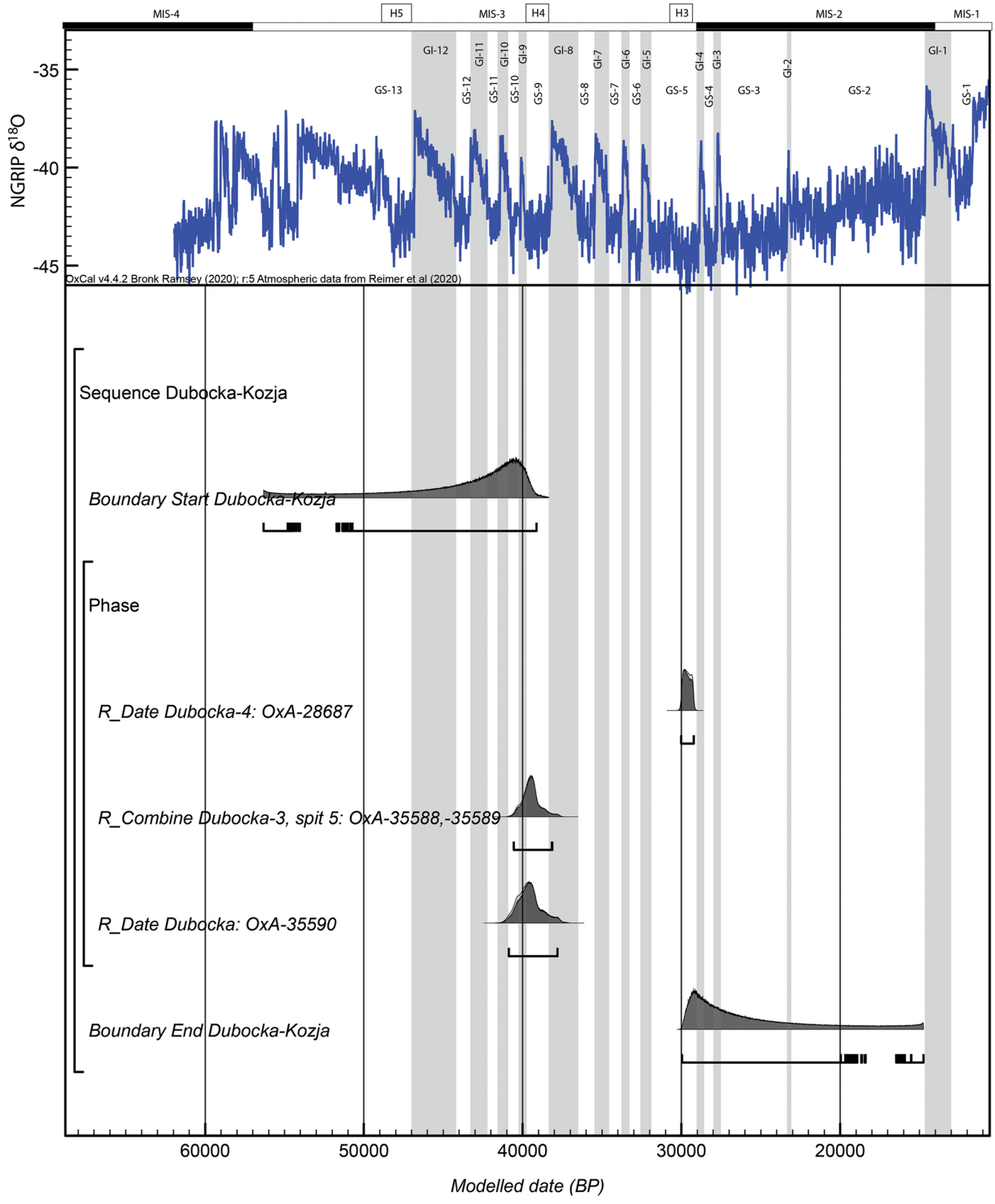

Figure 22. Bayesian modelling of all available dates from DK plotted against the North Greenland (NGRIP) $\delta^{18}O_{ice}$ record and event stratigraphy; Greenland Stadial/Interstadial (GS/GI) cycles for the last 48 kyr BP (before 2000 AD). For the radiocarbon measurements, distributions in outline are the results of simple radiocarbon calibrations, solid distributions are the output from the chronological model. The large square brackets and OxCal v. 4.4 CQL2 keywords define the overall model exactly. [Color figure can be viewed at wileyonlinelibrary.com]

In fact, four *Ursus* sp. specimens (presumably *U. spelaeus*) from TT and DK identified on the basis of ZooMS analyses and directly AMS-dated have associated AMS burn isotope values and even if these values are only indicative values for the moment, all $\delta^{15}N$ values for these specimens are below 10‰ with some significant differences in trophic levels among these specimens (two specimens from TT have $\delta^{15}N$ values as low as 1.6‰ and 1.5‰, respectively), while also their low $\delta^{13}C$ values are all clustered away from herbivorous taxa. The highest $\delta^{15}N$ values for cave bear to date are around 10‰ from late Pleistocene individuals at Peștera cu Oase in Romania, interpreted as pertaining to an omnivorous diet (Richards *et al.*,

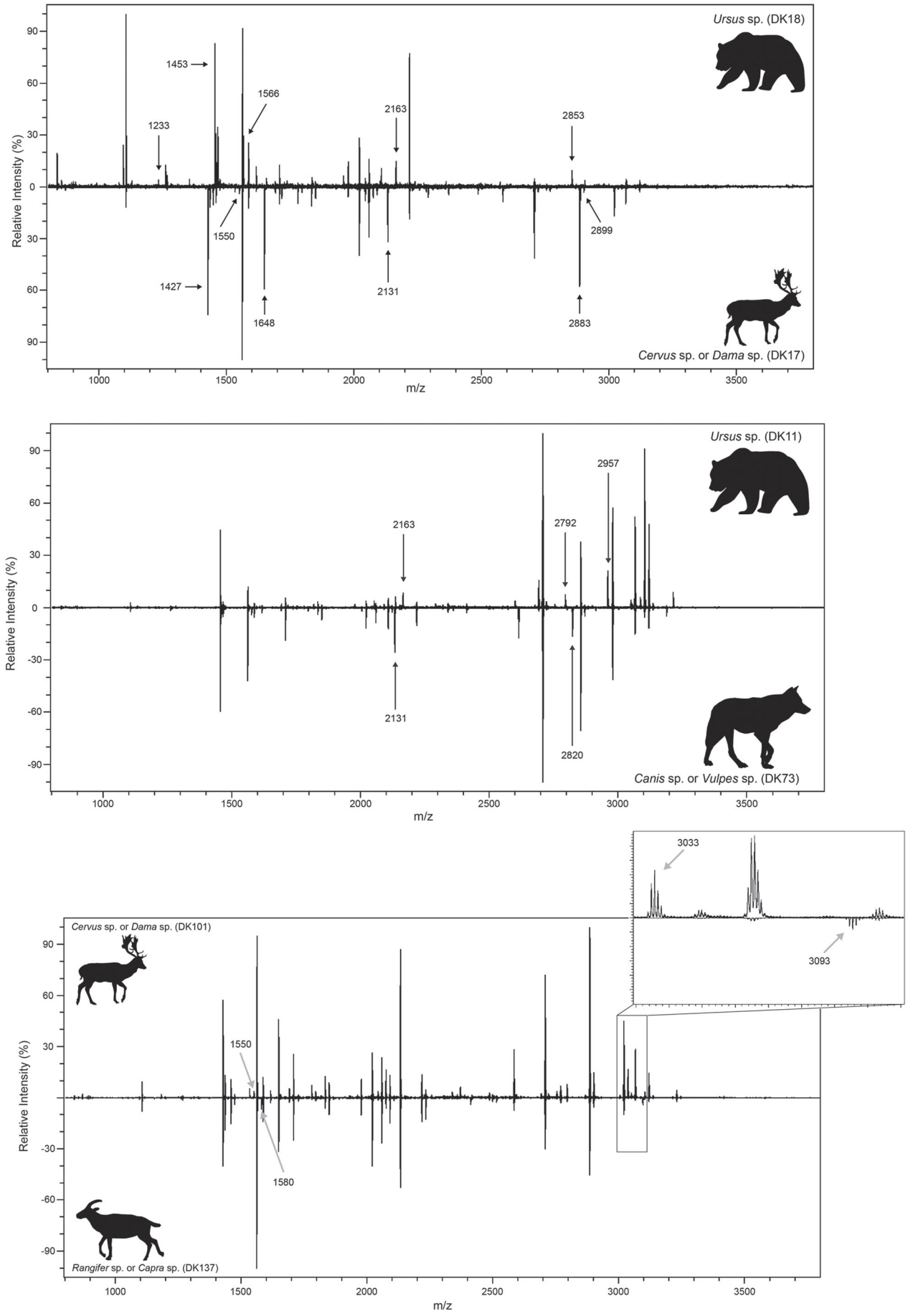

Figure 23. MALDI spectra identifications of fragmented bone specimens from DK. Masses of the key markers used for taxonomic identification are indicated with arrows. The inset highlights a key, high mass, marker (*m/z* 3093) that is highly distinctive for *Capra* and *Rangifer*. While in some cases not all markers were present to provide the lowest level taxonomic identification, partial identification was possible.

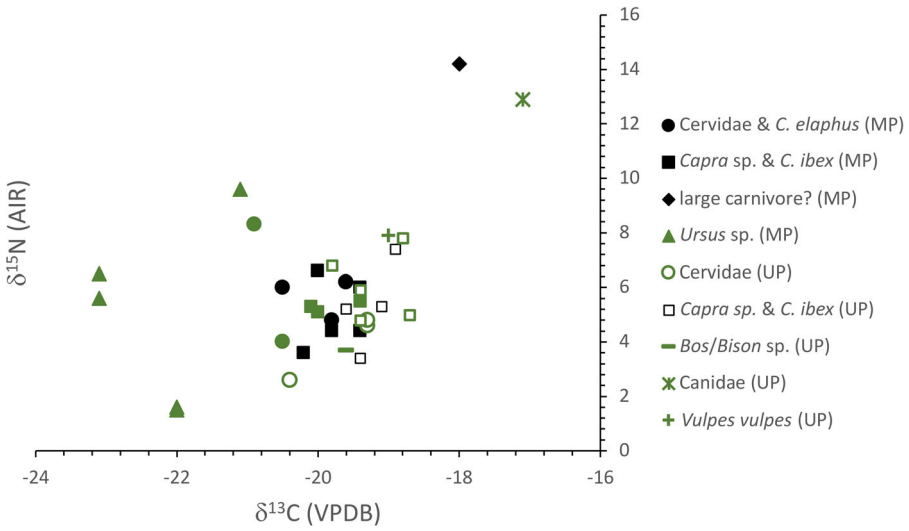

Figure 24. Available $\delta^{13}C$ and $\delta^{15}N$ values ($n = 34$) plotted against main periods at TT and DK. Black symbols indicate specimens analysed specifically for C and N isotopes from Tabula Traiana only ($n = 13$, Table 7); green symbols indicate stable isotope values from AMS burns ($n = 21$, Table 6) that lack the three-point calibration standard and are only indicative values. [Color figure can be viewed at wileyonlinelibrary.com]

2008), although recent compound-specific amino acid analysis of nitrogen isotopes of further Pleistocene cave bears in Romania has indicated an exclusively herbivorous diet, with higher $\delta^{15}N$ values reflecting niche portioning within nitrogen zones in the landscape (Naito *et al.*, 2020). Effects such as hibernation for longer durations during colder periods can produce inflated $\delta^{15}N$ values in cave bears (Fernández-Mosquera, *et al.*, 2001; D'Anglade and Mosquera, 2008). Younger or sub-adult bears may also have inflated $\delta^{15}N$ values, reflecting a combination of residual breastfeeding in addition to their mother's hibernation effect (Bocherens 2004; Grandal-D'Anglade, *et al.*, 2011). The value of specimen TAB04 would be extreme even considering these possible effects, especially given that this individual is >2 years of age. Hence the sampled specimen probably does not come from a cave bear. Similarly, although brown bear (*U. arctos*) can be omnivorous, isotopic studies of UP specimens from Austria have shown them to have $\delta^{15}N$ values of around 3‰ (Bocherens *et al.*, 2011). Even accounting for baseline differences between regions, and the possibilities of nursing and hibernation signatures, a $\delta^{15}N$ value of 14‰, as seen at TT would be hard to achieve, suggesting that this individual is probably not a brown bear. The isotopic result on TAB04 would be consistent with a carnivore feeding at a high trophic level, consuming a diet rich in animal protein. Based on the size of the vertebra, it likely belonged to a larger carnivore, which have also been identified in TT sediments. In the broadly contemporaneous deposits of the site of Šalitrena (Fig. 1), cave hyena, wolf, leopard and cave lion were identified (Marín-Arroyo and Mihailović, 2017), attesting to the presence of large carnivores in central Serbia at this time. Future ZooMS analysis on the specimens should be able to clarify this dilemma.

As previously emphasised, while stable isotope values associated with AMS burns cannot be used in comparisons with data specifically obtained for stable isotopes in an unproblematic way due to problems of using calibration standards (Szpak *et al.*, 2017), it could be informative to have a quick look at some of these data. Apart from a fox specimen with the $\delta^{15}N$ value of 7.9‰, one AMS-dated specimen of *Canis* sp. clusters together with the previously discussed TAB04, both exhibiting high trophic levels. This *Canis* sp. specimen also has a relatively high $\delta^{13}C$ value of −17.1‰, and these elevated isotope values in this area close to the Danube River could be indicative of the consumption of fish species, both freshwater fish and anadromous sturgeon (cf. Borić 2011). The isotope values of the *Canis* sp. specimen are similar to isotope values obtained on dog specimens from Mesolithic forager sites (Borić *et al.*, 2004). There remains a possibility that this specimen comes from a dog feeding on human forager-fisher leftovers or, alternatively, a wolf significantly feeding on fish remains washed out by the Danube. Stable isotope values for one AMS-dated cave lion specimen from TT measured at the Arizona lab with a very low $\delta^{13}C$ (Table 6) is considered problematic and lacks information on bone chemistry, and hence is not taken into consideration.

Discussion

Over the past decade or so, a revised chronology for the Upper Danube region gave some support to the idea that the 'Danube corridor' (Conard and Bolus, 2003) might have played an important role as one of the main axes for the dispersal of modern humans and their assumed association with material remains of Protoaurignacian and Aurignacian provenance and/or transitional industries (Nigst, 2012; Teyssandier, 2008; Tsanova, 2008), pushing its start in central Europe to *c.* 43 kya cal BP (Higham *et al.*, 2012). Yet, while a decade ago, early dates started to pop up for deposits with modern human remains elsewhere in Europe (e.g. Benazzi *et al.*, 2011; Higham *et al.*, 2011), the assessment of radiocarbon chronology from south-eastern Europe did not live up to the expectations of the earliest dated IUP occurrences on the continent, as would be expected assuming the Danube corridor as the main conduit for dispersal. Over the past several years, this situation led some authors to suggest that the Danube corridor was unlikely to be the dispersal route for modern humans into Europe and to propose instead a northern route through the Russian steppes as the likely dispersal axis for modern humans reaching central Europe and beyond (Bae *et al.*, 2017). However, the results of the most recent excavations at the site of Bacho Kiro in northern Bulgaria (Fig. 1) have now positively confirmed the earliest directly AMS-dated modern human remains in Europe found in Layer I of this site, and associated material culture, including personal ornaments made from cave bear teeth, with the modelled boundary of 45 820–43 650 cal BP (Hublin *et al.*, 2020; Fewlass *et al.*, 2020). These recent findings have an important role to play both in understanding the role of the Danube corridor as the dispersal axis of modern humans into Europe and in assessing the last Neanderthal settlement of the Balkans (cf. Mihailović 2020).

If it is likely that the two taxa, i.e. Neanderthals and modern humans, were sympatric, and given the possibility for rapid dispersals, the Danube Basin must surely be a likely region for

this to have occurred, as aDNA results of one of the Oase Cave fossils suggest, with Neanderthal ancestry as early as 4–6 generations or 2–3 lifespans (cf. Fu *et al.*, 2015). Yet, there are only a few sites across the Balkans that provide some secure evidence for late Neanderthal occupation dated to MIS3, albeit with slim chances of overlap with modern humans (e.g. see the case of Vindija, Devièse *et al.*, 2017). Hence, it remains difficult to understand the extent of chronological overlap and the nature of social interactions of Neanderthals and modern human groups in different parts of the region. Few known MIS3 industries in the Balkans are generally characterised by a reduction strategy using the discoid method, and a strong denticulate component found on retouched tools (Mihailović 2020: 49).

Using different chronological proxies, the MP deposits of Mujina Cave in Croatia (Fig. 1) have recently been securely dated to between *c.* 49 and 39 kya with no evidence of modern human presence at the site in this temporal interval (Boschian *et al.*, 2017). Farther south, in the hinterland of the southern part of the Adriatic catchment, a recent assessment of the upper part of the MP deposits at the deeply stratified sequence of Crvena Stijena in Montenegro (Fig. 1) seems to suggest no MP hominin presence later than 46 kya cal BP (Mercier *et al.*, 2017). On the other hand, facing shallow Pleistocene-age palimpsest deposits with low artefact yields in the central Balkans and based on increased chronological datasets from the sites Hadži Prodanova and Pešturina caves in Serbia, Alex *et al.* (2019) suggest a working hypothesis that hominins occupying sites before 39 kya cal BP were Neanderthals producing MP industries, followed by a gap until 34 kya cal BP, when the earliest phases of the Gravettian can securely be linked to modern humans. However, these authors do cite earlier published data from TT as rare evidence in the central Balkans of EUP/Protoaurignacian presence at the site prior to 39 kya cal BP.

The evidence from Level VII (Layer 5c) at the site of Kozarnika in north-western Bulgaria places the EUP industry between 43 and 40 kya cal BP (Tsanova, 2012). Like TT, Layer 5c at Kozarnika contained CI-Y5 tephra (Lowe *et al.*, 2012). The finds from Level VIII (Layer 6/7) at Kozarnika would correspond to a transitional MP and IUP industry still poorly defined (Sirakov *et al.*, 2010), and based on two published radiocarbon measurements (GifA-101051: 43 600 ± 1200 BP; GifA-101052: 42 700 ± 1000 BP), put this occupation between 49 and 44 kya cal BP (Guadelli *et al.*, 2005), thus making these levels contemporaneous with previously mentioned IUP occupation at Bacho Kiro. In the same general region of north-western Bulgaria, at the site of Samuilitsa II Cave (Fig. 1), the MP assemblage of Levallois Mousterian is dated to between 48 and 43 kya cal BP (GRN-5181: 42 780 ± 1270 BP) and shows some evidence of UP blade production alongside the presence of a typical Levallois-based industry (Tsanova, 2008, 2012). On the other hand, the late MP assemblage, characterised as Denticulate Mousterian on quartz in Layer 2 and containing CI-Y5 tephra, at the site of Golema Pešt in North Macedonia is dated to *c.* 39 kya cal BP (Blackwell *et al.*, 2020) and might have been broadly contemporaneous with the UP assemblage at TT. In western Serbia, an important sequence covering the Middle to Upper Palaeolithic transitional interval is found at the cave site of Šalitrena (Marín-Arroyo and Mihailović 2017; Mihailović *et al.*, 2011). Here, MP levels (5b, 5c and 6) are characterised as the typical Balkan Mousterian with sidescrapers, Mousterian points, Levallois artefacts and leaf-like points. There are two infinite dates from these levels while two other AMS dates from MP levels suggest a late MP occupation between 42.8 and 39.2 kya cal BP. Early Upper Palaeolithic level 5a at this site dates to between 36.6 and 33.2 kya BP and is characterised by the Aurignacian industry with carinated endscrapers, burins and retouched and unretouched bladelets. A small assemblage of Initial/Early Upper Palaeolithic tools is found in Layer 4b at the cave site of Baranica in eastern Serbia, which is absolutely dated by only one measurement (OxA–13828: 35 780 ± 320 BP) to *c.* 41.5–40.2 kya cal BP (Mihailović *et al.*, 2011).

Adjacent to the Danube Gorges area, along a possible modern human dispersal route into Europe, there is a concentration of EUP open-air Aurignacian sites (Anghelinu *et al.*, 2012; Bălțean, 2011; Chu, 2018; Chu *et al.*, 2014, 2015; Hauck *et al.*, 2018): Tincova, Românești-Dumbrăvița (dated by luminiscence to between 41 and 37 kya cal BP, Schmidt, *et al.*, 2013), Coșava I and Crvenka-At (dated by luminiscence to 36.4 ± 2.8 kya cal BP, Nett *et al.*, 2021) (Fig. 1). In the Danube Gorges area (Fig. 2), previous MP finds come from the cave site of Peștera Hoților at Băile Herculane as well as from a concentration of several open-air locations in the vicinity of the village of Gornea in south-western Romania, on the edge of the Liubcova Basin – the hill of Căunita, where a small area of 28 m^2 was excavated in 1969 and 1970, yielding a small assemblage of 154 pieces with the characteristics of a MP industry (Levallois flakes and points, sidescrapers), and the hill of Păzăriște where some 180 pieces were found and were characterised as Aurignacian (Bălțean, 2011: 52). Also, at the small cave site of Pescari-Livadiței on the banks of the Danube, not far from the two previously mentioned open-air sites, Pleistocene levels were discovered in the 1970s, and a small lithic assemblage is characterised as 'Mousterian' with the presence of sidescrapers and several Levallois flakes.

Some 50 km north of DK, at the cave site of Peștera cu Oase on the Romanian side of the Danube, cranial and dental remains of two modern human individuals showing recent Neanderthal ancestry (Fu *et al.*, 2015; Trinkaus *et al.*, 2012) are dated to 42–37 kya cal BP and are broadly contemporaneous with the dated deposits at TT and DK. On the Serbian side of the Danube, at around 40 km distance from DK, two nearby cave sites – Kozja and Mala caves near Blizna – were recently investigated documenting both Middle and Early Upper Palaeolithic occupations, with Kozja containing hominin remains possibly coming from the Neanderthals (D. Mihailović, pers. comm.).

So, how does the presented evidence from TT and DK fit these wider regional patterns, and how do the two sites compare with each other? TT and DK are located in the same general area of the Danube Gorges at the distance of some 60 km as the crow flies, and in part their occupation is broadly contemporaneous. When it comes to MP knapped stone assemblages, there are striking differences in the type and knapping quality of raw material used at the two locations, with quartz and quartzite almost exclusively found at TT while at DK good quality flint raw materials were almost exclusively used. In addition, the MP assemblage at DK contains non-local raw materials, such as Balkan/Upper Cretaceous flint originating in northern Bulgaria some 150 km away. If future dating of the MP assemblage from DK reconfirms the current late date and if we could unambiguously show the association of this assemblage with Neanderthals, and also assuming the movement of modern humans from the east along the Danube, this presence of non-local raw materials could be a possible indication of a westward displacement of Neanderthal groups during the transitional interval. The absence of late MP (and by proxy Neanderthal) assemblages in the eastern Balkans might have been an effect of such a displacement.

There are also differences in the general density of artefacts between the two sites – while TT Cave conforms to the wider pattern of low artefact yields seen in the central Balkans (cf. Alex *et al.*, 2019), DK shows a surprisingly abundant and diverse assemblage with all stages of core reduction sequence

present. While little trace of human presence is evidenced in MP deposits of TT based on micromorphological analysis, the presence of very small bone fragments in micromorphological sections of Pleistocene deposits at DK may be an indication of *in situ* activities for marrow extraction, resulting in smashed and kneaded bones. This pattern would be consistent with the rather fragmented and small faunal assemblage found at this site. Possible hunting/consumption of cave bear is evidenced at both sites based on cutmarked and directly dated bones identified through proteomic analysis and may conform to the wider pattern of cave bear use in other MP sequences (e.g. Bacho Kiro, Samuilitsa II). Yet, it seems that this species might have had a significance also for slightly later and/or broadly contemporaneous modern human populations during the IUP phases, as evidenced by Bacho Kiro pendants from cave bear teeth (Hublin *et al.*, 2020) and other Gravettian-age ornaments from south-eastern Europe (Borić and Cristiani, 2019).

A combination of different chronological and chronostratigraphic proxies suggests that TT had been used by Neanderthals likely several thousand years before the site was used by modern humans sometime between 42.3 and 36.9 kya cal BP, which is consistent with the pattern of MP settlement abandonment prior to 44 kya BP seen in other areas of the Balkans (Mihailović 2020: 56). The likely gap in the sequence between c. 47 and 42 kya cal BP coincides with the duration of the Greenland Stadial (GS) 13-Heinrich 5 event, which was a global cooling episode associated with severe aridity in south-eastern Europe (Müller *et al.*, 2011), as well as GS12, *c.* 44.3–43.3 (Fig. 19). These stadials are recorded in speleothems from Romania, albeit characterised here by a smaller amplitude and less severe cooling and aridity than in other parts of Europe, especially the Atlantic and Mediterranean (Staubwasser *et al.*, 2018). The UP presence at TT possibly precedes the CI eruption, which can be used at this site as a chronostratigraphic marker based on the presence of cryptotephra glass shards consistent with CI materials in cave deposits. The micromorphological analyses of MP sediments from both TT and DK suggest cold conditions characterised by freezing and thawing cycles. The chronological situation and association with material culture remains less clear at DK at present. The flint assemblage from this site bears strong similarities both with the assemblage from Mujina Cave to the west (highly reduced, a high presence of denticulates, faceted platforms), but also to the east of the Balkans in the late MP assemblage from Samuilitsa II Cave. Yet it remains unclear how best to interpret the dates for cutmarked bones that place a hominin presence at the site sometime between 41 and 38 kya cal BP. There is a distinct possibility that these dates relate to the use of the site by late Neanderthals at a very close proximity to modern humans found in the wider region, but more work on chronological and contextual understanding of the site's sediments is needed in order to either confirm or reject this possibility. If in the future we could confirm the late presence of Neanderthals at DK in association with a distinct MP industry, it would mean that in this area along the Danube Neanderthals and modern humans might have indeed crossed their paths and were sympatric.

Conclusions

In this paper, relying on multiple analytical proxies, we have presented preliminary chronostratigraphic insights into Pleistocene sediments of two cave sites located on the southern, Serbian side of the Lower Danube Basin in the Danube Gorges area. While the site of TT is located on the sheer cliffs of the Danube in the downstream part of the region, DK is located some 10 km into the hinterland of the Danube in a more upstream area of the region. We have been able to identify and document an EUP presence at TT around 41–37 kya cal BP characterised by a very small lithic assemblage made on non-local materials with some characteristics of the Protoaurignacian (Dufour bladelet), while the lower strata of the cave contain evidence of the MP occupation, characterised by a Levallois industry on quartz and quartzite, currently dated to between 52.3 and 46.7 kya cal BP. The presence of CI-Y5 cryptotephra at the site provides an important chronostratigraphic marker for the hominin use of the cave and suggests the occupation of the site by likely modern humans prior to the CI eruption. The site was likely used and abandoned by Neanderthals several millennia before the arrival of modern humans. The Neanderthal disappearance at TT coincides broadly with the arrival of first modern humans farther to the east of the Danube Gorges area *c.* 47 to 45 kya cal BP.

In this paper, we have presented for the first time the chronostratigraphic sequence at DK, which suggests a late MP hominin occupation of the site *c.* 41 to 37.5 kya cal BP based on three AMS dates on two cutmarked bones. While more extensive radiometric dating of this sequence remains a priority, this occupation possibly continues from the older hominin use of the site based on several infinite AMS dates from the bottom of the sequence. At DK, there is a relatively large assemblage of knapped stone artefacts made on flint characterised by good knapping properties, some of which might have come from sources 150 km away (in northern Bulgaria). Based on the presence of a Levallois technology with a prominence of denticulates and convergent scrapers, along with a small presence of some UP categories of tools (endscrapers, points, borers), on the face of the current evidence, we suggest that the occupation of DK could probably be associated with the refugial occupation of some of the latest Neanderthal groups who were contemporaneous with the first modern humans in the wider region of the Balkans.

Acknowledgements. Research at TT and DK was supported by the High Risk Research in Archaeology grant of the National Science Foundation (BCS-0442096) in 2004, British Academy Small Grant 40967 in 2005, the McDonald Institute for Archaeological Research in Cambridge grants in 2005, 2008 and 2009, Cardiff University in 2013 and 2017, the NOMIS Foundation in 2019–2020 (all to DB), and the European Research Council Starting Grant Project HIDDEN FOODS grant agreement no. 639286 (to EC) in 2017. Research on cryptotephra and several AMS radiocarbon dates were funded through the UK Natural Environment Research Council (NERC) consortium 'RESponse of Humans to Abrupt Environmental Transitions' (RESET, NE/E015670/1 and NE/E015913/1). Stable isotope analyses were supported by the European Research Council Starting Grant Project SUBSILIENCE grant agreement no. 818299 (to AMB). CAIF thanks Tonko Rajkovača, McBurney Geoarchaeology Laboratory, Department of Archaeology University of Cambridge, for making the thin section slides and Chris Rolfe and Dr Steve Boreham of the Department of Geography, University of Cambridge are thanked for conducting the pollen preservation assessment. Als Chemex of North Vancouver is thanked for producing the multi-element figures. DB thanks Brandon Fowler for his help with the MALDI-TOF at the Department of Chemistry, Columbia University, Maria Gurova for drawings 1 and 3 of flint artefacts on Fig. 7, Miljana Botunjac for drawings on Figs. 11 and 12, and Andrea Zupancich for the base map in Fig. 1. We also thank two anonymous reviewers for their constructive comments that improved the presentation of our results. The radiocarbon dating was supported in the main by the European Research Council (ERC) under the European Union's Seventh Framework Programme (FP7/2007–2013)/ERC grant agreement 324139 "Palaeo-Chron," awarded to Professor Tom Higham, University of Oxford. This funding also supported Rachel Hopkins'' doctoral research. Open access funding provided by Universita degli Studi di Roma La Sapienza within the CRUI-CARE Agreement.

Supporting information

Additional supporting information can be found in the online version of this article. This article includes online-only Supplemental Data.

References

Alex B, Mihailović D, Milošević S *et al*. 2019. Radiocarbon chronology of Middle and Upper Palaeolithic sites in Serbia. *Journal of Archaeological Science: Reports* **25**: 266–279.

Aitken MJ. 1985. *Thermoluminescence Dating*. Academic Press: London.

Anghelinu M, Niță L, Sitlivy V *et al*. 2012. Looking around Peștera Cu Oase: The beginnings of Upper Paleolithic in Romania. *Quaternary International* **274**: 136–157.

Bae CJ, Douka K, Petraglia MD. 2017. On the origin of modern humans: Asian perspectives. *Science* **358**: eaai9067.

Bălțean IC. 2011. The Palaeolithic in Banat. In *The Prehistory of Banat*, Tasić N, Drașovean F (eds). The Publishing House of the Romanian Academy: Bucharest; 21–76.

Banerjee D, Murray AS, Bøtter-Jensen L *et al*. 2001. Equivalent dose estimation using a single aliquot of polymineral fine grains. *Radiation Measurements* **33**: 73–94.

Binford LR. 1981. *Bones: Ancient Men and Modern Myths*. Academia Press: New York.

Behrensmeyer AK. 1978. Taphonomic and ecological information from bone weathering. *Paleobiology* **4**: 150–162.

Benazzi S, Douka K, Fornai C *et al*. 2011. Early dispersal of modern humans in Europe and implications for Neanderthal behaviour. *Nature* **479**: 525–528.

Blackwell BAB, Šalamanov-Korobar L, Huang CLC *et al*. 2020. Sedimentary radioactivity in an Upper Paleolithic-Middle Paleolithic (MP-UP) transition site: Increasing ESR tooth dating accuracy at Golema Pešt, North Macedonia. *Radiation Protection Dosimetry* **186**(1): 94–112.

Blockley SPE, Pyne-O'Donnell SDF, Lowe JJ *et al*. 2005. A new and less destructive laboratory procedure for the physical separation of distal glass tephra shards from sediments. *Quaternary Science Reviews* **24**: 1952–1960.

Blumenschine RJ, Marean CW, Capaldo SD. 1996. Blind tests of inter-analyst correspondence and accuracy in the identification of cut marks, percussion marks, and carnivore tooth marks on bone surfaces. *Journal of Archaeological Science* **23**:493–507.

Bocherens H. 2004. Cave bear palaeoecology and stable isotopes: Checking the rules of the game. In *Cahiers scientifiques du Muséum d'histoire naturelle de Lyon*. Departément du Rhone: Lyon; 183–188.

Bocherens H, Drucker D. 2003. Trophic level isotopic enrichment of carbon and nitrogen in bone collagen: Case studies from recent and ancient terrestrial ecosystems. *International Journal of Osteoarchaeology* **13**(1–2): 46–53.

Bocherens H, Stiller M, Hobson KA *et al*. 2011. Niche partitioning between two sympatric genetically distinct cave bears (*Ursus spelaeus* and *Ursus ingressus*) and brown bear (*Ursus arctos*) from Austria: Isotopic evidence from fossil bones. *Quaternary International* **245**(2): 238–248.

Bonsall C. 2008. The mesolithic of the Iron gates. In *Mesolithic Europe, Bailey GN*, Spikins P (ed). Cambridge University Press: Cambridge; 238–279.

Borić D. 2011. Adaptations and transformations of the Danube Gorges foragers (c. 13,000–5500 cal BC): An overview. In *Beginnings – New Research in the Appearance of the Neolithic between Northwest Anatolia and the Carpathian Basin*, Krauß R (ed). Verlag Marie Leidorf GmbH: Rahden/Westf; 157–203.

Borić D, Cristiani E. 2019. Taking Beads seriously: Prehistoric forager ornamental traditions in southeastern. *Europe. PaleoAnthropology (Special Issue: Early Personal Ornaments)* **2019**: 208–239.

Borić D, Grupe G, Peters J *et al*. 2004. Is the Mesolithic-Neolithic subsistence dichotomy real? New stable isotope evidence from the Danube Gorges. *European Journal of Archaeology* **7**(3): 221–248.

Borić D, Dimitrijević V, White D *et al*. 2012. Early Modern Human settling of the Danube corridor: the Middle to Upper Palaeolithic site of Tabula Traiana Cave in the Danube Gorges (Serbia). *Antiquity* **86issue 334**.

Boscato P, Boschian G, Caramia F *et al*. 2009. Il Riparo del Poggio a Marina di Camerota (Salerno): culture ed ambiente. *Rivista di Scienze Preistoriche* **59**: 5–40.

Boschian G, Montagnari-Kokelj E. 2000. Prehistoric shepherds and caves in the Trieste Karst (Northeastern Italy). *Geoarchaeology: An International Journal* **15**(4): 31–371.

Boschian G, Gerometta K, Ellwood BB *et al*. 2017. Late Neandertals in Dalmatia: Site formation processes, chronology, climate change and human activity at Mujina Pećina, Croatia. *Quaternary International* **450**: 12–35.

Brennan BJ. 2003. Beta doses to spherical grains. *Radiation Measurements* **37**: 299–303.

Brochier JE, Villa P, Giacomarra M. 1992. Sheperds and sediments: Geoethnoarchaeology of pastoral sites. *Journal of Anthropological Archaeology* **11**: 47–102.

Bronk Ramsey C, Higham T, Bowles A *et al*. 2004a. Improvements to the pre-treatment of bone at Oxford. *Radiocarbon* **46**: 155–163.

Bronk Ramsey C, Higham T, Leach P. 2004b. Towards high precision AMS: Progress and limitations. *Radiocarbon* **46**: 17–24.

Buckley M, Collins M, Thomaes-Oates J *et al*. 2009. Species identification by analysis of bone collagen using matrix-assisted laser desorption/ionisation time-of-flight mass spectrometry. *Rapid Communications in Mass Spectrometry* **23**: 3843–3854.

Buckley M, Harvey VL, Chamberlain AT. 2017. Species identification and decay assessment of Late Pleistocene fragmentary vertebrate remains from Pin Hole Cave (Creswell Crags, UK) using collagen fingerprinting. *Boreas* **46**(3): 402–411.

Buckley M. 2016. Species identification of bovine, ovine and porcine type 1 collagen; comparing peptide mass fingerprinting and LC-based proteomics methods. *International Journal of Molecular Sciences* **17**(4): 445.

Bullock P, Fedoroff N, Jongerius A *et al*. 1985. *Handbook for Soil Thin Section Description*. Waine Research Publications: Wolverhampton.

Casana J, Kantner J, Wiewel A *et al*. 2014. Archaeological aerial thermography: A case study at the Chaco-era Blue J community, New Mexico. *Journal of Archaeological Science* **45**: 207–219.

Chu W. 2018. The Danube corridor hypothesis and the Carpathian Basin: Geological, environmental and archaeological approaches to characterizing Aurignacian dynamics. *Journal of World Prehistory* **31**: 117–178.

Chu W, Hauck T, Mihailović D. 2014. Crvenka-At– preliminary results from a lowland Aurignacian site in the Middle Danube catchment. In *Palaeolithic and Mesolithic Research in the Central Balkans*, Mihailović D (ed). Serbian Archaeological Society: Belgrade; 69–75.

Chu W, Mihailović D, Pantović I *et al*. 2015. Archaeological excavations at the site of At (Vršac, Serbia). *Antiquity*, Project Gallery, https://www.antiquity.ac.uk/projgall/chu352

Collins MJ, Buckley M, Grundy H *et al*. 2010. ZooMS, the collagen barcode and fingerprints. *Spectroscopy Europe* **22**(2): 11–13.

Comer DC, Harrower MJ. 2013. *Mapping archaeological landscapes from space*. Springer: New York.

Conard NJ, Bolus M. 2003. Radiocarbon dating the appearance of modern humans and timing of cultural innovations in Europe: New results and new challenges. *Journal of Human Evolution* **44**: 331–371.

Constantin S, Lauritzen S-E, Știucă E *et al*. 2001. Karst evolution in the Danube Gorge from U-series dating of a cave-bear skull and calcite speleothems from Pestera de la Gura Ponicovei (Romania). *Theoretical and Applied Karstology* **13–14**(2000–2001): 39–55.

Cvijić J. 1895a. *Karst: geografska monografija*. Štamparija Kraljevine Srbije: Beograd.

Cvijić J. 1895b. Pećine i podzemna hidrografija u Istočnoj Srbiji. *Glas Srpske Kraljevske Akademije* **46**: 1–101.

D'Anglade AG, Mosquera DF. 2008. Hibernation can also cause high δ15N values in cave bears: A response to Richards *et al*. *Proceedings of the National Academy of Sciences of the United States of America* **105**: E14–E14.

De Corte F, Vandenberghe D, Buylaert J-P *et al*. 2006. Relative and k_0-standardized INAA to assess the internal (Th, U) radiation dose rate in the "quartz coarse-grain protocol" for OSL dating of sediments: unexpected observations. *Nuclear Instruments and Methods in Physics Research (A)* **564**: 743–751.

DeNiro MJ, Epstein S. 1978. Influence of diet on the distribution of carbon isotopes in animals. *Geochimica et Cosmochimica Acta* **42**(5): 495–506.

Devièse T, Karavanic I, Comeskey D *et al*. 2017. Direct dating of Neanderthal remains from the site of Vindija Cave and implications

for the Middle to Upper Paleolithic transition. *PNAS* **114**(40): 10606–10611.

Diefendorf AF, Mueller KE, Wing SL *et al*. 2010. Global patterns in leaf 13C discrimination and implications for studies of past and future climate. *Proceedings of the National Academy of Sciences of the United States of America* **107**(13): 5738–5743.

Dimitrijević V, alić-Ljubojević J, Bogićević K. 2002. Cave bear (*Ursus spelaeus* Rosenmüller & Heinroth) males' den from Velika Pećina in Duboka near Kučevo (eastern Serbia). *Geološki anali Balkanskog poluostrva* **64**(2001): 153–165.

Dogandžić T, McPherron S, Mihailović D. 2014. Middle and Upper Paleolithic in the Balkans: Continuities and discontinuities of human occupations. In *Palaeolithic and Mesolithic Research in the Central Balkans*, Mihailović D (ed). Serbian Archaeological Society: Belgrade; 83–96.

Douka K, Grimaldi S, Boschian G *et al*. 2012. A new chronostratigraphic framework for the Upper Palaeolithic of Riparo Mochi (Italy). *Journal of Human Evolution*. **62**: 286–299.

Drucker D, Bocherens H, Bridault A *et al*. 2003. Carbon and nitrogen isotopic composition of red deer (*Cervus elaphus*) collagen as a tool for tracking palaeoenvironmental change during the Late-Glacial and Early Holocene in the northern Jura (France). *Palaeogeography, Palaeoclimatology, Palaeoecology* **195**(3–4): 375–388.

Drucker DG, Bridault A, Hobson KA *et al*. 2008. Can carbon-13 in large herbivores reflect the canopy effect in temperate and boreal ecosystems? Evidence from modern and ancient ungulates. *Palaeogeography, Palaeoclimatology, Palaeoecology* **266**(1–2): 69–82.

Drucker DG, Bridault A, Cupillard C *et al*. 2011. Evolution of habitat and environment of red deer (*Cervus elaphus*) during the Late-glacial and early Holocene in eastern France (French Jura and the western Alps) using multi-isotope analysis (δ13C, δ15N, δ18O, δ34S) of archaeological remains. *Quaternary International* **245**(2): 268–278.

Duller GAT. 2015. The Analyst software package for luminescence data: Overview and recent improvements. *Ancient TL* **33**: 35–42.

Durcan JA, King GE, Duller GAT. 2015. DRAC: Dose rate and age calculator for trapped charge dating. *Quaternary Geochronology* **28**: 54–61.

Ehleringer JR, Comstock JP, Cooper TA. 1987. Leaf-twig carbon isotope ratio differences in photosynthetic-twig desert shrubs. *Oecologia* **71**(2): 318–320.

Farquhar GD, O'Leary MH, Berry JA. 1982. On the relationship between carbon isotope discrimination and the intercellular carbon dioxide concentration in leaves. *Australian Journal of Plant Physiology* **9**(2): 121–137.

Farquhar GD, Hubick KT, Condon AG *et al*. 1989. Carbon isotope fractionation and plant water-use efficiency. In *Stable Isotope in Archaeological Research*, Rundel PW, Ehleringer JR, Nagy KA (eds). Springer-Verlag: New York; 21–40.

Fernández-Jalvo Y, Andrews P, Denys C. 1999. Cut marks on small mammals at Olduvai Gorge Bed-I. *Journal of Human Evolution* **36**: 587–589.

Fernández-Mosquera D, Vila-Taboada M, Grandal-d'Anglade A. 2001. Stable isotopes data (δ13C, δ15N) from the cave bear (*Ursus spelaeus*): A new approach to its palaeoenvironment and dormancy. *Proceedings of the Royal Society B: Biological Sciences* **268**(1472): 1159–1164.

Fewlass H, Talamo S, Wacker L *et al*. 2020. A 14C chronology for the Middle to Upper Palaeolithic transition at Bacho Kiro Cave. *Bulgaria. Nature Ecology & Evolution* **4**: 794–801.

Fisher JW. 1995. Bone surface modifications in zooarchaeology. *Journal of Archaeological Method and Theory* **2**: 7–68.

Fleisher J, Sulas F. 2015. Deciphering public spaces in urban contexts: Geophysical survey, multi-element analysis, and artefact distributions at the 15th–16th-century AD Swahili settlement of Songa Mnana, Tanzania. *Journal of Archaeological Science* **55**: 55–70.

Fu Q, Hajdinjak M, Moldovan OT *et al*. 2015. An early modern human from Romania with a recent Neanderthal ancestor. *Nature* **524**(7564): 216–219.

Giaccio B, Hajdas I, Isaia R *et al*. 2017. High-precision ^{14}C and $^{40}Ar/^{39}Ar$ dating of the Campanian Ignimbrite (Y-5) reconciles the time-scales of climatic-cultural processes at 40 ka. *Scientific Reports* **7**(1): 1–10.

Goldberg P. 1980. Micromorphology in archaeology and prehistory. *Paléorient* **6**: 159–164.

Grandal-D'Anglade A, Pérez-Rama M, Fernandez-Mosquera D. 2011. Diet, physiology and environment of the cave bear. In *Fragments of Ice Age Environments. Proceedings in Honour of Ivan Turk's Jubilee*. Toškan B (ed). Založba ZRC: Ljubljana; 111–125.

Grignolio S, Rossi B, Bassano R *et al*. 2004. Seasonal variations of spatial behaviour in female alpine ibex (*Capra ibex ibex*) in relation to climatic conditions and age. *Ethology Ecology and Evolution* **16**(3): 255–264.

Gröcke DR, Bocherens H, Mariotti A. 1997. Annual rainfall and nitrogen-isotope correlation in macropod collagen: Application as a palaeoprecipitation indicator. *Earth and Planetary Science Letters* **153**(3–4): 279–285.

Grün R, Fenton C. 1990. Internal dose rates of quartz grains separated from fault gouge. *Ancient TL* **8**: 26–28.

Guadelli J-L, Sirakov N, Ivanova S *et al*. 2005. Une sequence du Paleolithique Inferieur au Paleolithique Recent dans les Balkans: La grotte Kozarnika a orechets (nord-ouest de la Bulgarie). In *Les Premiers Peuplements en Europe* (BAR Int. Ser. 1364), Molines N, Moncel M-H, Monnier J-L (eds). Archaeopress: Oxford; 87–103.

Guérin G, Mercier N, Adamiec G. 2011. *Dose-rate conversion factors: Update. Ancient TL* **29**: 5–8.

Gurova M, Andreeva P, Stefanova E *et al*. 2016. Flint raw material transfers in the prehistoric Lower Danube Basin: An integrated analytical approach. *Journal of Archaeological Science: Reports* **6**: 422–441.

Hansen V, Murray AS, Buylaert J-P *et al*. 2015. A new irradiated quartz for beta source calibration. *Radiation Measurements* **81**: 123–127.

Harangi S, Lukács R, Schmitt AK *et al*. 2015. Constraints on the timing of Quaternary volcanism and duration of magma residence at Ciomadul volcano, east–central Europe, from combined U–Th/He and U–Th zircon geochronology. *Journal of Volcanology and Geothermal Research* **301**: 66–80.

Harangi S, Molnar K, Schmitt AK *et al*. 2007. Fingerprinting the Late Pleistocene tephras of Ciomadul volcano,eastern–central Europe. *Journal of Quaternary Science* **35**(1-2): 232–244.

Harvati K, Roksandic M (eds). 2016. *Palaeoantrhopology of the Balkans and Anatolia: Human Evolution and its Context*. Springer: New York.

Hauck TC, Lehmkuhl F, Zeeden C *et al*. 2018. The Aurignacian way of life: Contextualizing early modern human adaptation in the Carpathian Basin. *Quaternary International* **485**: 150–166.

Heaton THE. 1999. Spatial, species, and temporal variations in the $^{13}C/^{12}C$ ratios of C_3 plants: Implications for palaeodiet studies. *Journal of Archaeological Science* **26**(6): 637–649.

Higham T, Compton T, Stringer C. 2011. The earliest evidence for anatomically modern humans in northwestern Europe. *Nature* **479**: 521–524.

Higham T, Basell L, Jacobi R *et al*. 2012. Testing models for the beginnings of the Aurignacian and the advent of figurative art and music: The radiocarbon chronology of Geißenklösterle. *Joural of Human Evolution* **62**: 664–676.

Hublin J-J, Sirakov N, Aldeias V *et al*. 2020. Initial Upper Palaeolithic *Homo sapiens* from Bacho Kiro Cave, Bulgaria. *Nature* **581**: 299–302.

Hultine KR, Marshall JD. 2000. Altitude trends in conifer leaf morphology and stable carbon isotope composition. *Oecologia* **123**(1): 32–40.

Iovita R, Dobos A, Fitzsimmons KE *et al*. 2014. Geoarchaeological prospection in the loess steppe: Preliminary results from the Lower Danube Survey for Paleolithic Sites (LoDanS). *Quaternary International* **351**: 98–114.

Jones JR, Richards MP, Straus LG *et al*. 2018. Changing environments during the Middle-Upper Palaeolithic transition in the eastern Cantabrian Region (Spain): Direct evidence from stable isotope studies on ungulate bones. *Scientific Reports* **8**(1): 84–88.

Jones JR, Richards MP, Reade H *et al*. 2019. Multi-Isotope investigations of ungulate bones and teeth from El Castillo and Covalejos caves (Cantabria, Spain): Implications for paleoenvironment reconstructions across the Middle-Upper Palaeolithic transition. *Journal of Archaeological Science: Reports* **23**: 1029–1042.

Jorayev G, Wehr K, Benito-Calvo A *et al*. 2016. Imaging and photogrammetry models of Olduvai Gorge (Tanzania) by Unmanned Aerial Vehicles: A high-resolution digital database for research and conservation of Early Stone Age sites. *Journal Archaeological Science* **75**: 40–56.

Jovanović B. 1951. Veika pećina kod Duboke – prilog morfologiji i hidrografiji krasa istočne Srbije, *Zbornik radova SAN, knj. VIII*. Geografski institut, knj. 1: Beograd; 135–165.

Kapuran A, Jevtić M, Borić D. 2007. Novi nalazi keramike matalnih doba na teritoriji Đerdapa (Eneolithic and Iron Age pottery from two newly discovered caves in the Danube Gorges). *Journal of the Serbian Archaeological Society* **23**: 103–124.

Karkanas P, Goldberg P. 2010. Phosphatic features. In *Interpretation of Micromorphological Features of Soils and Regoliths*, Stoops G, Marcelino V, Mees F (eds). Elsevier: Amsterdam; 521–542.

Karátson D, Wulf S, Veres D *et al*. 2016. The latest explosive eruptions of Ciomadul (Csomád) volcano, East Carpathians—a tephrostratigraphic approach for the 51–29 ka BP time interval. *Journal of Volcanology and Geothermal Research* **319**: 29–51.

Karavanić I, Miracle P, Culiberg M *et al*. 2008. The Middle Palaeolithic from Mujina Pećina, Dalmatia, Croatia. *Journal of Field Archaeology* **33**(3): 259–277.

Kohn MJ. 2010. Carbon isotope compositions of terrestrial C3 plants as indicators of (paleo)ecology and (paleo)climate. *Proceedings of the National Academy of Sciences of the United States of America* **107**(46): 19691–19695.

Kolska Horwitz L, Goldberg P. 1989. A study of Pleistocene and Holocene hyaena coprolites. *Journal of Archaeogical Science* **16**: 71–94.

Körner C, Farquhar GD, Wong SC. 1991. Carbon isotope discrimination by plants follows latitudinal and altitudinal trends. *Oecologia* **88**(1): 30–40.

Kreutzer S, Schmidt C, Fuchs M *et al*. 2012. Introducing an R package for luminescence dating analysis. *Ancient TL* **30**(1): 1–8.

Law IA, Hedges REM. 1989. A semi-automated pre-treatment system and the pretreatment of older and contaminated samples. *Radiocarbon* **31**: 247–253.

Lindbo DL, Stolt MH, Vepraskas MJ. 2010. Redoximorphic features. In *Interpretation of Micromorphological Features of Soils and Regoliths*, Stoops G, Marcelino V, Mees F (eds). Elsevier: Amsterdam; 129–148.

Lowe J, Barton N, Blockley S *et al*. 2012. Volcanic ash layers illuminate the resilience of Neanderthals and early Modern Humans to natural hazards. *Proceedings of the National Academy of Sciences of the United States of America* **109**(34): 13532–13537.

Lyman L. 1994. *Vertebrate Taphonomy*. Cambridge University Press: Cambridge.

Macphail RI, Goldberg P. 2010. Archaeological materials. In *Interpretation of Micromorphological Features of Soils and Regoliths*, Stoops G, Marcelino V, Mees F (eds). Elsevier: Amsterdam; 569–622.

Mandić M, Borić D. 2015. Pećina kod Trajanove Table. In *Caves in the Djerdap National Park*, Ćalić J (ed). JP Nacionalni Park Đerdap: Donji Milanovac; 84–89.

Marín-Arroyo AB, Mihailović B. 2017. The chronometric dating and subsistence of late Neanderthals and early anatomically modern humans in the central Balkans insights from Šalitrena Pećina (Mionica, Serbia). *Journal of Anthropological Research* **73**(3): 413–447.

Mejdahl V. 1987. Internal radioactivity in quartz and feldspar grains. *Ancient TL* **5**: 10–17.

Mercier N, Rink WJ, Rodrigues K *et al*. 2017. Radiometric Dating of the Crvena Stijena Sequence. In *Crvena Stijena in Cultural and Ecological Setting: Multidisciplinary Archaeological Research in Montenegro*, Whallon R (ed). Montenegrin Academy of Sciences and Arts: Podgorica; 140–49.

Mihailović D. 2009. *Middle Palaeolithic Settlement at Petrovaradin Fortress*. City Museum of Novi Sad: Novi Sad.

Mihailović D. 2020. Push-and-pull factors of the Middle to Upper Paleolithic transition in the Balkans. *Quaternary International* **551**: 47–62.

Mihailović D, Mihailović B, Lopičić M. 2011. The Palaeolithic in northern Serbia. In *The Prehistory of Banat*, Tasić N, Drașovean F (eds). The Publishing House of the Romanian Academy: Bucharest; 78–101.

Milošević S. 2020. *Competition Between Humans and Large Carnivores: Case Studies from the Late Middle and Upper Palaeolithic of the Central Balkans* (British Archaeological Reports Int. Ser. 2961). BAR Publishing: Oxford.

Molnár K, Lukács R, Dunkl I *et al*. 2019. Episodes of dormancy and eruption of the Late Pleistocene Ciomadul volcanic complex (Eastern Carpathians, Romania) constrained by zircon geochronology. *Journal of Volcanology and Geothermal Research* **373**: 133–147.

Müller UC, Pross J, Tzedakis PC *et al*. 2011. The role of climate in the spread of modern humans into Europe. *Quaternary Science Reviews* **30**(3–4): 273–279.

Murphy CP. 1986. *Thin Section Preparation of Soils and Sediments*. A. B. Academic: Berkhamsted.

Murray AS, Wintle AG. 2000. Luminescence dating of quartz using an improved single-aliquot regenerative-dose measurement protocol. *Radiation Measurements* **32**: 57–73.

Naito YI, Meleg IN, Robu M *et al*. 2020. Heavy reliance on plants for Romanian cave bears evidenced by amino acid nitrogen isotope analysis. *Scientific Reports* **10**(1): 6612.

Nett JJ, Chu W, Fischer P *et al*. 2021. The early Upper Paleolithic site Crvenka-At, Serbia – the first Aurignacian lowland occupation site in the southern Carpathian Basin. *Frontiers in Earth Science* **9**: 599986.

Nigst P. 2012. *Early Upper Palaeolithic of the Middle Danube Basin*. Leiden University Press: Leiden.

Parrini F, Cain JW, Krausman PR. 2009. *Capra ibex* (Artiodactyla: Bovidae). *Mammalian Species* **830**: 1–12.

Prescott JR, Hutton JT. 1994. Cosmic ray contributions to dose rates for luminescence and ESR dating: large depths and long-term time variations. *Radiation Measurements* **23**: 497–500.

Privat KL, O'Connell TC, Richards MP. 2002. Stable isotope analysis of human and faunal remains from the Anglo-Saxon cemetery and Berinsfield, Oxfordshire: Dietary and social implications. *Journal of Archaeological Science* **29**(7): 779–790.

Rabinovich R, Hovers E. 2004. Faunal analysis from Amud Cave: Preliminary results and interpretations. *International Journal of Osteoarchaeology* **14**(3–4): 287–306.

Rees-Jones J, Tite MS. 1997. Optical dating results for British archaeological sediments. *Archaeometry* **39**: 177–187.

Rees-Jones J. 1995. Optical dating of young sediments using fine-grained quartz. *Ancient TL* **13**: 9–14.

Richards MP, Pacher M, Stiller M *et al*. 2008. Isotopic evidence for omnivory among European cave bears: Late Pleistocene *Ursus spelaeus* from the Peștera cu Oase, Romania. *Proceedings of the National Academy of Sciences of the United States of America* **105**(2): 600–604.

Richter D, Richter A, Kornich K. 2015. *Lexsyg Smart* – a luminescence detection system for dosimetry, material research and dating application. *Geochronometria* **42**: 202–209.

Riedesel S, Autze M, Burow C. 2020. scale_GammaDose: Calculate the gamma dose deposited within a sample taking layer-to-layer variations in radioactivity into account (according to Aitken, 1985). Function version 0.1.2. In *Luminescence: Comprehensive Luminescence Dating Data Analysis. R package version 0.9.9 et al.*, Kreutzer S, Burow C, Dietze M, Available at: https://CRAN.R-project.org/package=Luminescence

Schmidt C, Sitlivy V, Anghelinu M *et al*. 2013. First chronometric dates (TL and OSL) for the Aurignacian open-air site of Românești-Dumbrăvița I, Romania. *Journal of Archaeological Science* **40**: 3740–3753.

Shipman P. 1981. *Life History of a Fossil: An Introduction to Taphonomy and Paleoecology*. Harvard University Press: Cambridge, MA.

Sirakov N, Guadelli J-L, Ivanova S *et al*. 2010. An ancient continuous human presence in the Balkans and the beginnings of human settlement in western Eurasia: A Lower Pleistocene example of the Lower Palaeolithic levels in Kozarnika cave (NW Bulgaria). *Quaternary International* **223–224**: 94–106.

van der Merwe NJ, Medina E. 1989. Photosynthesis and $^{13}C^{12}C$ ratios in Amazonian rain forests. *Geochimica et Cosmochimica Acta* **53**(5): 1091–1094.

van der Merwe NJ, Medina E. 1991. The canopy effect, carbon isotope ratios and foodwebs in Amazonia. *Journal of Archaeological Science* **18**(3): 249–259.

van der Sluis LG *et al*. 2014. Combining histology, stable isotope analysis and ZooMS collagen fingerprinting to investigate the taphonomic history and dietary behaviour of extinct giant tortoises from the Mare aux Songes deposit on Mauritius. *Palaeogeography, Palaeoclimatology, Palaeoecology* **416**: 80–91.

Staubwasser M, Drăgușin V, Onac BP *et al*. 2018. Impact of climate change on the transition of Neanderthals to modern humans in Europe. *Proceedings of the National Academy of Sciences of the United States of America* **115**(37): 9116–9121.

Stevens RE, Hermoso-Buxán XL, Marín-Arroyo AB *et al*. 2014. Investigation of Late Pleistocene and Early Holocene palaeoenvironmental change at El Mirón cave (Cantabria, Spain): Insights from carbon and nitrogen isotope analyses of red deer. *Palaeogeography, Palaeoclimatology, Palaeoecology* **414**: 46–60.

Stewart GR, Turnbull MH, Schmidt S *et al*. 1995. ^{13}C natural abundance in plant communities along a rainfall gradient: A biological integrator of water availability. *Australian Journal of Plant Physiology* **22**(1): 51–55.

Stoops G. 2003. *Guidelines for Analysis and Description of Soil and Regolith Thin Sections*. Soil Science Society of America: Madison, WI.

Stoops G, Marcelino V, Mees F (eds). 2010. *Interpretation of Micromorphological Features of Soils and Regoliths*. Elsevier: Amsterdam.

Szpak P, Metcalfe JZ, Macdonald RA. 2017. Best practices for calibrating and reporting stable isotope measurements in archaeology. *Journal of Archaeological Science: Reports* **13**: 609–616.

Teyssandier N. 2008. Revolution or evolution? The emergence of the Upper Palaeolithic in Europe. *World Archaeology* **40**: 493–519.

Thomas H. 2016. Quantitative analysis of two low-cost aerial photography platforms: A case study of the site of Zagora, Andros, Greece. *Journal of Field Archaeology* **41**: 1–11.

Tomlinson EL, Thordarson T, Müller W *et al*. 2010. Microanalysis of tephra by LA-ICP-MS – Strategies, advantages and limitations assessed using the Thorsmörk ignimbrite (Southern Iceland). *Chemical Geology* **279**: 73–89.

Trinkaus E, Constantin S, Zilhão J (eds). 2012. *Life and Death at Peștera cu Oase: A Setting for Modern Human Emergence in Europe*. Oxford University Press: Oxford.

Tsanova T. 2008. *Les débuts du Paléolithique supérieur dans l'Est des Balkans. Réflexion à partir des études taphonomique et techno-économique des ensembles lithiques des grottes Bacho Kiro (couche 11), Temnata (couche VI et 4) et Kozarnika (niveau VII)* (BAR Int. Ser. 1752). Archaeopress: Oxford.

Tsanova T. 2012. A diachronic view of flake production from the beginning of the Upper Palaeolithic in the Eastern Balkans. In *Flakes Not Blades: The Role of Flake Production at the Onset of the Upper Palaeolithic in Europe*, Pastoors A, Peresani M (eds). Neanderthal Museum: Mettmann; 215–237.

Vandenberghe D, De Corte F, Buylaert J-P *et al*. 2008. On the internal radioactivity in quartz. *Radiation Measurements* **43**: 771–775.

Van Vliet-Lanoë B. 2010. Frost action. In *Interpretation of Micromorphological Features of Soils and Regoliths*, Stoops G, Marcelino V, Mees F (eds). Elsevier: Amsterdam; 81–108.

Verhoeven GJJ. 2009. Providing an archaeological bird's-eye view e an overall picture of ground-based means to execute low-altitude aerial photography (LAAP) in Archaeology. *Archaeological Prospection* **16**: 233–249.

Wallinga J, Murray AS, Bøtter-Jensen L. 2002. Measurement of the dose in quartz in the presence of feldspar contamination. *Radiation Protection Dosimetry* **101**: 367–370.

Wattez J, Courty M-A. 1987. Morphology of ash of some plant materials. In *Soil Micromorphology*, Fedoroff N, Bresson LM, Courty M-A (eds). AFES: Plaisir; 677–683.

Welker F, Soressi M, Rendu W *et al*. 2015. Using ZooMS to identify fragmentary bone from the late Middle/Early Upper Palaeolithic sequence of Les Cottés, France. *Journal of Archaeological Science* **54**: 279–286.

Wintle AG, Murray AS. 2006. A review of quartz optically stimulated luminescence characteristics and their relevance in single-aliquot regeneration dating protocols. *Radiation Measurements* **41**: 369–391.

Zlokolica-Mandić M, Mandić M, Stošić P *et al*. 2003. Novija istraživanja Dubočke pećine, *4. Simpozijum o zaštiti karsta, Despotovac 2000*. ASAK: Beograd; 135–141.

